

DISS. ETH NO. 20204

**Oxidative Transformation of Aromatic Amines:  
Mechanistic Insights from Multielement  
Stable Isotope Analyses**

A dissertation submitted to  
ETH ZURICH

for the degree of  
Doctor of Sciences

presented by  
MARITA SKARPELI-LIATI  
MSc. ETH Chemistry

born July 30<sup>th</sup>, 1983

citizen of  
Greece and Zürich, Switzerland

accepted on the recommendation of  
Prof. Dr. René P. Schwarzenbach, examiner  
Prof. Dr. A. Lynn Roberts, co-examiner  
PD Dr. Thomas B. Hofstetter, co-examiner

2012



# Dank

Ganz herzlich möchte ich mich bei meinen Betreuern, Thomas Hofstetter und René Schwarzenbach bedanken. Sie haben mir die Möglichkeit gegeben meine Dissertation in einem sehr interessanten und interdisziplinären Gebiet durchzuführen und mir das entsprechende Vertrauen entgegengebracht. Sie haben mich von der "Umwelt-Seite" der Chemie wirklich begeistern können! Thomas war immer sehr hilfsbereit in Computer-, Labor- und schreibtechnischen Angelegenheiten. Das ist wohl nicht selbstverständlich und dafür bin ich sehr dankbar. Ich habe durch die langen Diskussionen sehr viel gelernt und sein Enthusiasmus war immer motivierend! Ausserdem hoffe ich, dass der Tennis-Match in Frankreich nicht der Letzte war. Die Diskussionen mit René und sein Input während der Schreibphasen haben sehr zur Qualität der Arbeit beigetragen. Ausserdem hatte er immer einen Ratschlag wie "Man soll gescheiter aussehen" oder "Mach kein Seich" bereit. Ich war auch immer darüber erfreut, wie er von den Schönheiten meiner Heimat geschwärmt hat. I would also like to thank Prof. A. Lynn Roberts for traveling overseas for my examination and her valuable comments to my work.

Ein sehr grosses Dankeschön gehört meinen zwei sehr engagierten Masterstudenten, Martin Jiskra und Sarah Pati für ihre ausserordentliche Leistung und den sehr wichtigen Beitrag zu dieser Arbeit. Die stundenlangen Diskussionen mit ihnen über die Arbeit und das Leben waren immer spannend und extrem wertvoll!

Kov hat mich immer im Kampf mit (oder gegen) dem IRMS unterstützt, sogar per sms vom kroatischen Strand aus! Er hat mehrere Vorsäulen, Oxidationsreaktoren und Kreuzstücke ausgewechselt, viele Proben gemessen und immer gewusst, wann der richtige Zeitpunkt für ein neues Überraschungsei ist! Herzlichen Dank! Michael Sander und Michael Äschbacher haben mir bei den elektrochemischen Experimenten geholfen. Dankeschön! Bedanken möchte ich mich auch bei Maarten Nachtegaal, der mir wertvolle beam time an der SLS am PSI zur Verfügung gestellt hat. I would also like to thank Prof. Cris Cramer, Prof. Bill Arnold and Dr. Soren Eustis for performing thoretical calculations, which contributed a lot to the interpretation of my data and also for valuable

discussions. Ebenfalls danke an Michael Berg und Caroline Stengel, dass wir bei ihnen die HPLC benutzen durften.

Für die sehr konstruktive und angenehme Arbeitsatmosphäre möchte ich mich bei der ehemaligen Schwaba-Gruppe bedanken, vor allem Anke, Nicole, Akané, Michi M., Michi Ä., Michi S. und Jeanne. Ich durfte noch die berühmten "Grufos" miterleben, die eine sehr gute Möglichkeit zum Austausch geboten haben. Auch die Kaffeerunden mit Patricia, Tinu, Daniela, Christian, Sibyl, Michi M., Jeanne, Reto und Fabio bleiben mir in sehr guter Erinnerung. Thanks a lot to Fabio Ugolini, Tonya del Sontro, and Ilaria Stendardo, it was really fun to organize the IBP PhD Congress with you guys! Der UCHEM-Abteilung an der EAWAG gehört ein spezielles Dankeschön! Alle haben uns sehr herzlich willkommen geheissen als wir, die "Thomas-Gruppe", nach Dübendorf gezogen sind. Sowohl die Arbeitsatmosphäre als auch alle Kultur- und Sport-Events habe ich sehr genossen! Vielen Dank an die Truppe vom D-floor, Philipp, Jürgen, Sarah, Rebekka, Michi, Alfi, Baschi, Reto, Marco, Irene und die Kaffeemaschine, die uns, im D9, immer willkommenen Besuch (Tobi) beschert hat.

Vom ganzen Herzen möchte ich mich bei meiner Mutter, Anthi, und meinem Vater, Nikos, bedanken, die immer an meiner Seite stehen und mich ständig bei meinen Entscheidungen unterstützt haben! Σας αγαπώ πολύ! Auch Dieter hat mir während meiner ganzen Zeit in der Schweiz sehr geholfen, ich schätze es sehr!

Vielen Dank an Patricia Walker und Brigitte Rohner für das Verständnis während der letzten Wochen und der sehr coolen Atmosphäre in unserer WG. Merci auch an meine Freunde und Kollegen, vor allem meine seit dem Studium treuen ouzo-12 Truppe, Pippo, Gaby, Nathalie, Fränzi, Dirk, Thomi, Lo, Pascal, Tino, Fabian; die Zeit mit ihnen ist immer ein Highlight! Maurizio Gaffuri gehört ein grosses Dankeschön für das wunderschöne Design des Titelblattes!

Ein sehr grosses Dankeschön geht an Tinu, der trotz meiner einigermaßen strengen Betreuung auch nach seiner Masterarbeit an meiner Seite steht. Danke für die Unterstützung und das Verständnis während dem Endspurt und den sehr wertvollen Latex-Support!!

# Table of contents

Summary	vii
Zusammenfassung	ix
Περίληψη	xiii
<b>1 Introduction</b>	<b>1</b>
1.1 Assessing transformation processes of organic micropollutants in the environment . . . . .	2
1.2 Transformation processes of N-containing organic micropollutants . . . .	5
1.3 Objectives and approach of this thesis . . . . .	8
<b>2 pH-Dependent Equilibrium Isotope Fractionation Associated with the Compound Specific Nitrogen and Carbon Isotope Analysis of Substituted Anilines by SPME-GC/IRMS</b>	<b>11</b>
Abstract . . . . .	11
2.1 Introduction . . . . .	12
2.2 Experimental Section . . . . .	14
2.2.1 Reagents and materials . . . . .	14
2.2.2 Instrumentation . . . . .	14
2.2.3 SPME of aqueous samples . . . . .	15
2.2.4 Extraction efficiency . . . . .	15
2.2.5 Stable isotope measurements in buffered solutions with SPME-GC/IRMS . . . . .	16
2.2.6 Detection limits for accurate isotope ratio measurements . . . . .	17
2.2.7 DFT-Calculations . . . . .	18
2.3 Results and Discussion . . . . .	20
2.3.1 <sup>15</sup> N and <sup>13</sup> C Signatures determined by SPME- GC/IRMS . . . . .	20

2.3.2	Equilibrium isotope effect (EIE) associated with the protonation of substituted anilines . . . . .	24
2.3.3	Detection limits for accurate isotope analysis of substituted anilines	29
2.4	Conclusion . . . . .	29
<b>Supporting Information to Chapter 2</b>		<b>31</b>
<b>3 Using Nitrogen Isotope Fractionation to Assess the Oxidation of Substituted Anilines</b>		
<b>by Manganese Oxide</b>		<b>35</b>
	Abstract . . . . .	35
3.1	Introduction . . . . .	36
3.2	Experimental Section . . . . .	38
3.2.1	Experimental systems for the oxidation of substituted anilines . .	38
3.2.2	Analytical methods . . . . .	40
3.2.3	Data evaluation . . . . .	41
3.2.4	Computational methods . . . . .	43
3.3	Results and Discussion . . . . .	43
3.3.1	Isotope fractionation associated with the oxidation of substituted anilines in MnO <sub>2</sub> -suspensions. . . . .	43
3.3.2	Substituent effects on AKIE <sub>N</sub> s and implications for the reaction mechanism . . . . .	45
3.3.3	Reference experiments and density functional theory calculations . . . . .	47
3.3.4	Influence of substituted aniline speciation on AKIE <sub>N</sub> . . . . .	50
3.4	Environmental Significance . . . . .	51
<b>Supporting Information to Chapter 3</b>		<b>53</b>

<b>4 Carbon, Hydrogen, and Nitrogen Isotope Fractionation Associated with Oxidative Transformation of Substituted Aromatic <i>N</i>-Alkyl Amines</b>	<b>69</b>
Abstract . . . . .	70
4.1 Introduction . . . . .	70
4.2 Experimental Section . . . . .	73
4.2.1 Oxidation experiments in MnO <sub>2</sub> -suspensions . . . . .	73
4.2.2 Oxidation experiments with horseradish peroxidase . . . . .	74
4.2.3 Analytical methods . . . . .	75
4.2.4 Data evaluation . . . . .	76
4.2.5 Computational Methods . . . . .	78
4.3 Results and Discussion . . . . .	79
4.3.1 Isotope fractionation associated with the oxidative transformation of <i>para</i> -substituted <i>N</i> -methylanilines by MnO <sub>2</sub> . . . . .	79
4.3.2 Isotope fractionation associated with the oxidative transformation of substituted <i>N,N</i> -dimethylanilines by MnO <sub>2</sub> . . . . .	82
4.3.3 Isotope fractionation associated with the enzymatic oxidation by horseradish peroxidase . . . . .	84
4.4 Environmental Significance . . . . .	89
<b>Supporting Information to Chapter 4</b>	<b>90</b>
<b>5 Conclusions and Outlook</b>	<b>121</b>
5.1 Assessing oxidative transformations by CSIA . . . . .	122
5.2 Implications for other reaction pathways based on mechanistic considerations	125
<b>Literature</b>	<b>127</b>
<b>Curriculum Vitae</b>	<b>145</b>





# Summary

The industrial and domestic use of chemicals has led to large emissions of organic micropollutants into the environment. Knowledge of contaminants' degradability in environmental systems is essential for proper risk assessment and further development of adequate remediation strategies for contaminated sites. Transformation processes of contaminants can be identified and quantified by means of compound-specific isotope analysis (CSIA). Depending on the chemical bond(s) that are cleaved or formed during a reaction, the isotopic ratio of the reactant changes systematically as a consequence of kinetic isotope effects (KIE). This change can be indicative for the occurring reaction and the derived apparent KIEs provide important information on the reaction mechanism. Although many emerging micropollutants exhibit reactive N-containing functional groups, only few studies have used CSIA to assess their transformation. This PhD thesis focuses on the transformation of aromatic *N*-alkyl amines, which are widely used in the chemical industry and can also represent the reactive moiety in larger contaminant molecules. Once present in the environment they are subject to oxidative transformation via multiple reaction pathways, which may occur simultaneously.

In this work the C, H, and N isotope fractionation associated with N atom oxidation and oxidative *N*-dealkylation was explored in order to assess the potential for applying CSIA in the environment. We performed batch experiments with substituted primary, secondary, and tertiary aromatic amines and environmental model oxidants, that is MnO<sub>2</sub> and horseradish peroxidase (HRP). We determined the magnitude and variability of <sup>13</sup>C-, <sup>2</sup>H-, and <sup>15</sup>N-AKIEs and investigated the reaction mechanisms and rate-limiting steps with additional support from systematic product analysis and theoretical calculations.

First, an analytical method for accurate and precise  $\delta^{15}\text{N}$  and  $\delta^{13}\text{C}$  measurements of substituted anilines was established and the equilibrium isotope effect (EIE) pertinent to H<sup>+</sup>-exchange at the N atom was evaluated. Using SPME-GC/IRMS we found that deprotonation of the substituted aniline's conjugate acid gives rise to significant <sup>15</sup>N-EIE of 1.02. This implies slightly increased acidity of the <sup>14</sup>N-containing isotopologues by 0.008 pK<sub>a</sub>-units. Accurate  $\delta^{15}\text{N}$  measurements ( $\Delta\delta^{15}\text{N}=0.3\pm0.7\text{‰}$  and  $\Delta\delta^{13}\text{C}=0.9\pm0.7\text{‰}$ ) were

performed for almost all anilines at solution pH-values that exceeded the  $\text{pK}_a$  of the aromatic amines by 2 pH-units. The corresponding aqueous concentrations were 2.1 and 0.56  $\text{mg L}^{-1}$  for the  $\delta^{15}\text{N}$  and  $\delta^{13}\text{C}$  measurements, respectively.

Oxidation of substituted anilines by  $\text{MnO}_2$  was associated with inverse  $^{15}\text{N}$ -AKIE ranging between 0.992 and 0.999 due to formation of partial imine type  $\text{N}=\text{C}$  bond in the anilinium radicals upon initial electron transfer from the N atom. The magnitude of  $^{15}\text{N}$ -AKIE increased with increasing electron donating properties of the *para*-substituent and correlated with radical stability.  $^{15}\text{N}$ -AKIE was identical for *para*- and *ortho*-substituted anilines and for *meta*- and unsubstituted compounds due to preferential radical localization at the *ortho*- and *para*-positions. Owing to the  $^{15}\text{N}$ -EIE associated with N atom deprotonation, the observable N isotope fractionation was strongly pH-dependent and approached the product of  $^{15}\text{N}$ -EIE<sub>N</sub> and  $^{15}\text{N}$ -KIE at pH below the aniline's  $\text{pK}_{\text{BH}^+}$ .

Oxidative transformation of substituted *N*-methyl and *N,N*-dimethylanilines by  $\text{MnO}_2$  and HRP proceeds via initial electron transfer followed by either radical coupling or *N*-dealkylation. Inverse  $^{15}\text{N}$ -AKIEs (up to 0.991) and normal  $^{13}\text{C}$ -, and  $^2\text{H}$ -AKIEs (<1.002 and <1.4, respectively) revealed that compounds substituted with an electron donating substituent ( $-\text{OCH}_3$ ) react preferentially via the N atom oxidation pathway to radical coupling products. Substitution with an electron acceptor ( $-\text{Cl}$ ) led to vanishing or slightly normal  $^{15}\text{N}$ -AKIEs (0.999-1.007) and larger  $^{13}\text{C}$ -, and  $^2\text{H}$ -AKIEs (up to 1.074 and 3.1, respectively) as well as to high amounts of *N*-dealkylated product(s), indicating that *N*-dealkylation is the predominant reaction pathway. Compounds substituted with a weak electron donor ( $-\text{CH}_3$ ) and the unsubstituted ones reacted along both pathways. The second *N*-methyl group favored the occurrence of side chain reactions at the *para*- $\text{CH}_3$ - and  $-\text{OCH}_3$ -substituent, which can complicate the interpretation of isotope fractionation patterns.

This study provides the first systematic evaluation of isotope effects for oxidative transformations of substituted aromatic amines via N atom oxidation and *N*-dealkylation. It illustrates that these reaction pathways lead to very compound-specific and complex C, H, and N isotope fractionation trends. An extrapolation of the obtained data to structurally related compounds is therefore hardly possible. For a more comprehensive evaluation regarding the applicability of CSIA to assess transformation of substituted aromatic amines in the environment, additional reaction pathways of this compound class (that is, photo-oxidation, nucleophilic addition to natural organic matter and enzymatic dioxygenation), should be the subjects of future research.

# Zusammenfassung

Der verbreitete Einsatz von Chemikalien in der Industrie, der Landwirtschaft sowie in Haushalten hat zur Belastung der Umwelt mit organischen Mikroverunreinigungen geführt. Die Risikoabschätzung der Umweltverschmutzung sowie die Entwicklung von entsprechenden Sanierungsstrategien setzen fundierte Kenntnisse über das Verhalten der Schadstoffe in der Umwelt voraus. Die Auswirkungen der organischen Schadstoffe auf das Ökosystem und die Menschen wird weitgehend durch deren Abbau bestimmt. Ein qualitativer und quantitativer Nachweis von solchen Abbauprozessen wird durch die Einzelstoff-Isotopenanalyse (Compound-Specific Isotope Analysis, CSIA) ermöglicht. Die CSIA basiert darauf, dass die Bildung und/oder Spaltung einer chemischen Bindung während einer Reaktion dem kinetischen Isotopeneffekt (KIE) unterliegt. Der KIE führt zu einer systematischen Änderung der stabilen Isotopenzusammensetzung des Reaktanden, die charakteristisch für diese Reaktion ist. Obwohl zahlreiche organische Mikroverunreinigungen reaktive stickstoffhaltige funktionelle Gruppen enthalten, existieren bisher nur sehr wenige Studien, die die relevanten Transformationsprozesse mittels CSIA untersucht haben. Diese Arbeit befasst sich mit der Schadstoffklasse der aromatischen *N*-alkylierten Amine, weil diese in der chemischen Industrie sehr verbreitet eingesetzt werden und weil sie zudem als reaktive Strukturen in grösseren, strukturell komplexeren Schadstoffmolekülen, wie z.B. Antibiotika, vorkommen. Aromatische Amine werden in der Umwelt mittels verschiedener Oxidationsreaktionen zu Transformationsprodukten umgesetzt, wobei viele dieser Prozesse auch gleichzeitig stattfinden können.

In dieser Dissertation wurde die C-, H- und N-Isotopenfraktionierung, die durch Oxidation am N-Atom und durch oxidative *N*-Dealkylierung verursacht wird, untersucht um die Anwendbarkeit von CSIA als Werkzeug zur Identifikation dieser Abbaureaktionen in der Umwelt zu prüfen. Im Rahmen einer Laborstudie wurden Oxidationsexperimente mit primären, sekundären und tertiären aromatischen Aminen sowie zwei umweltrelevanten Modelloxidationsmitteln,  $\text{MnO}_2$  und dem Enzym Horseradish peroxidase (HRP) durchgeführt. Dabei wurden die Grössenordnung und Variabilität der apparenten kinetischen Isotopeneffekte (Apparent Kinetic Isotope Effect, AKIE)  $^{13}\text{C}$ -,  $^2\text{H}$ -, und  $^{15}\text{N}$ -AKIE

bestimmt. Mit Hilfe von systematischen Produktanalysen und theoretischen Berechnungen konnten wichtige Erkenntnisse über die untersuchten Reaktionsmechanismen und die geschwindigkeitsbestimmenden Reaktionsschritte gewonnen werden.

Als erstes wurde eine analytische Methode für die präzise und akurate Messung der N und C Isotopensignaturen von substituierten Anilinen mittels Festphasen-Mikroextraktion gekoppelt mit Gaschromatographie und Massenspektrometrie (solid-phase microextraction coupled with gas chromatography and mass spectrometry, SPME-GC/IRMS) entwickelt. Zudem wurde die Grössenordnung des durch den  $H^+$ -Austausch am N-Atom verursachten Gleichgewichts-Isotopeneffektes (equilibrium isotope effect, EIE) bestimmt. Die N-Isotopenfraktionierung während der Deprotonierung der konjugierten Säure der Aniline war signifikant,  $^{15}N$ -EIE=1.02, was eine um 0.008  $pK_a$ -Einheiten erhöhte Azidität für die  $^{14}N$ -haltigen Isotopologe bedeutet. Für beinahe alle substituierte Aniline konnte eine Genauigkeit von  $\Delta\delta^{15}N=0.3\pm0.7\text{‰}$  und  $\Delta\delta^{13}C=0.9\pm0.7\text{‰}$  erzielt werden, wenn der pH-Wert der umgebenden wässrigen Lösung den  $pK_a$ -Wert der Aniline um 2 pH-Einheiten überschritt und zwar bis zu Konzentrationen von 2.10 und 0.56  $mg\ L^{-1}$  für jeweils  $\delta^{15}N$  und  $\delta^{13}C$ .

Die Oxidation von substituierten Anilinen mit  $MnO_2$  hat inverse  $^{15}N$ -AKIE im Bereich von 0.992-0.999 verursacht. Diese kommen durch die Bildung einer  $C=N$  Bindung mit partiellem Imincharakter in den Aminium-Radikalen zustande, die durch den Elektronentransfer am N-Atom entstehen. Der  $^{15}N$ -AKIE wurde umso inverser, je stärker der Elektronendonator an der *para*-Stellung des aromatischen Rings war und korrelierte somit mit der Radikalstabilität. Die Grössenordnung des  $^{15}N$ -AKIE der *ortho*- und *para*-substituierten Aniline sowie der *meta*- und der unsubstituierten Substanzen war identisch, weil das Radikalelektron bevorzugt an der *para*- und *ortho*-Stellung lokalisiert ist. Aufgrund des durch das Säure-Base Gleichgewicht verursachten  $^{15}N$ -EIE, war die N-Isotopenfraktionierung der Oxidationsreaktion stark pH-abhängig. Bei pH-Werten tiefer als der  $pK_a$  der substituierten Aniline konvergierte der insgesamt beobachtete  $^{15}N$ -AKIE dem Produkt aus  $^{15}N$ -EIE und dem  $^{15}N$ -KIE.

Die Oxidation von substituierten *N*-Methyl- und *N,N*-Dimethylanilinen durch  $MnO_2$  und HRP wird durch einen Elektronentransfer initiiert. Anschliessend findet entweder Radikalkopplung oder *N*-Dealkylierung statt. Inverse  $^{15}N$ -AKIE (bis zu 0.991) in Kombination mit normalen  $^{13}C$ - und  $^2H$ -AKIE (jeweils  $<1.002$  und  $<1.4$ ) deuteten darauf hin, dass Substanzen mit einem Elektronendonator ( $-OCH_3$ ) bevorzugt über Oxidation am N-Atom zu Radikalkopplungsprodukten reagieren. Die Substitution mit einem Elektronenakzeptor ( $-Cl$ ) verursachte verschwindend kleine oder leicht normale  $^{15}N$ -AKIE (0.999

- 1.007) und grössere  $^{13}\text{C}$ - und  $^2\text{H}$ -AKIE (jeweils bis zu 1.074 und 3.1) sowie hohen Umsatz zu *N*-Dealkylierungsprodukten. Dies weist darauf hin, dass die *N*-Dealkylierung im vorliegenden Fall den bevorzugten Reaktionspfad darstellt. Unsubstituierte *N*-Methyl- und *N,N*-Dimethylaniline sowie diejenigen mit einem schwachen Elektronendonator ( $-\text{CH}_3$ ) werden durch beide Reaktionspfade abgebaut. Die zweite Methylgruppe am N-Atom hat Seitenkettenreaktionen am *para*- $\text{CH}_3$  und  $\text{OCH}_3$ -Substituenten begünstigt, was die Interpretation der Isotopendaten erschweren kann.

Diese Arbeit zeigt, dass der oxidative Abbau von aromatischen *N*-alkylierten Aminen durch Oxidation am N-Atom und *N*-Dealkylierung zu sehr substanzspezifischen C, H, und N Isotopenfraktionierungen führt. Aus diesem Grund ist es kaum möglich, aufgrund der hier präsentierten Resultate auf das Fraktionierungsverhalten von strukturell komplexeren Schadstoffmolekülen mit reaktiven aromatischen Amino-Gruppen zu schliessen. In Zukunft sollte eine vollständige Charakterisierung zusätzlicher umweltrelevanter Abbaureaktionen dieser Substanzklasse mittels CSIA erfolgen, wie z.B. photochemischer Abbau, nukleophile Addition an elektrophile Gruppen des natürlichen organischen Materials sowie enzymatische Dioxygenierung.



# Περίληψη

Η ευρεία χρήση χημικών στη βιομηχανία, στις αγροτικές καλλιέργειες και γενικότερα στην παραγωγή καταναλωτικών προϊόντων έχει συντελέσει σε μεγάλο βαθμό στη μόλυνση του περιβάλλοντος. Η αντιμετώπιση των κινδύνων που προκαλούνται από την εκτεταμένη εξάπλωση οργανικών ρυπογόνων χημικών ουσιών απαιτεί εφαρμογή μιας σωστής στρατηγικής, η οποία περιλαμβάνει κατ'αρχήν την αξιολόγηση κινδύνου και στη συνέχεια την ανάπτυξη μεθόδων αποκατάστασης. Για το λόγο αυτόν η κατανόηση των μηχανισμών που ελέγχουν τη συμπεριφορά ρυπογόνων οργανικών χημικών ουσιών σε διάφορα περιβαλλοντικά συστήματα είναι θεμελιώδους σημασίας. Ένας εύστοχος τρόπος μελέτης του μηχανισμού που διέπει τις αντιδράσεις αποδόμησης αυτών των ουσιών είναι η διερεύνηση ισοτοπικών λόγων επιλεγμένων στοιχείων των ουσιών που αποδομούνται.

Στα πλαίσια της Διατριβής αυτής, ερευνήθηκε η ομάδα των αρωματικών αμινών. Οι ανιλίνες (πρωτογενείς αρωματικές αμίνες) βρίσκουν ευρεία εφαρμογή στη χημική βιομηχανία σα διαλύτες, καθώς και σαν πρόδρομες ενώσεις για την παραγωγή βαφών, φαρμακευτικών προϊόντων και φυτοφαρμάκων. Μέσω βιομηχανικών αποβλήτων, οικιακών λυμάτων, καθώς και σαν προϊόντα αναγωγής άλλων χημικών ουσιών, όπως νιτροαρωματικών, καταλήγουν στο περιβάλλον, οπότε και οξειδώνονται με την παρουσία οξειδωτικών ουσιών. Στην εργασία αυτή μελετήθηκε πειραματικά η μεταβολή του ισοτοπικού λόγου των στοιχείων C, H και N κατά τη διάρκεια της οξείδωσης των αρωματικών αμινών με διάφορους υποκαταστάτες στο μορίό τους. Σαν μέσα οξείδωσης επιλέχθηκαν το  $\text{MnO}_2$  και το ένζυμο HRP (horseradish peroxidase), τα οποία αποτελούν κοινά οξειδωτικά στα εδάφη. Ο ισοτοπικός λόγος των στοιχείων των αρωματικών αμινών που συμμετέχουν σε αντιδράσεις αποδόμησης τους μεταβάλλεται με τρόπο χαρακτηριστικό για κάθε συγκεκριμένη αντίδραση. Αυτό οφείλεται στην ιδιότητα της κινητικής των ισοτόπων (kinetic isotope effect, KIE), σύμφωνα με την οποία οι αρωματικές αμίνες που περιέχουν το βαρύ ισότοπο αντιδρούν με διαφορετικούς ρυθμούς από αυτές που περιέχουν το ελαφρύ.

Ο προσδιορισμός της πορείας της ισοτοπικής κλασμάτωσης των στοιχείων C, H και N στις αρωματικές αμίνες κατά τη διάρκεια της οξείδωσής τους με  $\text{MnO}_2$  και HRP επιτρέπει να διαπιστωθεί εάν οι αντιδράσεις αυτές οδηγούν σε χαρακτηριστικές και μετρήσιμες μεταβολές

των ισοτοπικών λόγων. Σε μία τέτοια περίπτωση, είναι δυνατός ο ακριβής προσδιορισμός των επί μέρους αντιδράσεων που οδήγησαν στην αποδόμησή τους. Επίσης, μετρώντας τον εκάστοτε ισοτοπικό λόγο της αρωματικής αμίνης μπορεί να διαπιστωθεί σε ποιο στάδιο βρίσκεται η αποδόμησή της και επομένως σε τι ποσοστό έχει προχωρήσει η αντίδραση.

Για τα εργαστηριακά πειράματα που πραγματοποιήθηκαν ακολουθήθηκε η εξής μεθοδολογία: έγινε αναλυτικός προσδιορισμός των ισοτοπικών λόγων C, H και N σε πρωτογενείς, δευτερογενείς και τριτογενείς αρωματικές αμίνες με υποκαταστάτες και υπολογίστηκαν οι φαινόμενες κινητικές επιδράσεις (apparent kinetic isotope effect, AKIE). Επίσης, καθορίστηκαν οι παράγοντες που επηρεάζουν το μέγεθος και την ποικιλία των AKIE, όπως το pH και η χημική δομή (ο συντακτικός τύπος) των ανιλινών. Τέλος, προσδιορίστηκε η φύση των προϊόντων των οξειδωτικών αντιδράσεων και έγινε μια από σειρά θεωρητικούς υπολογισμούς.

Ένα σημαντικό μέρος αυτής της μελέτης αφιερώθηκε στην ανάπτυξη μιας νέας αναλυτικής μεθόδου αέριας χρωματογραφίας φασματογράφου μάζας (GC/IRMS), με σκοπό την ανάλυση των ισοτοπικών λόγων των C, H και N, με ικανοποιητική επαναληψιμότητα και ακρίβεια ταυτόχρονα. Επίσης έγινε αξιολόγηση των επιδράσεων ισοτοπικής ισορροπίας (equilibrium isotope effect, EIE) που σχετίζονται με την ανταλλαγή πρωτονίων στο άτομο του N και η τιμή που προέκυψε για το  $^{15}\text{N}$ -EIE ήταν 1.02. Από αυτό συμπεραίνεται ότι τα συζυγή οξέα των ανιλινών με  $^{14}\text{N}$  στο μόριό τους είναι κατά 0.008 οξύτερα από αυτά με  $^{15}\text{N}$ . Η ακρίβεια των μετρήσεων των ισοτοπικών λόγων ήταν  $\Delta\delta^{15}\text{N}=0.3\pm0.7$  και  $\Delta\delta^{13}\text{C}=0.9\pm0.7$  για διαλύματα με τιμές  $\text{pH}>\text{pK}_a+2$ . Η συγκέντρωση των ανιλινών εν διαλύσει βρέθηκε ότι ήταν 2.1mg/L για το N και 0.56mg/L για τον C.

Εφαρμόζοντας την πιο πάνω αναλυτική μέθοδο, προσδιορίστηκαν οι τιμές των AKIE που σχετίζονται με την οξείδωση των ανιλινών με  $\text{MnO}_2$  και βρέθηκε ότι κυμαίνονται μεταξύ 0.992 και 0.999. Από αυτές τις τιμές προκύπτει ότι υπάρχει αντίστροφο  $^{15}\text{N}$ -AKIE, πράγμα που οφείλεται στο σχηματισμό αρωματικών ιμινών, σαν αποτέλεσμα οξείδωσης μέσω ενός ηλεκτρονίου του N. Η τιμή των  $^{15}\text{N}$ -AKIE ήταν μεγαλύτερη για υποκαταστάτες ανιλινών που είναι ισχυρότεροι δότες ηλεκτρονίων, καθώς επηρεάζουν τη σταθερότητα των ριζών που σχηματίζονται με την απώλεια ενός ηλεκτρονίου του N. Λόγω της κανονικής  $^{15}\text{N}$ -EIE που συνδέεται με την απώλεια πρωτονίου από τα συζυγή οξέα των ανιλινών, βρέθηκε ότι η ισοτοπική κλασμάτωση του N εξαρτάται από το pH.

Η οξείδωση των δευτερογενών και τριτογενών αρωματικών αμινών με  $\text{MnO}_2$  και HRP πραγματοποιείται με τη μεταφορά ενός ηλεκτρονίου από το άτομο του N και συνεχίζεται είτε με σύζευξη των ριζών είτε με την απώλεια ενός μεθυλίου από το δεσμό με το N. Οι τιμές αντίστροφων  $^{15}\text{N}$ -AKIE (έως και 0.991) και οι τιμές κανονικών  $^{13}\text{C}$ - και  $^2\text{H}$ -AKIE που προέκυψαν ( $<1.002$  και  $<1.4$ , αντίστοιχα), οδηγούν στο συμπέρασμα ότι οι



ανιλίνες με ισχυρούς δότες ηλεκτρονίων αντιδρούν κατά προτίμηση μέσω της μεταφοράς ενός ηλεκτρονίου από το άτομο του N και σχηματίζουν διμερή προϊόντα. Οι τιμές των AKIE που συνδέονται με την οξείδωση των ανιλινών με ισχυρούς αποδέκτες ηλεκτρονίων ήταν είτε πολύ μικρές είτε ελαφρώς κανονικές για το N (0.999 - 1.007) και υψηλές για τον C (έως και 1.074) και το H (3.1). Επιπλέον, ανιχνεύθηκε υψηλό ποσοστό προϊόντων που είχαν ένα μεθύλιο λιγότερο από την αντιδρώσα ουσία. Από αυτό συμπεραίνεται ότι για αυτές τις ανιλίνες, η απώλεια ενός μεθυλίου από το δεσμό με το N ήταν ο επικρατέστερος μηχανισμός αντίδρασης. Ανιλίνες χωρίς υποκαταστάτες, καθώς και ανιλίνες με αδύναμους δότες ηλεκτρονίων αποδομήθηκαν μέσω και των δύο αντιδράσεων. Επίσης, διαπιστώθηκε επιπλέον οξείδωση των υποκαστατών  $-CH_3$  και  $-OCH_3$ , επηρεάζοντας τις αντίστοιχες τιμές AKIE, κάτι που κάνει πιο πολύπλοκη την ερμηνεία των ισοτοπικών δεδομένων.

Λαμβάνοντας υπόψη τα αποτελέσματα της Διατριβής αυτής προκύπτει το γενικότερο συμπέρασμα ότι η αποδόμηση ανιλινών μέσω οξειδωτικών αντιδράσεων οδηγεί σε συγκεκριμένες πορείες κλασμάτωσης των ισοτόπων C, H και N. Οι πορείες αυτές διαφοροποιούνται ανάλογα με τη χημική ένωση και τη δομή της. Είναι επομένως εξαιρετικά δύσκολο να προεκτείνει κανείς τα αποτελέσματα αυτής της εργασίας σε άλλες χημικές ενώσεις, οι οποίες περιέχουν αρωματικές αμίνες. Σε ένα επόμενο στάδιο θα ήταν σκόπιμο να διερευνηθούν και άλλοι πιθανοί μηχανισμοί αποδόμησης των ανιλινών, όπως φωτοχημικές αντιδράσεις, ενζυματική αποοξυγόνωση ή πυρινόφιλη προσθήκη.



# Chapter 1

## Introduction

## 1.1 Assessing transformation processes of organic micropollutants in the environment

Chemical pollution represents one of the major environmental problems worldwide. A large variety of organic compounds used as, for example, industrial chemicals, biocides, pharmaceuticals, or personal-care products enter the environment through municipal and industrial wastewater effluents, spills, landfills or runoff from agricultural areas.<sup>123,124,127,128</sup> Depending on the pollution source and the compound's behavior in the environment, organic micropollutants can be found in surface waters, aquifers, soils, sediments and the atmosphere. Once present in the environment they can have adverse effects on the aquatic and terrestrial life and affect human health via the food chain or contamination of drinking water resources. Since many of those chemicals are already of concern at very low concentrations, assessing the fate of organic micropollutants in the environment is crucial for evaluating the risks of contamination.<sup>12,126</sup>

Risk assessment of chemicals includes an assessment of the compound's exposure in the environment, and its effects to organisms. Exposure assessment requires the availability of input data as well as knowledge of the pollutant's behavior in environmental systems, including transport (diffusion, advection), partitioning between environmental compartments and transformation processes. Transformations of organic micropollutants in natural and engineered systems can occur at different rates, via different reaction mechanisms and can lead to the formation of a variety of transformation products. Transformation products can exhibit similar or different modes of toxic action as the parent compound and contribute to the overall mixture toxicity.<sup>12,32,103</sup> Identifying degradation processes of contaminants in the environment is not a trivial task because besides (bio)transformation, physical processes such as sorption, volatilization, as well as transport by diffusion and advection can lead to concentration changes. Concentration measurements for assessment of mass balances can be analytically challenging. Detection and quantification of reactants and transformation products in complex environmental matrices require appropriate techniques including several extraction and enrichment steps.<sup>70,128</sup> Moreover, most transformation products have not yet been identified whereas those susceptible to rapid degradation may not be detectable.<sup>32</sup> Therefore, unambiguous determination of the underlying processes by means of concentration measurements can be difficult.

One tool for assessing the transformation of organic contaminants in the environment is compound-specific isotope analysis (CSIA). By analyzing the stable isotope composition of the reactant, the source of contamination can be allocated and transformation

processes can be identified and quantified, even if contaminants are degraded via competing reactions.<sup>28,29,58,125</sup> Moreover, CSIA may provide important information on the underlying reaction mechanism. For a given compound the relative abundance of the heavy  $^h\text{E}$  and light  $^l\text{E}$  isotopes of element E is commonly expressed by the isotopic signature  $\delta^h\text{E}$  and reported as difference in ‰ relative to an international reference standard:<sup>29,130</sup>

$$\delta^h\text{E} = \frac{(^h\text{E}/^l\text{E})_{\text{sample}}}{(^h\text{E}/^l\text{E})_{\text{reference}}} - 1 \quad (1.1)$$

The most established analytical methods for measuring the isotopic composition of organic contaminants at natural abundance levels in environmental samples with high precision and accuracy are gas and liquid chromatography coupled to isotope ratio mass spectrometry (GC/ and LC/IRMS, respectively).<sup>28,53</sup> Each transformation pathway leads to a characteristic change in the compound’s isotopic signature, which can be indicative for the relevant degradation process. This is because bond-cleavage or bond-formation during the rate-determining step of a reaction are subject to a kinetic or equilibrium isotope effect (KIE or EIE, respectively). Kinetic isotope effects reflect the energy differences between the reactant isotopologues carrying the light and heavy isotope at the reactive site in the ground and the transition state. This gives rise to different activation energies and the isotopologues react therefore with different rate constants  $^lk$  and  $^hk$ , respectively:<sup>28,29,58</sup>

$$\text{KIE}_\text{E} = \frac{^lk}{^hk} \quad (1.2)$$

Equilibrium isotope effects (EIE) are related to bonding changes between reactant and product and are defined as the ratio of the KIEs associated with the forward and backward reaction.<sup>58</sup> Changes in isotopic signatures due to an EIE are characteristic for the underlying equilibrium reaction.

Because KIEs are related to the transition state structure and changes of the bonding environment of the reactive atoms, they are indicative of the type of occurring reaction and may thus provide insight into the reaction mechanism. To infer the origin and determine the magnitude of the KIE the change in the reactant’s isotopic signature  $\delta^h\text{E}$  compared to the initial one  $\delta^h\text{E}_0$  is measured in the remaining fraction  $C/C_0$  of the reactant over time or distance from the pollution source. The enrichment of the slower reacting isotopologues, caused by the occurring reaction, can be determined using the Rayleigh equation:<sup>29,58</sup>

$$\frac{\delta^h E + 1}{\delta^h E_0 + 1} = \left( \frac{C}{C_0} \right)^{\epsilon_{E,\text{bulk}}} \quad (1.3)$$

Bulk isotope enrichment factors  $\epsilon_{E,\text{bulk}}$  reflect the average change in isotopic composition of the entire molecule. Identification of transformation processes on the basis of  $\epsilon_{E,\text{bulk}}$  is feasible if they are converted to position specific enrichment factors and bond-specific apparent kinetic isotope effects  $\text{AKIE}_E$ s. Based on an assumption regarding the reaction mechanism and kinetics of the elementary reactions,  $\text{AKIE}_E$ s can be calculated according to Equation 1.4 by taking into account the number  $n$  of total isotopic atoms, i.e. including those at nonreactive positions, the number  $x$  of atoms at the reactive site, and the number  $z$  of isotopic atoms that compete at the reactive position:<sup>58</sup>

$$\text{AKIE}_E = \frac{1}{1 + (n/x) \cdot z \cdot \epsilon_{E,\text{bulk}}} \quad (1.4)$$

By comparing the calculated  $\text{AKIE}_E$  with expected KIEs of reference reactions the hypothesized degradation mechanism can be confirmed or excluded. Due to the wide variety of organic micropollutants and possible reactions in the environment KIE reference data are scarce. Therefore, the interest for elucidating reaction mechanisms is increasing and numerous studies have focused on relevant transformation processes of organic micropollutants.<sup>10,30,49,50,74,113,165</sup> Once the mechanisms are identified, the extent of transformation can also be quantified using Equation 1.3.

Additional evidence for identifying the underlying reaction even if the intrinsic KIE is masked due to rate-limiting processes other than degradation and for distinguishing between competing pathways is provided by multielement isotope analysis. The simultaneous change of isotopic signatures for the elements at the reactive site is evaluated by plotting  $\delta^h E_1$  vs.  $\delta^h E_2$ , where the slope is approximately equal to the ratio of the enrichment factors (Equation 1.5):

$$\frac{\delta^h E_1}{\delta^h E_2} \approx \frac{\epsilon_{E_1,\text{bulk}}}{\epsilon_{E_2,\text{bulk}}} \quad (1.5)$$

The slope is diagnostic for the reaction in question, since it reflects the change in isotope ratios for the elements involved in bond-cleavage or formation. Relative changes in isotopic signatures  $\delta^h E_1/\delta^h E_2$  remain the same as under non-masking conditions.<sup>28,132,165</sup> Comparison of isotope effects and reaction mechanisms between different compounds is only possible with derived AKIEs.

Physical processes, i.e. transport, phase transfer, dilution, can lead to small changes in the contaminant's isotopic composition under certain conditions. In contaminant plumes at non-steady state and in the unsaturated zone small isotope fractionations due to diffusion and sorption have been observed and need to be considered when estimating degradation.<sup>11,28,73,77</sup>

## 1.2 Transformation processes of N-containing organic micropollutants

To date most applications of CSIA focused on the isotope fractionation of the elements C and H and included transformation of chlorinated solvents,<sup>2,10,56</sup> BTEX compounds,<sup>61,86,142</sup> and MTBE.<sup>62,74</sup> Because of the highly diverse molecular structures of biologically active micropollutants, which exhibit a wide range of reactive functional groups containing heteroatoms, the interest to apply CSIA to other elements increased.<sup>53</sup> An important class of priority contaminants consists of compounds exhibiting N-containing functional groups, which often represent the site of initial attack during abiotic and enzymatic reactions. N isotope analysis has been much less frequently applied compared to C isotope analysis since it is associated with certain analytical limitations. The presently established method for measuring N isotope signatures of organic contaminants is GC/IRMS, i.e. isotope analysis is restricted to volatile compounds.<sup>53</sup> The major problem for environmental applications is the high detection limits, which is related to the low abundance of <sup>15</sup>N isotopes (0.37%), the target analyte gas N<sub>2</sub>, and instrumental procedures.<sup>6,31,130</sup> Higher sensitivity can be achieved by using efficient pre-concentration steps, e.g. solid-phase microextraction (SPME) or purge and trap.

Despite the analytical challenges, precise and accurate  $\delta^{15}\text{N}$  values have been measured for nitroaromatic compounds (NACs)<sup>6</sup>, and triazine and phenylurea herbicides.<sup>94,111</sup> Consequently, CSIA has been successfully applied to study relevant transformation processes of these typical N-containing micropollutants, i.e. abiotic reduction of NACs,<sup>48,49</sup> photochemical and microbial degradation of atrazine<sup>50,95</sup> and abiotic and microbial transformation of isoproturon.<sup>112,113</sup> Furthermore, N isotope fractionation associated with biodegradation of RDX was measured using instrumentation other than GC/IRMS.<sup>7</sup> These studies revealed variable <sup>15</sup>N fractionation and showed that interpreting measured bulk enrichment factors  $\epsilon_{\text{N,bulk}}$  and deriving AKIE<sub>N</sub>s can be very difficult due to the complexity of the molecular mechanisms that govern the transformation processes of these

compounds. Therefore, additional knowledge is required to understand the reactions of N-containing functional groups in environmentally relevant systems on a molecular level, which is a prerequisite for applying CSIA.

This thesis focused on the isotopic investigation of oxidative transformation(s) of the aromatic (*N*-alkyl) amino functional group. Aromatic amines are of environmental concern because they are manufactured on a large scale due to their extensive use in chemical industry as precursors for the synthesis of dyes, polyurethanes, rubber products, and drugs. They are toxic to the ecosystem and carcinogenic and mutagenic to humans.<sup>72,122</sup> They can enter the environment either directly, i.e. through spills or waste water effluents, or indirectly as transformation products of the reduction of nitroaromatic explosives,<sup>55,71</sup> pesticides,<sup>5</sup> and azo-dyes.<sup>154</sup> Furthermore, the aromatic amino functional group is contained as a substructure in larger contaminant molecules such as antibacterial agents and agrochemicals, where they often represent the reactive moieties during oxidative transformations.<sup>8,82,159</sup>

Aromatic (*N*-alkyl) amines can react along multiple pathways in the environment and can lead to the formation of a wide variety of transformation products (Figure 1.1). N atom oxidation and oxidative *N*-dealkylation can be catalyzed at mineral surfaces or by enzymes and can lead to the formation of radical coupling and *N*-dealkylated product(s), respectively.<sup>46,72,78,159</sup> Indirect photolysis by transient oxidants, such as  $\text{CO}_3^{\bullet-}$ -radicals, excited triplet states of dissolved organic material (DOM),  $\text{OH}^{\bullet}$  radicals, or singlet oxygen  $^1\text{O}_2$ , leads to oxidized transformation products but their structure is not always clear.<sup>17</sup> During direct photolysis unsubstituted and/or hydroxylated aromatic amines as well as coupling products can be formed.<sup>43</sup> Furthermore, aromatic (*N*-alkyl) amines can be transformed via enzymatic dioxygenation of the aromatic ring to catechols,<sup>132</sup> and via 1,2- and 1,4-nucleophilic addition of the amino group to electrophilic quinone moieties of natural organic matter (NOM) to form anilinoquinones.<sup>19,155</sup> Because degradation along these pathways can take place simultaneously and the reaction products are partly unknown or difficult to analyze, identification of the relevant transformation process remains a challenging task. Although oxidative transformation of aromatic (*N*-alkyl) amines is of great importance during degradation of a variety of contaminants, proper analytical methods for N isotope analysis are not yet available, isotope effects of the oxidation reactions remain largely unknown and the potential for using CSIA to assess their degradation has not yet been evaluated.

The present work focused on the mineral and enzyme catalyzed N-atom oxidation and *N*-dealkylation of substituted *N*-alkyl aromatic amines (Figure 1.1). Previous work



on oxidation of substituted anilines by manganese oxide, an important heterogeneous oxidant in soils, revealed that the reaction proceeds via initial electron transfer from the lone pair of the N atom followed by formation of arylamino radical species.<sup>72,78,119</sup> Radical coupling leads to the formation of dimer or trimer products, as shown in Figure 1.1. The correlation of initial reaction rates with the Hammett constants  $\sigma$  of aromatic substituents and half-wave potentials  $E_{1/2}$  of the anilines suggests that the initial electron transfer also represents the rate-determining step of the reaction.

Aromatic *N*-alkyl amines can be subject to oxidative *N*-dealkylation catalyzed by heme enzymes such as horseradish peroxidase (HRP) and cytochrome P450.<sup>46,147</sup> Most studies agree that oxidation by HRP proceeds via initial electron transfer, whereas cytochrome P450 enzymes react via hydrogen atom abstraction.<sup>45,67,107</sup> Subsequent electron and proton transfer(s) lead to the formation of the *N*-dealkylated product and formaldehyde. Determination of  $^2\text{H}$  kinetic isotope effects of selected  $^2\text{H}$ -labelled substituted *N,N*-dimethylanilines revealed that substitution of the aromatic ring can lead to shifts of the rate-determining step of the reaction (electron vs. proton transfer).<sup>24,46,98</sup>

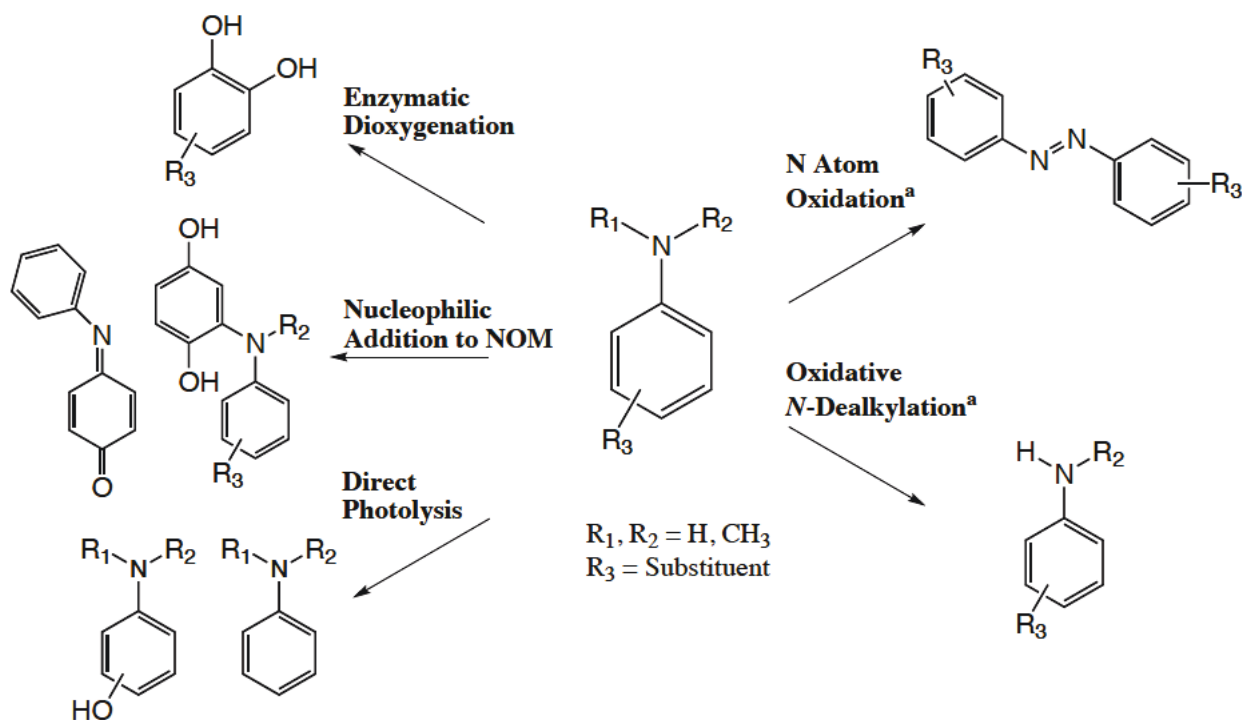


Figure 1.1: Possible degradation pathways of aromatic *N*-methyl amines in the environment and characteristic reaction products. <sup>a)</sup>Enzyme- and mineral-catalyzed reactions as well as photo-oxidation can proceed via N atom oxidation and oxidative *N*-dealkylation.

## 1.3 Objectives and approach of this thesis

Applying CSIA to investigate oxidative transformation processes of aromatic *N*-alkyl amines can provide important information about the elementary steps and contribute to the understanding of these complex reactions. Since the amino moiety (N-R<sub>1</sub>R<sub>2</sub>, Figure 1.1) is directly involved in the oxidation reactions and the bonding environment of the N, C, and H atoms is directly affected, changes in  $\delta^{15}\text{N}$ ,  $\delta^{13}\text{C}$ , and  $\delta^2\text{H}$  signatures could be measurable by CSIA. Earlier studies of reduction of nitroaromatic radical anions showed that small bonding changes induced by electron transfer can also cause measurable  $^{15}\text{N}$ -fractionation.<sup>42,49</sup>

Therefore, the goals of the present work were the following:

1. to develop an analytical method for the precise and accurate determination of the isotope composition of substituted aromatic amines, including high extraction efficiencies and low detection limits
2. to use CSIA to determine C, H, and N isotope fractionation trends during oxidative transformations of substituted *N*-alkyl aromatic amines in the environment and to assess the potential of CSIA for distinguishing between those sometimes competing reactions
3. to elucidate the reaction mechanism by determining the associated apparent kinetic isotope effects,  $\text{AKIE}_\text{E}$ , and the factors that influence their magnitude and variability, i.e. molecular structure and experimental conditions

To this end, laboratory batch experiments were performed with primary, secondary, and tertiary aromatic amines carrying substituents of variable electron donating properties (-Cl, -H, -CH<sub>3</sub>, -OCH<sub>3</sub>). Two oxidative transformation pathways, i.e. N atom oxidation and oxidative *N*-dealkylation, were investigated using the mineral MnO<sub>2</sub> and the enzyme horseradish peroxidase (HRP), which have been previously used to mimic the corresponding reactions in soils and aquatic environments.<sup>72,131,133,147</sup> Experimental conditions, i.e. pH, were varied in order to examine the influence of substituted aniline speciation (typical  $pK_\text{a}$ -values between 2.5 and 7),<sup>84,126</sup> on the isotope fractionation. Additional information was obtained by qualitative and quantitative product analysis and the interpretation of the results was supported by independent reference experiments and theoretical calculations.

The work presented in Chapter 2 describes the analytical method developed for precise and accurate determination of N and C isotope signatures of substituted anilines by SPME-GC/IRMS. This method was used to determine the magnitude of equilibrium isotope effects (EIE) associated with aromatic amine protonation.

Chapter 3 focuses on the N atom oxidation pathway and deals with the N isotope fractionation associated with the oxidation of substituted primary aromatic amines by  $\text{MnO}_2$ . Insights into the reaction mechanisms are gained by investigating the influence of aromatic substituents on  $\text{AKIE}_{\text{N}}$ , reference experiments with other oxidizing agents and computations of  $^{15}\text{N}$ -KIEs. Furthermore, the influence of aniline acid/base speciation on the observable  $^{15}\text{N}$  fractionation is evaluated.

Chapter 4 deals with the  $\text{MnO}_2$ - and HRP-catalyzed transformation of substituted secondary and tertiary aromatic amines. Multielement (C, H, and N) isotope fractionation trends were examined and apparent  $^{13}\text{C}$ -,  $^2\text{H}$ -, and  $^{15}\text{N}$ -KIEs were studied systematically to obtain evidence for the reactions occurring simultaneously along the N atom oxidation and the oxidative *N*-dealkylation pathway (Figure 1.1).

The general conclusions of the thesis as well as open questions for future research work are discussed in chapter 5.



## Chapter 2

# pH-Dependent Equilibrium Isotope Fractionation Associated with the Compound Specific Nitrogen and Carbon Isotope Analysis of Substituted Anilines by SPME-GC/IRMS

M. Skarpeli-Liati, W. A. Arnold, A. Turgeon, C. J. Cramer, and T. B. Hofstetter.  
pH-dependent equilibrium isotope fractionation associated with compound-specific nitrogen and carbon isotope analysis by SPME-GC/IRMS. *Anal. Chem.*, 83(5):1641-1648, 2011

## Abstract

Solid-phase microextraction (SPME) coupled to gas chromatography/isotope ratio mass spectrometry (GC/IRMS) was used to elucidate the effects of N-atom protonation on the analysis of N and C isotope signatures of selected aromatic amines. Precise and accurate isotope ratios were measured using polydimethylsiloxane/divinylbenzene (PDMS/DVB) as the SPME fiber material at solution pH-values that exceeded the  $pK_a$  of the substituted aniline's conjugate acid by two pH-units. Deviations of  $\delta^{15}\text{N}$  and  $\delta^{13}\text{C}$ -values from reference measurements by elemental analyzer IRMS were small ( $<0.9\text{‰}$ ) and within the typical uncertainties of isotope ratio measurements by SPME-GC/IRMS. Under these conditions, the detection limits for accurate isotope ratio measurements were between 0.64 and 2.1  $\text{mg L}^{-1}$  for  $\delta^{15}\text{N}$  and between 0.13 and 0.54  $\text{mg L}^{-1}$  for  $\delta^{13}\text{C}$ , respectively. Substantial inverse N isotope fractionation was observed by SPME-GC/IRMS as the fraction of protonated species increased with decreasing pH leading to deviations of  $-20\text{‰}$  while the corresponding  $\delta^{13}\text{C}$ -values were largely invariant. From isotope ratio analysis at different solution pHs and theoretical calculations by density functional theory, we derived equilibrium isotope effects, EIEs, pertinent to aromatic amine protonation of 0.980 and 1.001 for N and C, respectively, which were very similar for all compounds investigated. Our work shows that N-atom protonation can compromise accurate compound-specific N isotope analysis of aromatic amines.

## 2.1 Introduction

Assessing transformation processes of organic micropollutants is crucial for addressing the risks of soil and water contamination. Compound-specific isotope analysis (CSIA) offers a complementary approach for identifying contaminant sources and degradation pathways, as well as for quantifying the extent of a transformation reaction even if several processes take place simultaneously. Because CSIA reveals the reactive position within an organic compound via detection of changes in isotopic composition, stable isotope ratio measurements also provide crucial information about the underlying reaction mechanism.<sup>53</sup> While CSIA is widely applied for the investigation of ground-water contaminants such as chlorinated solvents (polychlorinated alkenes<sup>2,23,63,149</sup>) and fuel components (methyl-tert butyl ether,<sup>62,74,165</sup> benzene,<sup>35</sup> toluene<sup>142,143,150</sup>), combined multielement isotope-fractionation analysis involving the elements C, H, and N is emerging for the transformation assessment of agrochemicals, explosives, and other priority

pollutants.<sup>6,7,94</sup> In fact, micropollutants exhibiting N-containing functional groups are the most promising target molecules for CSIA, because the presence of N functional groups is key for many transformation processes including reductions, oxidations, substitutions, and eliminations.<sup>126</sup> Despite the importance of these reaction pathways, only few N-containing organic micropollutants are amenable to CSIA.

To date, nitrogen isotope fractionation has been successfully measured by GC/IRMS of amino acids,<sup>52,85,138</sup> selected N-containing herbicides,<sup>50,94,111</sup> and nitroaromatic compounds.<sup>6,49,57,142</sup> To expand the applicability of CSIA, this study targets the N isotope analysis of substituted aromatic amines by GC/IRMS. Substituted anilines represent a class of toxic and mutagenic environmental pollutants<sup>36</sup> and they have also served as model compounds for studying the transformation of emerging contaminants such as sulfonamide antibiotics.<sup>159</sup> In contaminated environments, abiotic as well as microbial oxidation and addition reactions occur either directly at the nitrogen atom of the primary amino group<sup>78,108,133</sup> or via oxidation at the aromatic ring.<sup>132</sup> The availability of analytical methods for the precise and accurate measurement of N and C isotope ratios is therefore essential for assessing degradation pathways of substituted anilines in the environment.

Current approaches to isotope ratio measurements of substituted anilines in aqueous solutions by GC/IRMS coupled to solid phase microextraction (SPME), however, showed poor accuracy, that is, deviations from the correct N isotope signatures were above 2‰.<sup>6</sup> Moreover, the consequences of aromatic amine protonation on the sensitivity and accuracy of CSIA is unexplored. Protonation of the anilines at pH values <7 deteriorates extraction efficiencies of the analytes from the aqueous solution to the SPME-fiber, because only neutral species can be expected to adsorb to the nonpolar fiber coating and thus be measured by CSIA. Given that environmentally relevant pH-ranges coincide with the pK<sub>a</sub>-values of many protonated aromatic amines (typical pK<sub>a</sub> between 2.5 and 7,<sup>84,126</sup>) and that N atom protonation might be key for understanding the isotope fractionation of N-containing micropollutants,<sup>95,112</sup> the impact of equilibrium isotope fractionation on the isotope ratio analysis of aromatic amines requires closer examination.

It was the goal of this study to investigate how aromatic amino group protonation affects the sensitivity and accuracy of N and C isotope signatures,  $\delta^{15}\text{N}$  and  $\delta^{13}\text{C}$ , of substituted primary aromatic amines while measured by SPME-GC/IRMS and whether significant N and C equilibrium isotope effects (EIE) are associated with proton exchange reactions. To this end, we examined the accuracy and precision of  $\delta^{15}\text{N}$  and  $\delta^{13}\text{C}$ -values of a series of substituted anilines in aqueous samples in the pH-range 2.0-7.0 in the presence

of various buffers. The compounds were chosen so that their  $pK_a$ -values (2.5-5.1) enabled us to study the effect of protonation on SPME-GC/IRMS under the chosen experimental conditions. Equilibrium isotope effects associated with aromatic amine protonation were determined experimentally and compared to independent estimates obtained from density functional theory calculations.

## 2.2 Experimental Section

### Safety Considerations

Substituted anilines are toxic and potentially carcinogenic. When dealing with anilines, wear suitable clothing, gloves, and work in a well-ventilated fume hood.

#### 2.2.1 Reagents and materials

All chemicals in this study were used as received. The substituted anilines examined included aniline ( $\geq 99.5\%$ , Fluka), 2-methylaniline ( $\geq 99.5\%$ , Merck), 4-methylaniline ( $\geq 99\%$ , Merck), 2-chloroaniline ( $\geq 99.5\%$ , Aldrich), and 4-chloroaniline ( $\geq 99\%$ , Fluka). Buffers used were sodium acetate trihydrate ( $\text{NaC}_2\text{H}_3\text{O}_2 \cdot 3\text{H}_2\text{O}$ , puriss, Riedel-de Haën), potassium phosphate dibasic ( $\text{K}_2\text{HPO}_4$ , puriss, Riedel-de Haën), sodium citrate tribasic dihydrate ( $\text{Na}_3\text{C}_6\text{H}_5\text{O}_7 \cdot 2\text{H}_2\text{O}$ ,  $\geq 99\%$ , Fluka) and 2-morpholinoethanesulfonic acid monohydrate (MES,  $\text{C}_6\text{H}_{13}\text{NO}_4\text{S} \cdot \text{H}_2\text{O}$ ,  $\geq 99\%$ , Fluka). All buffer solutions were prepared in deionized water ( $18.2 \text{ M}\Omega\cdot\text{cm}$ , NANO-pure) and solution pH-values were adjusted with hydrochloric acid (Sigma Aldrich) and sodium hydroxide solution (Fluka). Solvents used were methanol ( $>99.9\%$ , Scharlau, Spain) and ethyl acetate ( $>99.8\%$ , Riedel-de Haën). High purity Ar was used for deoxygenation of water and methanol and helium, nitrogen, and carbon dioxide were used for GC/MS and GC/IRMS measurements (all  $\geq 99.999\%$ , Carbagas).

#### 2.2.2 Instrumentation

Prior to nitrogen and carbon isotope analysis, extraction efficiencies of the substituted anilines from the buffered aqueous solutions to the SPME-fibers were evaluated by means of GC/MS analysis. Instrumentation and procedures for chromatographic separation used for GC/MS analysis were similar to that of previous studies.<sup>6</sup> A GC (Trace GC Ultra, Thermo Electron Corp.) was combined with a quadrupole MS (Trace DSQ ESI 250,



Thermo Electron Corp.) and a CombiPAL autosampler (CTC) and equipped with a cold on-column and a split/splitless injector with a Merlin Microseal (Merlin Instrument Co.). The isotope analysis was carried out using a TraceGC (Thermo Electron Corp.) coupled to an isotope ratio mass spectrometer (IRMS; Delta V PLUS, Thermo Electron Corp.) via a combustion interface (GC Combustion III).<sup>164</sup> Helium carrier gas was used at constant pressure of 100 kPa. For chromatographic separation, 1 m of a deactivated guard column (530  $\mu\text{m}$  i.d., BGB, Boeckten, Switzerland) and a 30 m  $\times$  0.32 mm fused-silica column (Zebron, ZB-5-ms, 0.25  $\mu\text{m}$ , Phenomenex) were used. The applied temperature program was 1 min at 50  $^{\circ}\text{C}$ , followed by a 10  $^{\circ}\text{C}/\text{min}$  ramp to 250  $^{\circ}\text{C}$  and 5 min at 250  $^{\circ}\text{C}$ .

For the  $\delta^{13}\text{C}$  measurements the NiO/CuO/Pt wires of the combustion unit were oxidized with  $\text{O}_2$  during 12 h prior to use at 940  $^{\circ}\text{C}$ . The N isotope signatures were measured with the same oxidation reactor but without preoxidation at 980  $^{\circ}\text{C}$ . The temperature of the reduction reactor was 650  $^{\circ}\text{C}$ . Additionally, liquid nitrogen was used to trap the  $\text{CO}_2$  produced during combustion of the analytes to prevent isobaric interferences by  $\text{CO}^+$ -fragments.<sup>13</sup>

### 2.2.3 SPME of aqueous samples

The SPME fiber coating polyacrylate (PA, 85  $\mu\text{m}$ , Supelco), used for the nitroaromatic compounds,<sup>6</sup> was compared to polydimethylsiloxane/divinylbenzene (PDMS/DVB, 65  $\mu\text{m}$ , Supelco). Both materials led to reproducible measurements and enabled more than 100 injections per fiber according to the following procedure. 1.3 mL of buffered solution was transferred into 2 mL autosampler glass vials, which contained 0.30 g of NaCl (final ionic strength I of 4 M). The samples were shaken on a Vortex shaker to dissolve NaCl. The SPME fiber was immersed directly into the buffered aqueous solutions and the analytes were allowed to adsorb on the fiber for 45 min at 40  $^{\circ}\text{C}$ . Thermal desorption from the SPME fiber was performed in a split/splitless injector equipped with a deactivated liner at 270  $^{\circ}\text{C}$  for 3 min. All measurements were carried out in triplicates. The SPME fiber was conditioned for 30 min at 250  $^{\circ}\text{C}$  after 20 samples.

### 2.2.4 Extraction efficiency

To determine the efficiency of substituted aniline extraction from buffered aqueous solutions by the SPME fibers, calibration curves of the analytes were measured on the GC/MS after cold on-column injection and compared to peak areas obtained after solid-phase microextraction. The ratio of the slopes of the calibration curves for SPME- vs

on-column-GC/MS (i.e., peak areas per amount of analyte in water vs ethyl acetate) was used as a measure of the extraction efficiency of each compound (Table 2.1). Additionally, the preconcentration factors for both SPME-fibers were determined as ratios of the analyte concentrations in water or ethyl acetate, which are necessary for the detection of identical peak areas by SPME- vs on-column-GC/MS. Analyte solutions for cold on-column measurements (25 °C, 1  $\mu$ L injection volume) were prepared in ethyl acetate and covered a concentration range of 5-50  $\mu$ M. The SPME measurements were prepared in 10 mM MES buffer at pH 7 and the concentrations were typically between 1 and 10  $\mu$ M to obtain peak areas similar to those measured by the cold on-column injection. Extraction efficiencies with the PDMS/DVB coated fiber were higher than with PA by a factor of 2 (4-Cl-aniline) to 13 (aniline, Table 2.1) for all substituted anilines used in this study. If not mentioned explicitly, the presented  $\delta^{15}\text{N}$  and  $\delta^{13}\text{C}$  values are measured with the PDMS/DVB-coated fiber.

### 2.2.5 Stable isotope measurements in buffered solutions with SPME-GC/IRMS

$^{15}\text{N}$  and  $^{13}\text{C}$  signatures of the substituted anilines were measured after SPME and compared to isotope ratio measurements after on-column injection and to reference isotope ratios determined by elemental analyzer (EA, Carlo Erba) coupled to IRMS (Fisons Optima).<sup>79</sup> These comparisons were performed to evaluate whether isotopic fractionation occurred during SPME and/or combustion to analyte gases. Isotope signatures were measured as single compounds by SPME-GC/IRMS to avoid potential interferences from competitive adsorption of the analytes on the SPME fiber. The concentration range of the investigated anilines varied from 25 to 500  $\mu$ M and 1-30  $\mu$ M at pH 7 for  $\delta^{15}\text{N}$  and  $\delta^{13}\text{C}$ , respectively, depending on the SPME extraction efficiency of each compound. The sensitivity of the  $\delta^{15}\text{N}$ -SPME analysis was 1.5 orders of magnitude lower compared to  $\delta^{13}\text{C}$ -SPME analysis as noted previously.<sup>6</sup> All  $\delta^{15}\text{N}$ - and  $\delta^{13}\text{C}$ -values are reported relative to air ( $\delta^{15}\text{N}_{\text{air}}$ ) and Vienna PeeDee Belemnite ( $\delta^{13}\text{C}_{\text{VPDB}}$ ), respectively, in per mil (‰).

$$\delta^h\text{E} = \left( \frac{R_{\text{sample}}}{R_{\text{standard}}} - 1 \right) \times 1000 \quad (2.1)$$

where  $\delta^h\text{E}$  is the element's isotope signature,  $R_{\text{sample}}$  and  $R_{\text{standard}}$  are the isotope ratio of sample and standard, respectively. To exclude nonlinearity effects, which may arise due to variations of the introduced mass into the IRMS and lead to inaccurate isotope sig-

natures,<sup>92</sup> we determined the concentration range within which isotope signatures, both  $\delta^{15}\text{N}$  and  $\delta^{13}\text{C}$ , did not show any mass bias. The accuracy of the isotope measurements,  $\Delta\delta^h\text{E}$ , was expressed as deviation of the isotope signature measured by SPME-GC/IRMS,  $\delta^h\text{E}_{\text{SPME-GC/IRMS}}$ , from the reference isotope signature determined by EA-IRMS,<sup>93</sup>  $\delta^h\text{E}_{\text{ref}}$  (Equation 2.2).

$$\Delta\delta^h\text{E} = \delta^h\text{E}_{\text{SPME-GC/IRMS}} - \delta^h\text{E}_{\text{ref}} \quad (2.2)$$

Isotope fractionation during the adsorption of aromatic amines to SPME fibers was ruled out from measurements of  $\delta^{15}\text{N}$  and  $\delta^{13}\text{C}$ -values measured with two different fiber materials (PA and PDMS/DVB) and comparison to isotope signatures determined after cold on-column injection of the analytes into the GC/IRMS system. No significant difference in accuracy between the two fiber coating materials was observed under optimized conditions (see discussion below), except for 4-Cl-aniline where extraction with the PDMS/DVB fiber decreased the  $\Delta\delta^{15}\text{N}$  value by approximately 4‰.

pH-dependent isotope fractionation was investigated by SPME-GC/IRMS at several pH-values using 10 mM solutions of the following buffers (parentheses indicate  $\text{pK}_a$ -values) at ionic strength of 4 M (NaCl): MES (6.15) was used for the pH-range 5.0-7.0, acetate (4.76) for the pH 4.0-5.0, citrate (3.13 and 4.76) for pH 3.0-5.5, succinate (4.21 and 5.64) for pH 3.5-6.5, and phosphate (2.15) for pH 2.0. To avoid potential artifacts from acid-catalyzed modification of SPME-fibers, experiments were not run at pH-values below 2.0 thus limiting the extent to which the effect of protonation on N and C isotope analyses could be studied with some substituted anilines.

To verify whether the presence of dissolved oxygen causes aniline oxidation and thus biases isotope ratio measurements, we carried out SPME-GC/IRMS of samples that were prepared with anoxic stock and buffer solutions of the analytes at all relevant pH values in an anoxic glovebox (data not shown). Isotope signatures were identical regardless of the dissolved oxygen content of the solution and thus no effort to deoxygenate solutions was made in this study.

### 2.2.6 Detection limits for accurate isotope ratio measurements

The operational detection limits for accurate stable isotope analysis of the investigated substituted anilines were derived from repeated  $^{15}\text{N}$ - and  $^{13}\text{C}$ -SPME-GC/IRMS measurements using PDMS/DVB fibers, aqueous solutions buffered with 10 mM MES at pH 7 ( $I = 4$  M), and different analyte concentrations corresponding to peak amplitudes

between 300 and 2500 mV and 500 and 6000 mV for N and C isotope analysis, respectively. As specified in the discussion below, detection limits correspond to the lowest analyte concentration lying within a  $\Delta\delta^h\text{E}$ -interval defined by the precision and accuracy of  $\delta^{15}\text{N}$ - and  $\delta^{13}\text{C}$ -measurements.

### 2.2.7 DFT-Calculations

The geometries of all free base anilines and their protonated conjugate acids were fully optimized at the density functional (DFT) level using the gradient-corrected Perdew-Wang exchange and correlation functionals<sup>114,115</sup> as modified by Adamo and Barone<sup>1</sup> in conjunction with the 6-311+G-(d) basis set.<sup>51</sup> Stationary equilibrium structures were confirmed by analytical calculation of vibrational frequencies, which were also used in the construction of ideal-gas, rigid-rotator, harmonic oscillator partition functions, from which thermal contributions to free energies  $G$  were computed.<sup>21</sup> Equilibrium isotope effects were computed as

$$\text{EIE}_{\text{B-BH}^+}^{\text{N}} = \frac{{}^{14}\text{N}K_{\text{B}}}{{}^{15}\text{N}K_{\text{B}}} = \exp\left(\frac{-G_{14\text{BH}^+} + G_{14\text{B}} + G_{15\text{BH}^+} - G_{15\text{B}}}{RT}\right) \quad (2.3)$$

where  $\text{EIE}_{\text{B-BH}^+}^{\text{N}}$  is the N equilibrium isotope effect and  $K_{\text{B}}$  is the equilibrium constant associated with aromatic amine protonation. The isotopically sensitive free energy  $G$  was determined for the substituted anilines, that is the neutral ( $G_{14\text{B}}$ ,  $G_{15\text{B}}$ ) and protonated isotopologues ( $G_{14\text{BH}^+}$ ,  $G_{15\text{BH}^+}$ ).  $\text{EIE}_{\text{B-BH}^+}^{\text{N}}$  was calculated for *para*- and *ortho*-substituted anilines including aromatic substituents with different electron donating and accepting properties (i.e., 4-N(CH<sub>3</sub>)<sub>2</sub>, 4-OCH<sub>3</sub>, 4-CH<sub>3</sub>, 4-F, 4-Cl, 4-NO<sub>2</sub> and 2-CH<sub>3</sub>, 2-Cl). The corresponding  $\text{EIE}_{\text{B-BH}^+}^{\text{C}}$  was calculated only for 4-CH<sub>3</sub>-aniline and for each single carbon atom. All calculations made use of the Gaussian 03 electronic structure program suite.<sup>39</sup>

Table 2.1: Names and Abbreviations of the Investigated Substituted Anilines as well as  $pK_a$ -Values of the Conjugate Acids. Extraction Efficiencies (extr. efficiency) and Preconcentration Factors (preconc. factor) Obtained by SPME-GC/MS are Listed for Polyacrylate (PA) and Polydimethylsiloxane/Divinylbenzene (PDMS/DVB) as the Fiber Material.<sup>a</sup>

compound name (abbreviation)	$pK_a^{19,126}$	extr. efficiency <sup>b</sup>		preconc. factor		extr. efficiency		preconc. factor	
		PA-fiber (%)	PDMS/DVB-fiber (%)	PA-fiber (-)	PDMS/DVB-fiber (-)	PA-fiber (-)	PDMS/DVB-fiber (-)	PA-fiber (-)	PDMS/DVB-fiber (-)
aniline (An)	4.63	0.96 $\pm$ 0.03		12.5 $\pm$ 0.4	12.7 $\pm$ 0.4			165 $\pm$ 5	
2-methyl-aniline (2-CH <sub>3</sub> -An)	4.45	3.51 $\pm$ 0.10		45.6 $\pm$ 1.3	-			-	
4-methyl-aniline (4-CH <sub>3</sub> -An)	5.10	5.10 $\pm$ 0.20		66.3 $\pm$ 2.7	38.3 $\pm$ 1.1			497 $\pm$ 15	
2-chloro-aniline (2-Cl-An)	2.46	9.73 $\pm$ 0.22		127 $\pm$ 3	-			-	
4-chloro-aniline (4-Cl-An)	3.98	9.56 $\pm$ 0.38		124 $\pm$ 5	19.2 $\pm$ 1.1			250 $\pm$ 14	

<sup>a</sup> All extraction experiments were performed after addition of NaCl to 10 mM MES buffer solution at pH 7.0 ( $I = 4$  M).

<sup>b</sup> See text for definition of extraction efficiencies and preconcentration factors.

## 2.3 Results and Discussion

### 2.3.1 $^{15}\text{N}$ and $^{13}\text{C}$ Signatures determined by SPME- GC/IRMS

The N and C isotope signatures ( $\delta^{15}\text{N}$  and  $\delta^{13}\text{C}$ ) of the substituted anilines measured by SPME-GC/IRMS at pH 7 correspond well with independent isotope signature measurements by elemental analyzer-IRMS (EA-IRMS). As shown in Table 2.2 accuracies were  $< \pm 0.3\text{‰}$  for N and  $< \pm 0.5\text{‰}$  for C isotope signatures, respectively, as revealed by the differences measured by the two methods ( $\Delta\delta^{15}\text{N}_{\text{SPME-EA}}$  and  $\Delta\delta^{13}\text{C}_{\text{SPME-EA}}$ , Equation 2.2). These deviations were within typical uncertainties ( $\pm 0.5\text{‰}$ ,<sup>64</sup>) reported for  $\delta^{15}\text{N}$  and  $\delta^{13}\text{C}$ -measurements (Table 2.2). Only  $\Delta\delta^{15}\text{N}$ -value of 4-Cl-aniline showed a significant offset by  $-4\text{‰}$ . All isotope ratio measurements were highly linear within the amplitude range typically used for isotope analysis, that is, 300-5500 mV (see Experimental Section for details and example for 4-CH<sub>3</sub>-aniline in Figure 2.1).

Despite good linearity,  $\delta^{15}\text{N}$ -measurements of substituted anilines deviated substantially from the correct values if the solution pH approached or was below the  $\text{pK}_{\text{a}}$  of the substituted aniline’s conjugate acid. We observed a decrease of  $\delta^{15}\text{N}$  corresponding to a depletion of isotopically heavy nitrogen ( $^{15}\text{N}$ ) in the measured analyte with decreasing pH. The most substantial  $^{15}\text{N}$  depletion was observed for 4-CH<sub>3</sub>-aniline ( $-15\text{‰}$ ), 4-Cl-aniline ( $-22\text{‰}$ ), and aniline ( $-17\text{‰}$ ) at approximately 2 pH units below the  $\text{pK}_{\text{a}}$  of the conjugate acid. In contrast, no C isotope fractionation was found as the pH-value of solutions decreased under the identical conditions and  $\delta^{13}\text{C}$ -values remained constant within  $< 0.9\text{‰}$  ( 2.2a and 2.2b). The observation of pH-dependent N isotope fractionation coincided with decreasing extraction efficiencies of the analytes from aqueous solution. Figure 2.1 illustrates the  $m/z$  28 IRMS signal intensities of 4-CH<sub>3</sub>-aniline between pH-values 4.0 and 7.0, which suggest that only neutral molecules are adsorbed to the SPME fiber while protonated species remain dissolved. The same observation was made for other substituted anilines (data not shown). The decreasing  $\delta^{15}\text{N}$ -values measured in adsorbed analytes at low pH ( $^{15}\text{N}$  depletion) imply that protonated compounds are enriched with  $^{15}\text{N}$ , while the total analyte concentration in control solutions, which were not subject to SPME, remained unchanged. In contrast to earlier work,<sup>6</sup> our data suggest that accurate determination of  $\delta^{15}\text{N}$  and  $\delta^{13}\text{C}$  in substituted anilines measured by SPME-GC/IRMS is feasible if the pH of analyte solutions is controlled and maintained at least 2 pH-units above the  $\text{pK}_{\text{a}}$  of the conjugate acid.

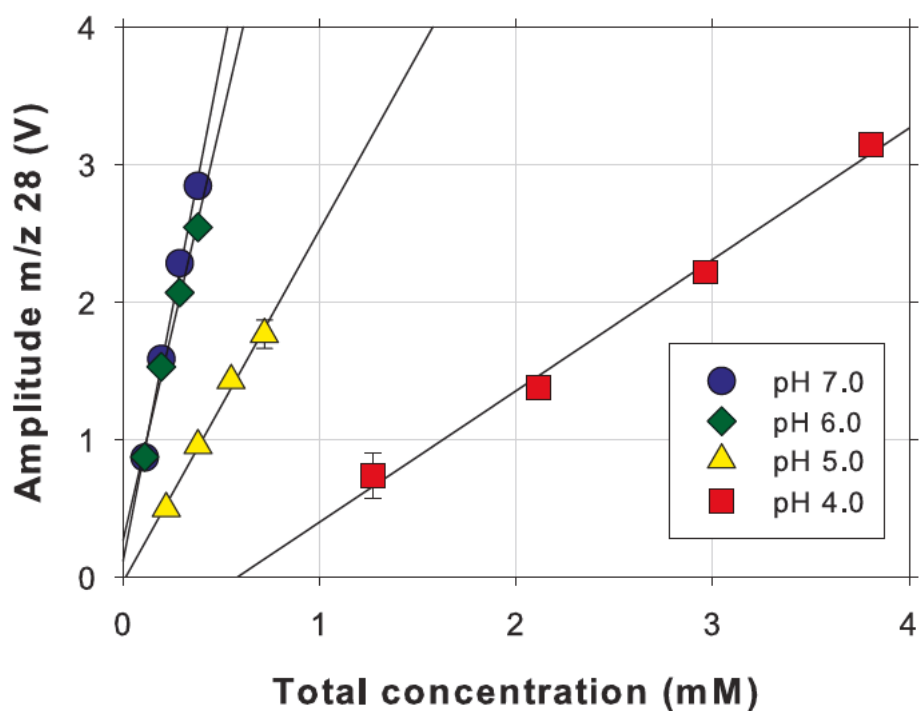


Figure 2.1: pH-dependence of 4-CH<sub>3</sub>-aniline  $m/z$  28 IRMS signal intensities for <sup>15</sup>N-SPME-GC/IRMS (fiber material PDMS/DVB) vs total aqueous 4-CH<sub>3</sub>-aniline concentration in 10 mM MES (pH 6.0 and 7.0) and 10 mM acetate (pH 4.0 and 5.0) buffered solutions. Uncertainties of signal intensities are  $\pm$  standard deviation (error bars mostly smaller than markers).

Table 2.2: Comparison of  $\delta^{15}\text{N}$ - and  $\delta^{13}\text{C}$ -Values of Substituted Anilines Measured by EA-IRMS and SPME-GC/IRMS<sup>a</sup>.

compound	$\delta^{15}\text{N}$ (‰)		$\Delta\delta^{15}\text{N}$	$\delta^{13}\text{C}$ (‰)		$\Delta\delta^{13}\text{C}$ (‰)
	EA-IRMS	SPME-GC/IRMS		EA-IRMS	SPME-GC/IRMS	
An	$7.6 \pm 0.3$	$7.9 \pm 0.3$	$0.3 \pm 0.5$	$-30.0 \pm 0.3$	$-29.1 \pm 0.2$	$0.9 \pm 0.4$
2-CH <sub>3</sub> -An	$3.7 \pm 0.3$	$3.9 \pm 0.3$	$0.2 \pm 0.4$	$-27.5 \pm 0.3$	$-27.8 \pm 0.6$	$-0.3 \pm 0.7$
4-CH <sub>3</sub> -An	$-5.1 \pm 0.3$	$-4.8 \pm 0.2$	$0.3 \pm 0.4$	$-28.3 \pm 0.3$	$-27.8 \pm 0.3$	$0.5 \pm 0.5$
2-Cl-An	$6.4 \pm 0.3$	$6.5 \pm 0.6$	$0.1 \pm 0.7$	$-26.7 \pm 0.3$	$-26.7 \pm 0.2$	$0.0 \pm 0.3$
4-Cl-An	$-3.1 \pm 0.3$	$-7.1 \pm 0.9$	$-4.0 \pm 0.9$	$-27.3 \pm 0.3$	$-26.8 \pm 0.5$	$0.5 \pm 0.6$

<sup>a</sup> SPME was performed in 10 mM MES buffered solutions at pH 7.0. The accuracy of the SPME-GC/IRMS measurements is expressed as deviation from reference measurements of the pure analytes by EA-IRMS ( $\Delta\delta^b\text{E-values}$ ). All uncertainties correspond to  $\pm 1$  standard deviation ( $n = 3$ ).



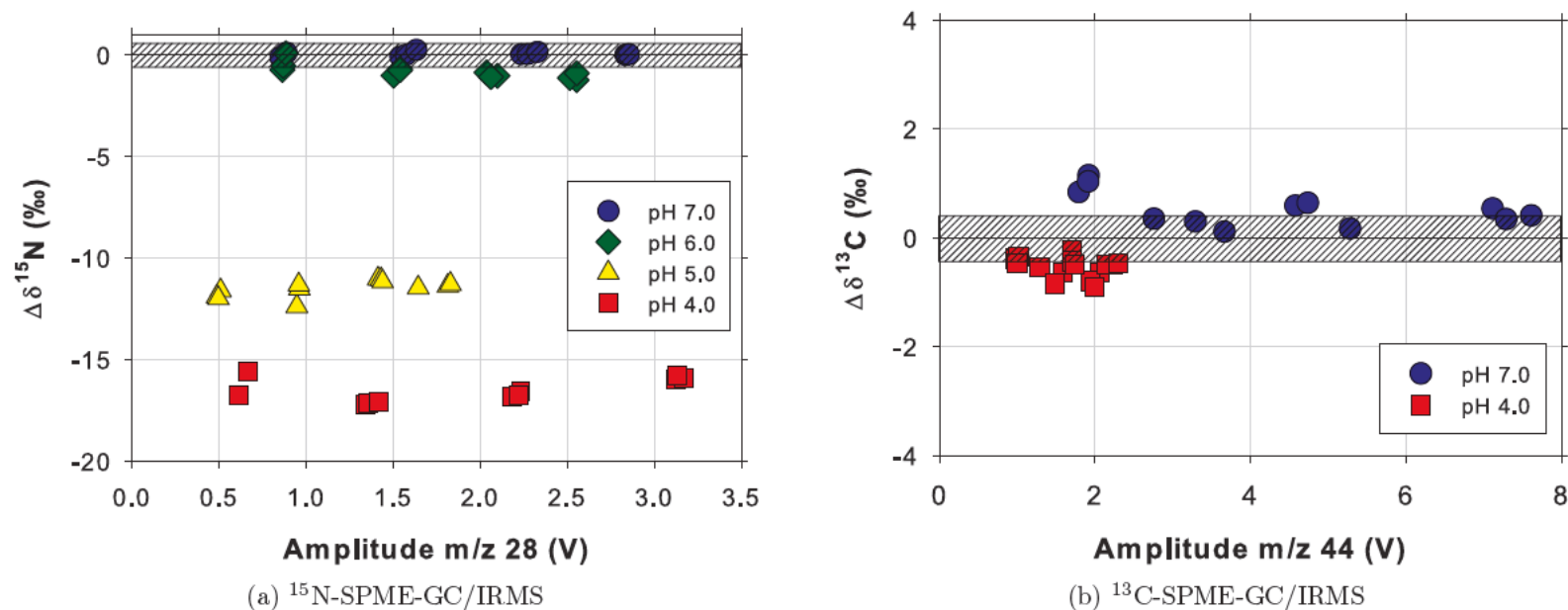


Figure 2.2: Accuracy of (a)  $^{15}\text{N}$ - and (b)  $^{13}\text{C}$ -SPME-GC/IRMS of 4-CH<sub>3</sub>-aniline,  $\Delta\delta^{15}\text{N}$  and  $\Delta\delta^{13}\text{C}$ , at solution pH-values between 4.0 and 7.0. Single  $\delta^{15}\text{N}$  measurements at pH 6.0 and 7.0 were carried out in 10 mM MES buffer, those at pH 4.0 and 5.0 in 10 mM acetate buffer. Single  $\delta^{13}\text{C}$  measurements at pH 4.0 and 7.0 were carried out in 10 mM acetate and MES buffer, respectively. The horizontal bar corresponds to the reference  $\delta^{15}\text{N}$  and  $\delta^{13}\text{C}$  ( $\pm$ standard deviation) of the pure 4-CH<sub>3</sub>-aniline determined by EA-IRMS.

### 2.3.2 Equilibrium isotope effect (EIE) associated with the protonation of substituted anilines

The observation of  $\delta^{15}\text{N}$ -decrease at lower solution pH values in combination with the preferential extraction of neutral substituted aniline species and the fact that a change of ambient pH did not affect C isotope composition implies a nitrogen equilibrium isotope effect originating from the protonation at the amino functional group. To obtain evidence for the magnitude of equilibrium isotope fractionation owing to N-atom protonation, we measured the  $\delta^{15}\text{N}$  of the substituted anilines in solutions buffered with different organic buffers at pH-values between 3.5 and 7.0 and compared the outcome with reference isotope signatures ( $\delta^{15}\text{N}_{\text{ref}}$ ) obtained by EA-IRMS as follows. According to the isotopic mass balance  $\delta^{15}\text{N}_{\text{ref}}$  corresponds to the sum of neutral and the protonated aniline species (Equation 2.4).

$$\delta^{15}\text{N}_{\text{ref}} = f_{\text{BH}^+} \times \delta^{15}\text{N}_{\text{BH}^+} + (1 - f_{\text{BH}^+}) \times \delta^{15}\text{N}_{\text{B}} \quad (2.4)$$

where  $f_{\text{BH}^+}$  is the fraction of the protonated species, and  $\delta^{15}\text{N}_{\text{BH}^+}$  and  $\delta^{15}\text{N}_{\text{B}}$  are the N isotope signatures of protonated and neutral species, respectively. The partitioning of N isotopes between protonated and neutral compounds is described by the isotopic fractionation factor  $\alpha_{\text{B-BH}^+}$  and corresponds to the ratio of isotopic composition in each species<sup>157</sup>

$$\alpha_{\text{B-BH}^+}^{\text{N}} = \frac{R_{\text{BH}^+}}{R_{\text{B}}} \quad (2.5)$$

where  $R_{\text{BH}^+}$  and  $R_{\text{B}}$  are the measured  $^{15}\text{N}/^{14}\text{N}$  ratios in the protonated and neutral species, respectively, typically reported in the per mil notation as in Equation 2.1. Substitution of a modified Equation 2.1 into Equation 2.5 results in an expression, which can be inserted into Equation 2.4 to yield the measured, neutral isotope signature  $\delta^{15}\text{N}_{\text{B}}$  at any solution pH as function of the degree of protonation,  $f_{\text{BH}^+}$ , the reference isotope signature,  $\delta^{15}\text{N}_{\text{ref}}$ , and the fractionation factor  $\alpha_{\text{B-BH}^+}$  (Equation 2.6).

$$\delta^{15}\text{N}_{\text{B}} = \frac{\delta^{15}\text{N}_{\text{ref}} - f_{\text{BH}^+} \times 1000 \times (\alpha_{\text{B-BH}^+}^{\text{N}} - 1)}{f_{\text{BH}^+} \times (\alpha_{\text{B-BH}^+}^{\text{N}} - 1) + 1} \quad (2.6)$$

For typical isotope effects, the term  $f_{\text{BH}^+} \times (\alpha_{\text{B-BH}^+}^{\text{N}} - 1)$  becomes negligible and Equation 2.6 simplifies to

$$\delta^{15}\text{N}_{\text{B}} \approx \delta^{15}\text{N}_{\text{ref}} - f_{\text{BH}^+} \times 1000 \times (\alpha_{\text{B-BH}^+}^{\text{N}} - 1) \quad (2.7)$$

Using N isotope enrichment factors instead of fractionation factors (Equation 2.8), the extent of equilibrium isotope fractionation is the slope of the correlation of measured  $\delta^{15}\text{N}$  (ascribed to neutral species) vs  $f_{\text{BH}^+}$  (Equation 2.9).

$$\epsilon_{\text{B-BH}^+}^{\text{N}} = 1000 \times (\alpha_{\text{B-BH}^+}^{\text{N}} - 1) \quad (2.8)$$

$$\delta^{15}\text{N}_{\text{B}} = \delta^{15}\text{N}_{\text{ref}} - f_{\text{BH}^+} \times \epsilon_{\text{B-BH}^+}^{\text{N}} = \delta^{15}\text{N}_{\text{ref}} + (1 - f_{\text{BH}^+}) \times \epsilon_{\text{B-BH}^+}^{\text{N}} \quad (2.9)$$

Figure 2.3 shows the correlation of the measured  $\delta^{15}\text{N}$  of aniline vs the fraction of neutral aniline species,  $(1 - f_{\text{BH}^+})$ , in solution buffered with different organic buffers over a wide pH range. Notice that  $(1 - f_{\text{BH}^+})$  was calculated after pH measurements at high ionic strength owing to the addition of NaCl for extraction of the analytes. The slope of the regression line corresponds to an  $\epsilon_{\text{B-BH}^+}^{\text{N}}$ -value of  $18.8 \pm 1.1\text{‰}$  or an inverse equilibrium isotope effect,  $\text{EIE}_{\text{B-BH}^+}^{\text{N}}$ , of  $0.9815 \pm 0.0011$  (Equation 2.10, Table 2.3). The inverse  $\text{EIE}_{\text{B-BH}^+}^{\text{N}}$  reflects the formation of an additional bond to N in the protonated species<sup>89</sup>

$$\text{EIE}_{\text{B-BH}^+}^{\text{N}} = \frac{{}^{14}\text{N}K_{\text{B}}}{{}^{15}\text{N}K_{\text{B}}} = \frac{1}{1 + \epsilon_{\text{B-BH}^+}^{\text{N}}/1000} = \frac{1}{(\alpha_{\text{B-BH}^+}^{\text{N}} - 1)} \quad (2.10)$$

Some of the  $\delta^{15}\text{N}$  of aniline measured in solutions containing citrate and succinate buffer deviated by up to 3‰ from the expected values. These deviations presumably originate from high ionic strength effects, which result in altered activities and ionization constants of dissolved ions, buffers, and substituted anilines due to ion pairing with the electrolyte (NaCl).<sup>96,117</sup> While ion pairing models allow for estimates of activity coefficients and ionization constants of typical ions in saline waters,<sup>97,118</sup> no data are available for assessing the buffers and substituted anilines used in this work. Ionic strength effects might ultimately lead to different estimates of the fraction of neutral and protonated aniline concentrations and thus explain the lack of correlation for selected data points in Figure 2.3. As illustrated in Figure S2.1 (Supporting Information to Chapter 2), however, this phenomenon does not alter the  $\epsilon_{\text{B-BH}^+}^{\text{N}}$ -value obtained from Equation 2.9 beyond experimental uncertainty.

The  $\text{EIE}_{\text{B-BH}^+}^{\text{N}}$  obtained from Figure 2.3 is in excellent agreement with data inferred from the chromatographic separation of  $^{14}\text{N}$  and  $^{15}\text{N}$  aniline isotopologues<sup>140</sup> and implies that the base dissociation constant of the  $^{15}\text{N}$ -containing aniline species  $^{15}\text{N}K_{\text{B}}$ , exceeds that of the light isotopologues,  $^{14}\text{N}K_{\text{B}}$ . An  $\text{EIE}_{\text{B-BH}^+}^{\text{N}}$  of 0.9815 in case of aniline (Table 2.3) implies that  $pK_{\text{B}}^{14\text{N}}$  exceeds  $pK_{\text{B}}^{15\text{N}}$  by 0.008 units. Thus, at any solution pH, the slightly higher basicity of the neutral  $^{15}\text{N}$ -aniline causes the heavy ( $^{15}\text{N}$ ) isotopologues to protonate to a larger extent compared to  $^{14}\text{N}$ -aniline species because of stronger N-H bonds in the heavy isotope-containing conjugate acid. As only the deprotonated, that is, neutral compound is extracted by SPME, one therefore observes a depletion of  $^{15}\text{N}$  and more negative  $\delta^{15}\text{N}$ -values unless aromatic amine protonation is negligible at the solution pHs exceeding the  $\text{pK}_{\text{a}}$  of the conjugate acid by at least 2 units.

We investigated the effects of aromatic substituents on the variability of  $\text{EIE}_{\text{B-BH}^+}^{\text{N}}$  with additional experiments for 4- $\text{CH}_3$ -aniline and 4- $\text{Cl}$ -aniline and through density functional theory (DFT) calculations for a wide set of compounds. The results are reported in Table 2.3 and in the SI. The  $^{13}\text{C}$ -EIE value reported in Table 2.3 corresponds to the average calculated for all carbon atoms 1 to 7. This accounts for the fact that the heavy carbon atom is more or less evenly distributed over all molecular positions so that the value measured by CSIA represents the average of all position-specific isotope effects. The data compiled in Table 2.3 show excellent agreement between experiment and theory confirming inverse  $\text{EIE}_{\text{B-BH}^+}^{\text{N}}$ -values for all substituted anilines. In addition,  $\text{EIE}_{\text{B-BH}^+}^{\text{N}}$ -values show little sensitivity to aromatic substitution albeit a slight trend to more inverse isotope effects with increasing electron-donating properties of the substituent (and vice versa) is observed. Note that our calculations also confirm the absence of significant C isotope fractionation (4- $\text{CH}_3$ -aniline  $\text{EIE}_{\text{B-BH}^+}^{\text{C}}$  of 1.0011, 2.2b and SI).

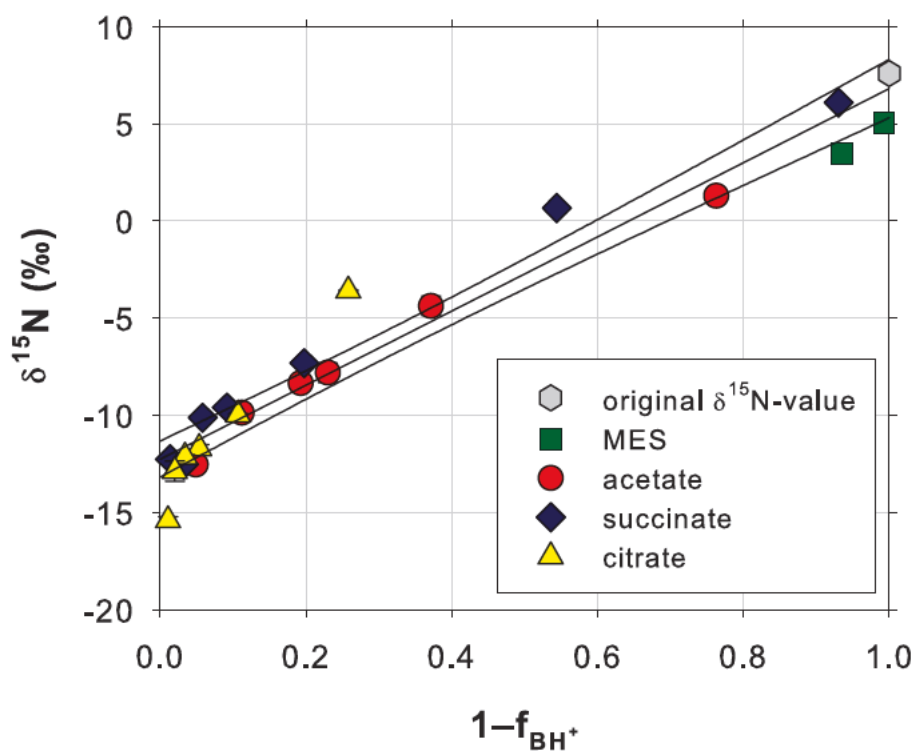


Figure 2.3:  $\delta^{15}\text{N}$ -values of aniline determined by SPME-GC/IRMS vs the fraction of neutral aniline species in aqueous solution at different pH-values. Organic buffers used include: MES (pH-range 5.0-7.0), acetate (4.0-5.0), citrate (3.0-5.5), and succinate (3.5-6.5). The slope of the regression line corresponds to the enrichment factor  $\epsilon_{\text{B-BH}^+}^{\text{N}}$ . Error bars of triplicate  $\delta^{15}\text{N}$  measurements ( $\pm$ standard deviation) are smaller than the corresponding markers.

Table 2.3: Nitrogen Isotope Enrichment Factors,  $\epsilon_{\text{B-BH}^+}^{\text{N}}$ , and N Equilibrium Isotope Effects,  $\text{EIE}_{\text{B-BH}^+}^{\text{N}}$ , Associated with the Protonation of the Substituted Anilines: Comparison of Experimental (exp) and Theoretical Data (calc).

compound	experimental		theoretical
	$\epsilon_{\text{B-BH}^+}^{\text{N}}$ (‰)	$\text{EIE}_{\text{B-BH}^+}^{\text{N}}$ , exp —	$\text{EIE}_{\text{B-BH}^+}^{\text{N}}$ , calc —
An	$18.8 \pm 1.1$	$0.9815 \pm 0.0011$	0.9811
2-CH <sub>3</sub> -An	$17.2 \pm 1.8$	$0.9831 \pm 0.0018$	0.9811
4-CH <sub>3</sub> -An	$19.9 \pm 4.1$	$0.9804 \pm 0.0041$	0.9811
2-Cl-An	$17.2 \pm 1.2$	$0.9831 \pm 0.0012$	0.9811
4-Cl-An	$18.6 \pm 2.0$	$0.9817 \pm 0.0020$	0.9821
4-N(CH <sub>3</sub> ) <sub>2</sub> -An	-	-	0.9718
4-OCH <sub>3</sub> -An	-	-	0.9800
4-F-An	-	-	0.9894
4-NO <sub>2</sub> -An	-	-	0.9842

Table 2.4: Concentration Limits for Accurate N and C Isotope Analysis of Substituted Anilines by SPME-GC/IRMS Using PDMS/DVB Fibers.

compound	$\delta^{15}\text{N}$	$\delta^{13}\text{C}$
	(mg L <sup>-1</sup> )	(mg L <sup>-1</sup> )
An	1.4	0.37
2-CH <sub>3</sub> -An	1.3	0.21
4-CH <sub>3</sub> -An	2.1	0.54
2-Cl-An	1.9	<0.13
4-Cl-An	<0.64	0.26

### 2.3.3 Detection limits for accurate isotope analysis of substituted anilines

Current recommendations<sup>9,60,64,66,83</sup> regarding detection limits for isotope ratio measurements by GC/IRMS not only include the precision of repeated measurements but also account for accuracy and the rather narrow linear range continuous-flow isotope ratio measurements. To this end, we determined the lowest analyte concentrations, at which the  $\delta^{15}\text{N}$ - and  $\delta^{13}\text{C}$ -values did not deviate from the reference isotope signatures determined by EA-IRMS by more than the accuracy of the proposed method (i.e., between 0.3‰ and 0.9‰ in  $\Delta\delta^{15}\text{N}$  and  $\Delta\delta^{13}\text{C}$  (SPME vs EA, Table 2.2)). The results summarized in Table 2.2 and 2.4 for five substituted anilines illustrate that the use of buffered solutions and PDMS/DVB fibers for SPME not only improved accuracy but also allowed for more sensitive quantification of isotope ratios in the  $\mu\text{g}$  to  $\text{mg L}^{-1}$ -range, which represents an improvement by a factor of 2 compared to earlier approaches.<sup>6</sup>

Note that previous contributions, which focus predominantly on  $\delta^{13}\text{C}$  measurements, refer to typical intervals of  $\pm 0.5\text{‰}$  as acceptable uncertainties, from which the lowest acceptable concentration is deduced.<sup>66,83</sup> Unfortunately, these limits are not as established for less common isotope systems such as N and O isotope ratios. Uncertainties of  $\delta^{15}\text{N}$ -values for organic compounds determined by GC/IRMS lack widely accepted limits across different isotope laboratories because these measurements are carried out less frequently than C isotope analyses. Given these ambiguities, we feel that it is more appropriate in the present case to define the acceptable limit of uncertainty for every compound individually because factors such as SPME extraction efficiency and the efficacy of combustion (and reduction) to analyte gases ( $\text{N}_2$  and  $\text{CO}_2$ ) cannot be assumed to be identical for all organic compounds analyzed for a specific isotope ratio.

## 2.4 Conclusion

Our study demonstrates the importance of adjusting the solution pH prior to compound-specific isotope ratio measurements of substituted anilines by SPME-GC/IRMS. Because the conjugate acids of many substituted anilines exhibit  $\text{pK}_\text{a}$ -values between 2.5 and 7,<sup>84,126</sup> the fraction of protonated species will be significant given the range of pH-values of natural waters (pH 5-8,<sup>137</sup>). Besides compromising the sensitivity of the analytical method,  $\delta^{15}\text{N}$ -measurements by SPME-GC/IRMS might deviate by up to  $-20\text{‰}$  depending on the contaminant's basicity and the pH of the aqueous sample.

Moreover, the equilibrium N isotope fractionation associated with protonation of aryl N atoms could potentially interfere with the quantification of N isotope fractionation during contaminant transformation if the latter involves reactions at N-containing functional groups. Even though the magnitude of C and N isotope fractionation for (bio)degradation processes of substituted anilines are currently unknown, recent work with structurally related organic contaminants supports this conclusion. Protonations of alkyl-, aryl-, and triazine-bound N atoms are important elementary reaction steps during hydrolysis of phenylurea and triazine herbicides.<sup>26,94,95,112</sup> For the hydrolysis of isoproturon, an inverse N equilibrium isotope effect of 0.992 was reported for the alkyl-N protonation during initial zwitterion formation,<sup>112</sup> which contributed partly to the overall, observable N isotope fractionation. The N-heteroatom protonation in the triazine ring of atrazine associated with its acid-catalyzed and biotic hydrolysis led to apparent kinetic N isotope effects of similar inverse magnitude (0.974-0.995<sup>95</sup>). These inverse isotope effects were rationalized as a consequence of N atom hybridization changes or additional bonds to N in the transition state. Our interpretation of stronger N-H bonds in protonated heavy N isotopologues of substituted anilines due to inverse N equilibrium isotope effects in a similar range fully agrees with these findings.

## Acknowledgment

This work was supported by the Swiss National Science Foundation (grant no. 200020-116447/1). We thank Jakov Bolotin for experimental support as well as Martin Elsner and C. Annette Johnson for valuable comments.



## Supporting Information to Chapter 2

## Sensitivity of $\epsilon_{\text{B-BH}^+}^{\text{N}}$ -values for variations of proton activities and buffer ionization at high ionic strength

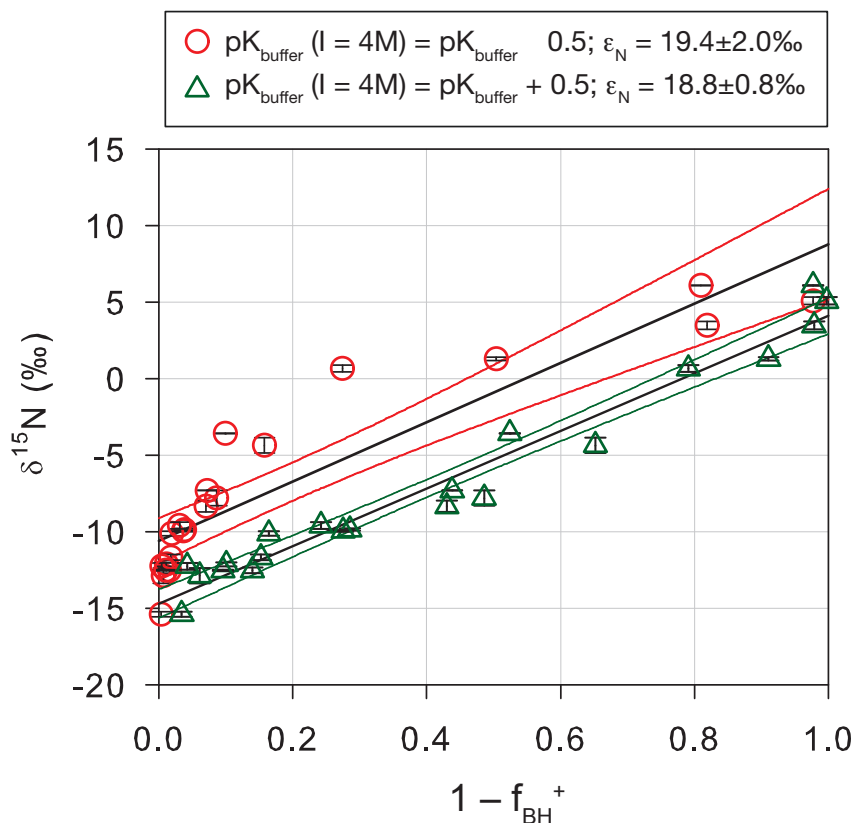
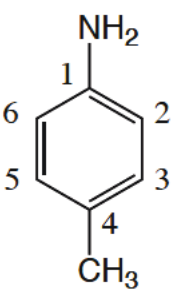


Figure S2.1: Correlation of  $\delta^{15}\text{N}$ -values of aniline determined by SPME-GC/IRMS vs. the fraction of neutral aniline species ( $1 - f_{\text{BH}^+}$ ) for two different scenarios for ionic strength effects (4 M NaCl) on buffer ionization constants and, ultimately, on the N isotope enrichment factor  $\epsilon_{\text{B-BH}^+}^{\text{N}}$  associated with aniline protonation. The  $\delta^{15}\text{N}$  data are the same as in Figure 2.3 of the manuscript while ( $1 - f_{\text{BH}^+}$ ) varied according to two scenarios for deviations of the buffer ionization constants by  $\pm 0.5$  pK-units. Even substantial changes of buffer ionization constants do not alter the  $\epsilon_{\text{B-BH}^+}^{\text{N}}$ -value associated with aniline protonation significantly.

# Position specific $^{13}\text{C}$ -EIEs associated with the protonation of 4- $\text{CH}_3$ -aniline obtained by density functional theory calculations

Table S2.1:  $^{13}\text{C}$ -EIE for all carbon atoms of 4- $\text{CH}_3$ -aniline obtained by DFT-calculations.

	Nr. Carbon atom	$^{13}\text{C}$ EIE
	1	1.0001
	2	1.0000
	3	1.0101
	4	0.9989
	5	1.0000
	6	0.9979
	7	0.9989
	average	1.0011



## Chapter 3

# Using Nitrogen Isotope Fractionation to Assess the Oxidation of Substituted Anilines by Manganese Oxide

M. Skarpeli-Liati, M. Jiskra, A. Turgeon, A.N. Garr, W. A. Arnold, C. J. Cramer, R.P. Schwarzenbach and T. B. Hofstetter. Using Nitrogen Isotope Fractionation to Assess the Oxidation of Substituted Anilines by Manganese Oxide. *Environ. Sci. Technol.*, 45, 5596-5604, 2011

## Abstract

We explored the N isotope fractionation associated with the oxidation of substituted primary aromatic amines, which are often the position of initial attack in transformation processes of environmental contaminants. Apparent  $^{15}\text{N}$ -kinetic isotope effects,  $\text{AKIE}_{\text{N}}$ , were determined for oxidation of various substituted anilines in suspension of manganese oxide ( $\text{MnO}_2$ ) and compared to reference experiments in homogeneous solution and at electrode surfaces, as well as to density functional theory calculations of intrinsic  $\text{KIE}_{\text{N}}$  for electron and hydrogen atom transfer reactions. Owing to the partial aromatic imine formation after one-electron oxidation and corresponding increase in C–N bond strength,  $\text{AKIE}_{\text{N}}$ -values were *inverse*, substituent-dependent, and confined to the range between 0.992 and 0.999 in agreement with theory. However,  $\text{AKIE}_{\text{N}}$ -values became *normal* once the fraction of cationic species prevailed owing to  $^{15}\text{N}$ -equilibrium isotope effects,  $\text{EIE}_{\text{N}}$ , of 1.02 associated with N atom deprotonation. The observable  $\text{AKIE}_{\text{N}}$ -values are substantially modulated by the acid/base pre-equilibria of the substituted anilines and isotope fractionation may even vanish under conditions where normal  $\text{EIE}_{\text{N}}$  and inverse  $\text{AKIE}_{\text{N}}$  cancel each other out. The pH-dependent trends of  $\text{AKIE}_{\text{N}}$ -values provide a new line of evidence for the identification of contaminant degradation processes via oxidations of primary aromatic amino groups.

## 3.1 Introduction

Aromatic amino groups are often the position of initial attack in transformation processes of industrial chemicals, biocides, and pharmaceuticals in the environment.<sup>8,25,72,78,110,159</sup> A (quantitative) assessment of these processes is therefore essential for evaluating the exposure and impact of these micropollutants on human and environmental health.<sup>128</sup> However, aryl amines can react along different, sometimes competing pathways including the mineral- and enzyme-catalyzed oxidation of the N atom,<sup>72,78,159</sup> the microbial dioxygenation of the aromatic ring,<sup>132</sup> as well as through nucleophilic addition of the amino functional group to electrophilic sites of natural organic matter.<sup>141</sup> Identifying these transformation processes is also challenging because they give rise to products that are usually difficult to analyze quantitatively (e.g., radical coupling products, adducts to NOM etc.).

Compound specific isotope analysis (CSIA) has been shown to offer new avenues to track degradation processes of such N-containing contaminants, even if competing

reaction pathways occur and reaction products are partially unknown.<sup>28,53,58</sup> This is because stable isotope compositions measured in the remaining fraction of the contaminant molecule over time or distance from the pollution source change systematically depending on the type of chemical bond(s) that are broken or formed as a consequence of kinetic or equilibrium isotope effects.<sup>157</sup> As shown for nitroaromatic explosives,<sup>48,49,59</sup> phenylurea<sup>112,113</sup> and triazine herbicides,<sup>26,50,95</sup> their enzymatic, abiotic, and photochemical redox reactions lead to typical distinct trends of C, H, and N isotope signatures that are not only indicative for the active transformation processes but can also allow one to quantify the extent of their degradation. These observations are due to the fact that different (N-containing) functional groups are involved in reactions, which also exhibit distinct apparent <sup>13</sup>C-, <sup>2</sup>H-, and <sup>15</sup>N-kinetic isotope effects (AKIEs). Despite the importance of aromatic amine oxidation for contaminant transformations, their isotope effects are largely unknown.

The goal of the present study was to assess the isotope effects associated with the oxidation of aromatic amino groups under typical environmental conditions and to evaluate whether the isotope fractionation associated with contaminant transformation can be exploited by CSIA for tracking these processes in aquatic environments. As a first step, we investigated the magnitude and variability of apparent <sup>15</sup>N-kinetic isotope effects (AKIE<sub>N</sub>) during the abiotic oxidation of a series of substituted anilines in suspensions of manganese oxide (MnO<sub>2</sub>), which represents an important heterogenous oxidant in the environment. Oxidation of substituted anilines by MnO<sub>2</sub> was reported to proceed via initial electron transfer from the lone pair of the nitrogen leading to formation of arylamino radicals.<sup>72,78</sup> As shown recently for the reduction of nitroaromatic radical anions,<sup>42,49</sup> even such small bonding changes induced by electron transfer to and from N atoms are likely to generate N isotope fractionation than can be measured by <sup>15</sup>N-CSIA.

Here, we examine the N isotope fractionation of a series of *o*-, *m*- and *p*-substituted anilines covering more than one order of relative reactivities.<sup>72</sup> Product analysis was performed to corroborate the proposed initial reaction mechanism involving substituted aniline radicals. Because the investigated compounds exhibit pK<sub>BH+</sub>-values between 4.0 and 5.3, we examined potential effects of contaminant speciation and contributions of <sup>15</sup>N-equilibrium isotope effects due to aromatic amine deprotonation<sup>134</sup> to the observable AKIE<sub>N</sub> through experiments conducted in MnO<sub>2</sub> suspension at pH-values between 4.0 and 7.0. Finally, independent evidence for the interpretation of N isotope fractionation was obtained (i) from homogeneous and electrochemical oxidation experiments and (ii) from computations of <sup>15</sup>N-kinetic isotope effects (KIE<sub>N</sub>) pertinent to outer-sphere electron

transfer and H atom transfer from substituted anilines using density functional theory.

## 3.2 Experimental Section

A complete list of all used chemicals including purities and suppliers, as well as a detailed description of the preparation and characterization procedures of  $\text{MnO}_2$ -suspension can be found in the Supporting Information to Chapter 3.

### 3.2.1 Experimental systems for the oxidation of substituted anilines

#### $\text{MnO}_2$ -suspensions

$\text{MnO}_2$  particles were synthesized through oxidation of  $\text{Mn}^{2+}$  by  $\text{MnO}_4^-$  according to the method of Murray.<sup>101</sup> The suspensions were prepared in 10 mM acetate buffer for experiments carried out at pH 4.0 and 5.1 and in 10 mM phosphate buffer for experiments at pH 7.0. XRD-measurements indicated that the synthesized  $\text{MnO}_2$ -mineral was highly amorphous with Mn oxidation state  $3.9 \pm 0.3$  as determined by iodometric titration and the  $\text{pH}_{\text{IEP}}$  was  $3.25 \pm 0.09$  as obtained from  $\zeta$ -potential measurements (see SI, Chapter 3).

Oxidation of substituted anilines by  $\text{MnO}_2$  was carried out in batch reactors containing different concentrations of  $\text{MnO}_2$  in buffer solutions, NaCl (final ionic strength to 0.02 M), and a PTFE-coated magnetic stirring bar. All batch experiments were conducted at room temperature under oxic conditions. Losses of the reactants due to volatilization, oxidation by air and/or sorption to the Viton rubber stoppers were accounted for in reference experiments set up in the identical manner except for the addition of  $\text{MnO}_2$ . Note that lack of reactivity of some substituted anilines in  $\text{MnO}_2$ -suspensions as well as in reference experiments (oxidation by  $\text{ABTS}^{\bullet-}$  (2,2'-azino-bis(3-ethylbenzthiazoline-6-sulfonic acid) radical anion) in aqueous solution and at electrode surfaces) limited the selection of substituted anilines (SI, Chapter 3).

Experiments at pH 7.0 were conducted in duplicates. The reaction was initiated by the addition of variable amounts of substituted anilines from a methanolic stock solution to achieve initial concentrations of 400-600  $\mu\text{M}$ . The  $\text{MnO}_2$  concentrations were varied so that fast reactions did not exceed 50% conversion within the first minute of the experiment, while the oxidative turnover of slowly reacting compounds had to be >60% within 3 days. Samples were withdrawn at pre-defined time points with a gas



tight glass syringe and the oxidation reaction was stopped by filtering off  $\text{MnO}_2$ -particles with a  $0.2\ \mu\text{m}$  regenerated cellulose (RC) filter. Filtered solutions were stored in amber vials in the dark at  $4^\circ\text{C}$  until concentration measurements and isotope analysis. Because the disappearance of substituted anilines from  $\text{MnO}_2$ -suspensions at pH 4.0 and 5.1 was too fast to be sampled as described for pH 7.0, variable amounts of  $\text{MnO}_2$  were spiked to reactors containing the identical initial concentration of substituted aniline. This procedure was used to achieve different degrees of reactant conversion and was shown earlier for nitroaromatic compounds to enable the study of isotope fractionation of fast reactions.<sup>49</sup> Prior to concentration measurements and isotope analysis of substituted anilines, the pH of the filtered aqueous samples was adjusted to pH 7.0 with NaOH.

The loss of substrate due to adsorption and cation exchange to the mineral surface was assessed for aniline by experiments in which the compound's concentration was compared before and after reductive dissolution of the  $\text{MnO}_2$ -particles with ascorbic acid (0.3 M, pH 13) at different time points of the reaction. To this end, the aniline was extracted from the aqueous solution with ethyl acetate and the concentration in the extract was quantified by GC/MS. The extraction efficiency of aniline into ethyl acetate was  $99.5\pm 2.5\%$ .

For the identification of organic oxidation products by LC-MS/MS, samples of 1 mL  $\text{MnO}_2$ -suspension were reductively dissolved by ascorbic acid (0.3 M, pH 13) and diluted with 9 mL of nanopure water. Aqueous samples were processed following a modified procedure of Kern et al.<sup>70</sup> Inorganic salts were removed by solid phase extraction (SPE, HLB Extraction Cartridges,  $100\ \mu\text{m}$ , Oasis, Waters AG, U.S.) of the dilute aqueous samples. Organic analytes were eluted from the cartridges with MeOH, dissolved in  $\text{H}_2\text{O}$  and filtered with a  $0.45\ \mu\text{m}$  RC filter prior to LC-MS/MS.

## Homogeneous oxidation

Oxidation of substituted anilines in homogeneous solution was performed in an anoxic glovebox using anoxic stock and buffer solutions identical to experiments with  $\text{MnO}_2$ -suspensions at pH 4.0 and 5.1 (see above), except for the addition of variable amounts of electrochemically produced oxidant instead of  $\text{MnO}_2$  to achieve different degrees of contaminant conversion. The oxidant  $\text{ABTS}^{\bullet-}$  was generated through direct electrochemical oxidation of the  $\text{ABTS}^{2-}$  at an  $E_h$  of 0.667 V (SHE) in the electrochemical cell as described in Aeschbacher et al.<sup>3</sup> The ABTS dianion was added to buffer solutions (0.1 M phosphate at pH 7.0 and 0.1 M acetate at pH 4.0 in 0.1 M KCl as supporting electrolyte) and the oxidative working current was monitored until it dropped below background val-

ues (30  $\mu$ A). The ABTS $^{\bullet-}$  was used immediately after generation. All samples containing the residual substituted aniline were stored at 4°C until concentration and isotope ratio analysis.

### Direct electrochemical oxidation

All electrochemical experiments were conducted in an anoxic glovebox using anoxic stock and buffer solutions (0.1 M acetate and phosphate for pH 4.0 and 7.0, respectively) containing 0.1 M KCl as background electrolyte (see ref<sup>3</sup> for procedures). Direct electrochemical oxidation of the aromatic amines was performed in an electrolysis cell equipped with a glassy carbon (GC) working electrode, an Ag/AgCl reference electrode, and a coiled platinum wire auxiliary electrode as described in<sup>3</sup>. Currents were measured with an CHInstruments 630C instrument (Austin, TX, USA) and the potential was controlled by an Autolab PG 302 instrument (EcoChemieB.V., Utrecht, NL). The electrolysis cell was filled with the corresponding buffer solution and equilibrated at the desired reduction potential ( $E_h$  between 0.777 and 0.957 V vs. SHE, Table 3.1) applied to the working electrode. The oxidation was initiated by the addition of defined amounts of substituted aniline stock solution. At given time intervals, 2 mL aqueous samples were withdrawn and stored outside the glovebox at 4°C until further analysis.

### 3.2.2 Analytical methods

#### Chemical analysis

Concentration measurements of substituted anilines were performed by reversed-phase HPLC (Supelcosil LC-18, 25 cm  $\times$  4.6 mm, 5  $\mu$ m, Supelco) and UV-VIS detection at wavelengths corresponding to the absorption maxima of the anilines. Different eluent mixtures  $\text{KH}_2\text{PO}_4/\text{MeOH}$  were used for each compound varying between 40/60% to 70/30% at a flow rate of 1 mL min<sup>-1</sup> and sample injection volume of 10  $\mu$ L. Quantification of substituted anilines extracted into ethyl acetate was conducted on a GC/MS (Ultra Trace GC and DSQII, Thermo Electron Corporation) upon on-column injection using the instrumental setup and settings described previously.<sup>134</sup>

The analytical procedure for identification of transformation products was adapted from Kern et al.<sup>70</sup> The measurements were performed by liquid chromatography coupled to an LTQ (Linear Trap Quadrupole) Orbitrap mass spectrometer (Thermo Electron Corporation) with electrospray ionization (LC-MS/MS). For liquid chromatographic separation an XBridge C-18 column was used (2.1  $\times$  50 mm, 3.5  $\mu$ m particle size, Waters)

and a gradient was run from H<sub>2</sub>O/MeOH 90/10% to 5/95% containing 0.1% formic acid. Identification of coupling products was performed only qualitatively due to lack of commercial standards. To this end exact masses of expected reaction products were extracted from the chromatograms in order to obtain MS/MS-fragment spectra. Based on the exact molecular mass and fragmentation pattern of each detected product, most probable molecular structures were postulated and these are shown in Figure S3.1.

The aqueous Mn<sup>2+</sup>-concentration was measured by inductively coupled plasma mass spectrometry (ICP/MS 7500cx, Agilent Technologies). All samples were diluted with 0.1 M HNO<sub>3</sub> to final concentrations between 10 and 1000 µg Mn<sup>2+</sup> L<sup>-1</sup>.

### Stable isotope ratio measurements

Stable N and C isotope signatures ( $\delta^{15}\text{N}$  and  $\delta^{13}\text{C}$ ) of the substituted anilines were determined by solid-phase microextraction (SPME) coupled to a GC/IRMS (gas chromatography isotope-ratio mass spectrometry) with combustion interface.<sup>134</sup> SPME fiber material and extraction conditions were polydimethylsiloxane/divinylbenzene (PDMS/DVB, Supelco) and 45 min at 40 °C for all compounds except OCH<sub>3</sub>-substituted anilines. The latter required DVB-Carboxen-PDMS coated fibers and 45 min extractions at 70 °C. All N and C isotope signatures are reported as arithmetic mean ( $\pm 1\sigma$ ) of triplicate measurements relative to air ( $\delta^{15}\text{N}_{\text{air}}$ ) and Vienna PeeDee Belemnite ( $\delta^{13}\text{C}_{\text{VPDB}}$ ), respectively, in per mil (‰). To account for uncertainty due to instrument nonlinearity<sup>83</sup> all samples were diluted to concentrations yielding constant peak amplitudes (1-2 V for <sup>15</sup>N- and 4-5 V for <sup>13</sup>C-analysis). Accuracy of compound-specific isotope analysis was verified via standard bracketing procedures using a calibrated in-house standard (aniline) of known N and C isotope ratios.<sup>134</sup>

### 3.2.3 Data evaluation

Bulk compound N and C isotope enrichment factors,  $\epsilon_{\text{N}}$  and  $\epsilon_{\text{C}}$ , were derived from linear regression analysis of  $\delta^{15}\text{N}$ - and  $\delta^{13}\text{C}$ -values, respectively, vs. fractional amount of reactant conversion.<sup>28</sup> Data from replicate experiments were combined using the Pitman estimator<sup>129</sup> as shown previously.<sup>143</sup> While the extent of C isotope fractionation is reported as average  $\epsilon_{\text{C}}$  for all C atoms present in the reactant molecules, interpretation of N isotope fractionation is based on position-specific apparent <sup>15</sup>N-kinetic isotope effects, AKIE<sub>N</sub>, calculated from Equation 3.1. Uncertainties associated with  $\epsilon_{\text{N}}$ -,  $\epsilon_{\text{C}}$ -, AKIE<sub>N</sub>-values correspond to 95% confidence intervals.

$$\text{AKIE}_N = \frac{1}{1 + \epsilon_N/1000} \quad (3.1)$$

To account for effects of substituted aniline protonation on the observed  $\text{AKIE}_N$ s, data obtained at pH-values below 7.0 were modeled as follows (see SI to Chapter 3 for full mathematical derivation). N isotope fractionation of substituted aniline cations,  $\text{BH}^+$ , originates from the combination of an isotope-sensitive deprotonation step (Equation 3.2,<sup>134</sup>) and the subsequent oxidation reaction of the neutral species, B (Equation 3.3).



where  $k_1$ ,  $k_2$  and  $k_3$  are the reaction rate constants of the elementary reactions and P stands for the radical products of the oxidation reaction. Using the steady-state treatment for the proton-exchange pre-equilibrium, the rate constant for the reaction of protonated substituted aniline species  $k_{\text{obs}}^{\text{BH}^+}$  is given by Equation 3.4.

$$k_{\text{obs}}^{\text{BH}^+} = \frac{k_1 \times k_3}{k_2[\text{H}^+] + k_3} \quad (3.4)$$

where  $[\text{H}^+]$  is the proton concentration. Rewriting Equation 3.4 for  $^{14}\text{N}$ - and  $^{15}\text{N}$ -isotopologues (see SI to Chapter 3) reveals that an apparent  $^{15}\text{N}$ -kinetic isotope effect associated with species  $\text{BH}^+$ ,  $\text{AKIE}_N^{\text{BH}^+}$ , is the product of the deprotonation  $^{15}\text{N}$ -equilibrium isotope effect,  $\text{EIE}_N^{\text{BH}^+}$ , and the  $\text{AKIE}_N$  of the neutral substituted aniline,  $\text{AKIE}_N^{\text{B}}$  (Equation 3.5).

$$\text{AKIE}_N^{\text{BH}^+} = \text{EIE}_N^{\text{BH}^+} \times \text{AKIE}_N^{\text{B}} \quad (3.5)$$

As a consequence of the simultaneous reactions of protonated and neutral substituted aniline species, the overall observable  $\text{AKIE}_N$  is the weighted average of the two fractions and their respective isotope effect. In Equation 3.6,  $f_{\text{BH}^+}$  is the fraction of protonated compound, which equals  $\left(1 + 10^{(\text{pH} - \text{pK}_{\text{BH}^+})}\right)^{-1}$  (see Table S3.3 for  $\text{pK}_{\text{BH}^+}$ ).

$$\text{AKIE}_N = f_{\text{BH}^+} \times \text{EIE}_N^{\text{BH}^+} \times \text{AKIE}_N^{\text{B}} + (1 - f_{\text{BH}^+}) \times \text{AKIE}_N^{\text{B}} \quad (3.6)$$

### 3.2.4 Computational methods

The gas-phase geometries of all molecular species were fully optimized at the density functional (DFT) level using the gradient-corrected Perdew-Wang exchange and correlation functionals<sup>114,115</sup> as modified by Adamo and Barone<sup>1</sup> using either the 6-311+G(d) or 6-311+G(2df,2p) basis sets.<sup>51</sup> Stationary points were confirmed as minima or transition-state (TS) structures by analytical calculation of vibrational frequencies, which were also used in the construction of ideal-gas, rigid-rotator, harmonic oscillator partition functions, from which thermal contributions to free energies  $G$  were computed.<sup>21</sup> For outer-sphere electron-transfer rate constants,  $^{15}\text{N}$ -kinetic isotope effects ( $\text{KIE}_{\text{N}}$ ) were computed essentially according to the method of Kavner et al.<sup>68</sup> For hydrogen-atom transfer reactions involving active oxygen species, KIEs were computed from canonical transition-state theory. Full details of all  $\text{KIE}_{\text{N}}$  calculations are provided in the SI to Chapter 3.

## 3.3 Results and Discussion

### 3.3.1 Isotope fractionation associated with the oxidation of substituted anilines in $\text{MnO}_2$ -suspensions.

We observed measurable N isotope fractionation during the oxidation of neutral, substituted anilines in suspensions of  $\text{MnO}_2$  at pH 7.0, while C isotope composition did not change significantly. Nitrogen isotope fractionation was always *inverse*, that is,  $^{15}\text{N}$ -containing isotopologues reacted faster than molecules with  $^{14}\text{N}$  leading to a decreasing  $\delta^{15}\text{N}$  of the reactant with increasing conversion (Figure 3.1b). The extent of N isotope fractionation observed in suspensions of  $\text{MnO}_2$  did not exceed  $-12\text{‰}$  compared to the initial  $\delta^{15}\text{N}$  while the reactant turnover approached 55 to 88% (Table 3.1). Limited turnover was due to the biphasic disappearance kinetics of substituted aniline oxidation by  $\text{MnO}_2$  (Figure 3.1a), which, as reported previously,<sup>72,78,160</sup> exhibited fast initial transformation followed by a decreasing rate of reaction. Increasing the concentration ratio of  $\text{MnO}_2$  to substituted aniline slightly increased the oxidative turnover and thus the observable range of N isotope fractionation (Figure 3.1b) but did not influence the N isotope enrichment factors,  $\epsilon_{\text{N}}$ , which quantify the extent of isotope fractionation per incremental amount of reacted substrate (Figure 3.1b and 3.11c). As shown in Figure 3.1c,  $\epsilon_{\text{N}}$ -values of aniline oxidation were identical within experimental error. This observation suggests that despite biphasic reaction kinetics, N isotope fractionation was associated

with the identical elementary reaction step(s) of aromatic amine oxidation independent of the substituted aniline to oxidant ratio.

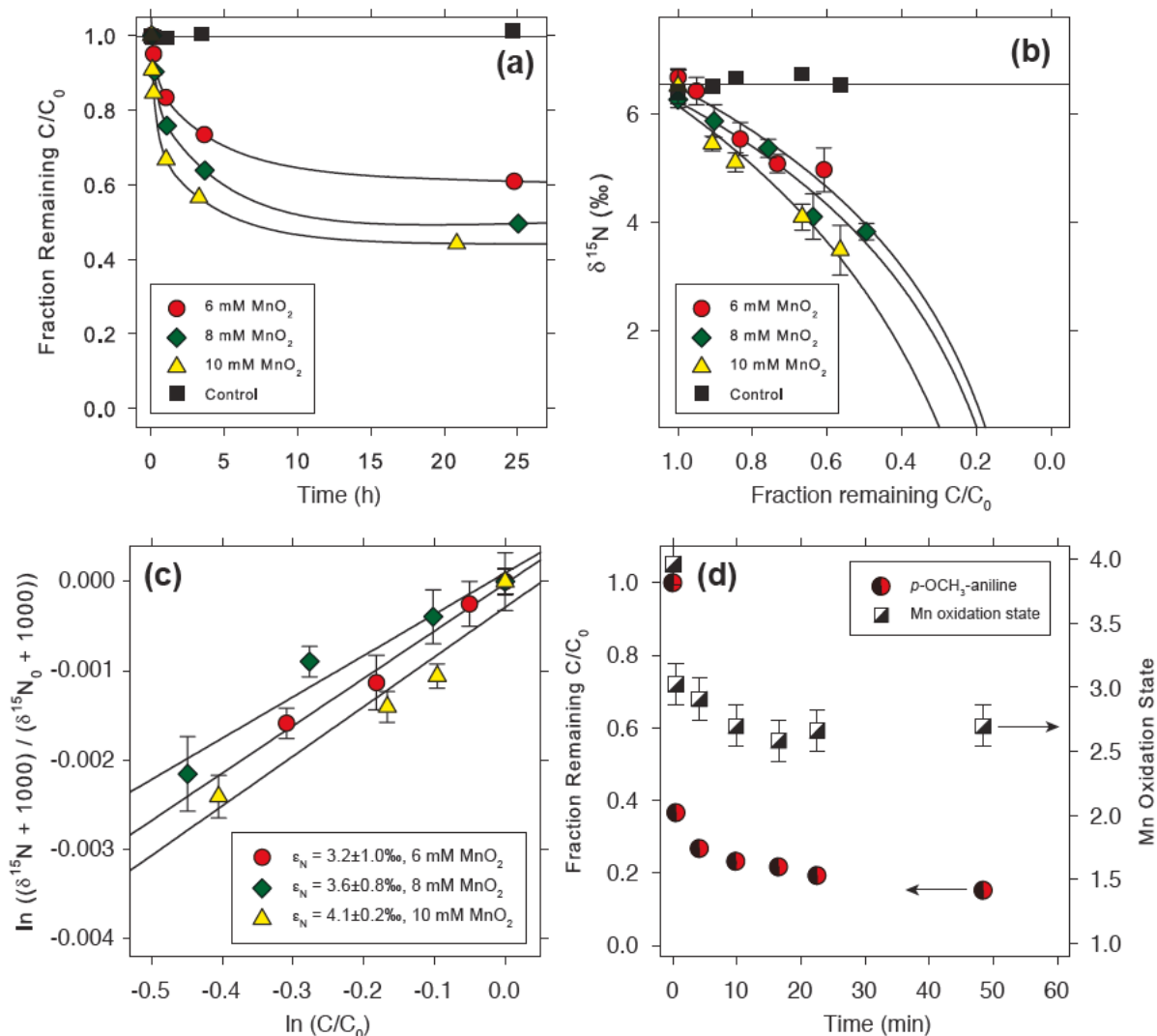


Figure 3.1: (a) Kinetics of aniline oxidation ( $C_0 = 0.6$  mM) in suspensions containing 6, 8, and 10 mM  $MnO_2$  at pH 7.0. Uncertainty of the concentration measurements ( $\pm\sigma$ ) is 2% (error bars are smaller than the markers); (b) N isotope fractionation during aniline oxidation in various  $MnO_2$ -suspensions:  $\delta^{15}N$ -values vs fraction of remaining reactant ( $C/C_0$ ); (c) linearized N isotope fractionation trends used for calculation of bulk N isotope enrichment factors:  $\epsilon_N$ ; (d) Oxidation of  $p$ -OCH<sub>3</sub>-aniline (4.8 mM initial concentration) in 10 mM  $MnO_2$  suspension at pH 7.0 and average Mn oxidation state.

The occurrence of a single isotope fractionating elementary reaction step was confirmed with a series of complementary experiments, which showed that the biphasic reaction kinetics were due to a decrease in  $MnO_2$  reactivity rather than a change in sub-

stituted aniline oxidation mechanism during the time course of the reaction. First, the decreasing rate of contaminant disappearance correlated with the decreasing average particulate Mn oxidation state monitored by X-ray absorption near edge structure (XANES) measurements, as illustrated in Figure 3.1d for the oxidation of *p*-OCH<sub>3</sub>-aniline by MnO<sub>2</sub>. The average Mn oxidation state decreased to 2.6 during the time course of the reaction pointing to an increased share of reduced Mn species in the mineral including Mn(II) adsorbed on the mineral surface. The corresponding decrease of average Mn oxidation state is indicative of the decreasing reactivity of the MnO<sub>2</sub>-particles. The same process has been invoked previously for the reductive dissolution of MnO<sub>2</sub> (e.g., by arsenious acid, H<sub>3</sub>AsO<sub>3</sub>), where formation of intermediate Mn(III)oxyhydroxide layers at the mineral surface blocked the access to reactive oxidized Mn(IV) sites and led to the overall decrease of the MnO<sub>2</sub> reduction rate.<sup>102,163</sup> Measurements of dissolved Mn<sup>2+</sup> at different time points of unsubstituted aniline oxidation by MnO<sub>2</sub> support the interpretation of XANES-data (Figure S3.3). After a conversion of > 400 μM of the initial 600 μM of aniline, only 130 μM of Mn<sub>aq</sub><sup>2+</sup> were recovered in solution. Therefore, only 65% of the oxidation equivalents of aniline could be detected as dissolved species, leaving Mn<sup>3+</sup>- and Mn<sup>2+</sup>-species bound to the mineral. Second, identical aniline disappearance kinetics were observed regardless whether aniline was measured in the supernatant or after dissolving the MnO<sub>2</sub>-particles (Figure S3.3). Similarly, no inhibition of the reaction was found if Mn<sup>2+</sup> and azobenzene had been added to the reactors in concentrations corresponding to the initial aniline oxidation-equivalents (Figure S3.4). These experiments indicate that under the experimental conditions, neither adsorption of aniline nor of co-solutes to MnO<sub>2</sub> did influence the rate of aniline oxidation.<sup>72,78</sup> Finally, identical ε<sub>N</sub>-values for different MnO<sub>2</sub>-loadings provide evidence that an electron transfer process is rate-limiting rather than any surface complex formation between the substituted aniline and the mineral. The assumption of an electron transfer as predominant rate-limiting step is also supported by the reported correlation of the half-wave potentials and substituent Hammett constants of the aromatic amines with experimentally determined initial oxidation rates.<sup>72,78</sup>

### 3.3.2 Substituent effects on AKIE<sub>N</sub>s and implications for the reaction mechanism

On the basis of the above discussion, the observable N isotope fractionation with ε<sub>N</sub>-values between 1.3‰ and 8.3‰ can be attributed to the oxidation of the N atom



in neutral substituted anilines resulting in apparent  $^{15}\text{N}$ -kinetic isotope effects,  $\text{AKIE}_\text{N}$  between 0.9987 and 0.9927 (Table 3.1, entries 1-8). The small C isotope fractionation represents an average secondary isotope effect for the C atoms that were not directly involved in the reaction ( $\epsilon_\text{C}$  of  $-1.1\pm 0.1\%$ , Figure S3.2).

We observed a marked influence of the position and type of the aromatic substituent on  $\text{AKIE}_\text{N}$ -values. *Meta*-substitution with  $-\text{CH}_3$  or  $-\text{OCH}_3$ -groups did not cause the  $\text{AKIE}_\text{N}$ -value to deviate significantly from that of aniline ( $0.9960\pm 0.0009$ ). Electron-donating substituents in *ortho* or *para* position, however, led to larger N isotope fractionation (lowest  $\text{AKIE}_\text{N}$  of  $0.9927\pm 0.0012$  for *p*- $\text{OCH}_3$ -aniline, entry 7, Table 3.1) compared to unsubstituted aniline, while electron-accepting substituents caused the opposite trend ( $\text{AKIE}_\text{N}$  of  $0.9987\pm 0.0004$  for *p*-Cl-aniline, entry 8, Table 3.1). The identical  $\text{AKIE}_\text{N}$ -values within experimental error found for *o*- $\text{CH}_3$  and *p*- $\text{CH}_3$ -aniline as well as *o*- $\text{OCH}_3$  and *p*- $\text{OCH}_3$ -aniline, respectively, indicate that substituents in these positions exhibited the same effects on the bonds to N during its oxidation.

The observed inverse isotope effects can be rationalized by the formation of a radical intermediate after one-electron oxidation, which is delocalized over the aromatic ring causing the C–N-bond to become stronger in the transition state, due to the formation of a partial imine-type bonding of N in the subsequent intermediates (illustrated by the resonance structures in Figure 3.2). Higher infrared stretching frequencies of C=N vs C–N bonds<sup>120</sup> imply stronger bonds to N in imines and support this interpretation. Similar findings of inverse N isotope fractionation have been reported for reactions in which additional bonds were formed to aromatic and heterocyclic N atoms and in amino acids.<sup>37,95,121,134</sup> In addition, the formation of radical intermediates gives rise to the sensitivity of the  $\text{AKIE}_\text{N}$ -values for aromatic substitution. The substituents' electron donating and accepting properties affect the radical stability, the preferential radical localization in *ortho*- and *para*-position, and thus the C–N bond strength in the transition state, which explains the observed variations of the  $\text{AKIE}_\text{N}$ . While electron donating substituents like *o*-/*p*- $\text{CH}_3$  and *o*-/*p*- $\text{OCH}_3$  cause the C–N-bond to become stronger in the transition state, electron-withdrawing *p*-Cl substitution has only moderate impact on C–N bonding and thus the magnitude of the  $\text{AKIE}_\text{N}$  compared to the unsubstituted aniline. Consequently, the lack of any radical stabilization and thus localization in *meta*-position is also responsible for the insensitivity of the  $\text{AKIE}_\text{N}$  for *meta*-substituents. Analysis of reactor solutions for reaction products by LC-MS/MS confirmed these substituent effects indirectly. As proposed in previous studies,<sup>78,159</sup> head-to-head (N–N), head-to-tail (N–C) and tail-to-tail (C–C) products were found in the reduced as well as in the oxidized form,



where radical coupling occurred at the *ortho*- and *para*- position (Figure S3.1).

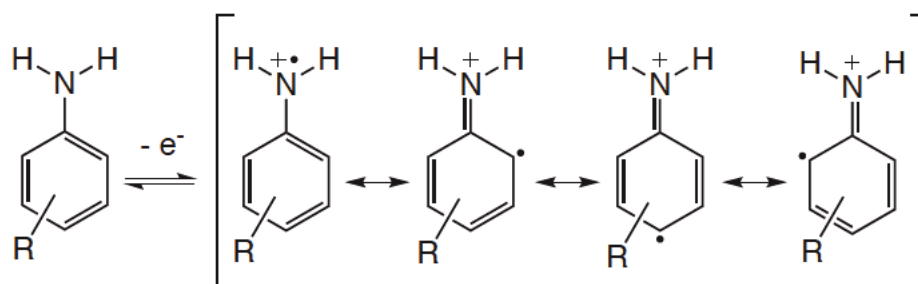


Figure 3.2: Resonance structures of aminium radical species after one-electron oxidation

### 3.3.3 Reference experiments and density functional theory calculations

Independent evidence for assigning the one-electron oxidation and subsequent partial imine-bond formation as isotope-sensitive and rate-limiting reaction step was obtained from measurements of N isotope fractionation of selected substituted anilines in homogeneous solution, in electrochemical experiments, and through calculation of  $\text{KIE}_\text{N}$  using density functional theory. Despite the different experimental conditions, oxidation of aniline and *p*- $\text{CH}_3$ -aniline by  $\text{ABTS}^{\bullet-}$  and at glassy carbon electrode surfaces at pH 7.0 also resulted in inverse  $\text{AKIE}_\text{N}$ s as observed in  $\text{MnO}_2$ -suspensions (Table 3.1).  $\text{AKIE}_\text{N}$ -values pertinent to electrochemical oxidation of *p*- $\text{CH}_3$ -aniline at oxidation potentials differing by 180 mV, which corresponds to three orders of magnitude in electron transfer driving force, did vary by less than 2.5‰ (Figure 3.3a, Table 3.1, entries 19-22). The insensitivity of N isotope fractionation towards oxidation potential lends further support to the hypothesis that N isotope fractionation during substituted aniline oxidation is not caused exclusively by the electron transfer but also by hybridization changes at the N atom and change in C–N bond strength during formation of partial imine bonds. This interpretation is also supported by theoretical considerations.

Density functional calculations were undertaken to predict  $\text{KIE}_\text{N}$ s that would be expected under conditions of outer-sphere electron transfer (ET) and hydrogen-atom transfer (HAT) by an active oxygen species (Table S3.1). In the former case, isotopically sensitive rate constants were predicted from Marcus theory; in the latter case, such constants were predicted from canonical transition-state theory (see SI to Chapter 3 for full theoretical details). Table S3.1 (entries 25-37) provides the predicted  $\text{KIE}_\text{N}$ s for aniline and various substituted cases. In general, there is good quantitative agreement

between the predicted  $\text{KIE}_{\text{NS}}$  for ET and those determined experimentally (at pH 7.0, see electrochemical data below) with electrodes having reduction potentials similar to those employed in the calculations. The HAT- $\text{KIE}_{\text{NS}}$  are also generally in good quantitative agreement with those determined experimentally at pH 7.0. All predicted  $\text{KIE}_{\text{NS}}$  are inverse (with the exception of HAT from *o*- $\text{NO}_2$ -aniline by hydroxyl radical), reflecting the increased  $\text{C}_1\text{--N}$  bonding in the anilinium radical cation or HAT transition state structure compared to the reactant aniline (Figure 3.2, for quantitative comparisons, see computed geometrical and bond order data in Table S3.2. The quantitative similarity for the two processes is primarily attributable to the small change in this bonding character, which leads to predicted inverse  $\text{KIE}_{\text{NS}}$  of substantially less than 10‰ in every instance consistent with experiments. Thus, theory indicates that the observed  $\text{AKIE}_{\text{NS}}$  cannot be considered to rule out HAT pathways in substituted aniline oxidation for cases where active oxygen species might be generated, but neither do they need to be invoked given the good agreement between theory and electrochemical oxidation results where ET processes would be likely to be the only ones active. We note that neither the computational predictions for outer-sphere ET nor those for HAT show substituent effects consistent with those observed experimentally. This must be assigned to the simplifications inherent in the computational models, which make it challenging to reproduce the small substituent effects.

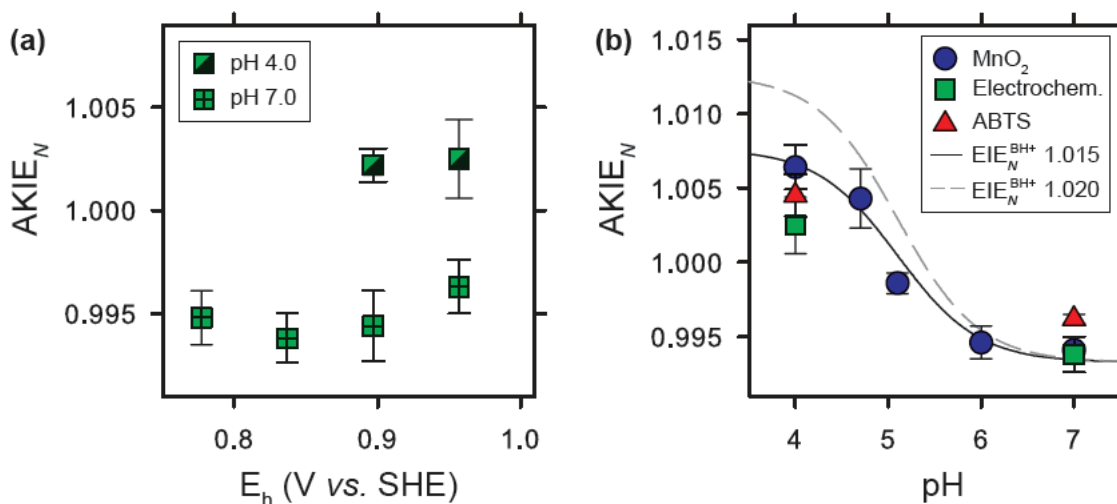


Figure 3.3: (a) Observed  $\text{AKIE}_{\text{N}}$  associated with the electrochemical oxidation of *p*- $\text{CH}_3$ -aniline at working electrode potential,  $E_{\text{h}}$ , between 0.78 and 0.96 V at pH 4.0 and 7.0 (see Table 3.1 for details); (b) Observed  $\text{AKIE}_{\text{N}}$  of *p*- $\text{CH}_3$ -aniline ( $\text{pK}_{\text{BH}^+}$  5.10) for oxidation by  $\text{MnO}_2$ ,  $\text{ABTS}^{\bullet-}$  (2,2'-azino-bis(3-ethylbenzthiazoline-6-sulfonic acid), and at a glassy carbon electrode in the pH-range 4.0 to 7.0.

Table 3.1: Bulk N isotope enrichment factors,  $\epsilon_N$ , Apparent <sup>15</sup>N-Kinetic Isotope Effects, AKIE<sub>N</sub>, of Substituted Anilines in Various Experimental Systems.

Entry	Compound	pH (–)	E <sub>h</sub> (V vs. SHE)	Conversion <sup>a</sup> (%)	$\epsilon_N$ <sup>b</sup> (‰)	AKIE <sub>N</sub> <sup>b</sup> (–)
<b>MnO<sub>2</sub>-suspensions</b>						
1	aniline <sup>c</sup>	7.0		55	3.6 ± 0.6	0.9960 ± 0.0009
2	<i>o</i> -CH <sub>3</sub> -aniline	7.0		65	6.0 ± 0.4	0.9948 ± 0.0009
3	<i>m</i> -CH <sub>3</sub> -aniline	7.0		53	3.7 ± 0.9	0.9963 ± 0.0006
4	<i>p</i> -CH <sub>3</sub> -aniline	7.0		63	6.0 ± 0.2	0.9941 ± 0.0003
5	<i>o</i> -OCH <sub>3</sub> -aniline	7.0		65	7.6 ± 0.2	0.9925 ± 0.0004
6	<i>m</i> -OCH <sub>3</sub> -aniline	7.0		52	4.9 ± 0.2	0.9952 ± 0.0001
7	<i>p</i> -OCH <sub>3</sub> -aniline	7.0		54	8.3 ± 0.6	0.9927 ± 0.0012
8	<i>p</i> -Cl-aniline	7.0		88	1.3 ± 0.2	0.9987 ± 0.0004
9	<i>p</i> -CH <sub>3</sub> -aniline	6.0		91	5.4 ± 1.1	0.9946 ± 0.0011
10	<i>p</i> -CH <sub>3</sub> -aniline	5.1		35	1.1 ± 0.4	0.9986 ± 0.0007
11	<i>p</i> -CH <sub>3</sub> -aniline	4.7		71	-4.3 ± 2.0	1.0043 ± 0.0020
12	<i>p</i> -CH <sub>3</sub> -aniline	4.0		53	-6.6 ± 0.7	1.0064 ± 0.0015
13	<i>p</i> -OCH <sub>3</sub> -aniline	4.0		45	-5.3 ± 0.9	1.0052 ± 0.0015
14	<i>p</i> -Cl-aniline	4.0		75	-1.9 ± 0.3	1.0019 ± 0.0006
<b>ABTS in homogeneous solution</b>						
15	aniline	7.0		75	2.3 ± 0.8	0.9977 ± 0.0021
16	<i>p</i> -CH <sub>3</sub> -aniline	7.0		80	3.8 ± 0.1	0.9962 ± 0.0003
17	aniline	4.0		74	-1.0 ± 0.2	1.0010 ± 0.0006
18	<i>p</i> -CH <sub>3</sub> -aniline	4.0		78	-4.5 ± 0.5	1.0045 ± 0.0014
<b>Electrochemical oxidation</b>						
19	<i>p</i> -CH <sub>3</sub> -aniline	7.0	0.777	56	5.2 ± 0.5	0.9948 ± 0.0013
20	<i>p</i> -CH <sub>3</sub> -aniline	7.0	0.837	58	6.2 ± 0.4	0.9938 ± 0.0012
21	<i>p</i> -CH <sub>3</sub> -aniline	7.0	0.897	50	5.6 ± 0.7	0.9944 ± 0.0017
22	<i>p</i> -CH <sub>3</sub> -aniline	7.0	0.957	52	3.7 ± 0.5	0.9963 ± 0.0013
23	<i>p</i> -CH <sub>3</sub> -aniline	4.0	0.897	73	-2.2 ± 0.3	1.0022 ± 0.0008
24	<i>p</i> -CH <sub>3</sub> -Aniline	4.0	0.957	71	-2.5 ± 0.7	1.0025 ± 0.0019

<sup>a</sup> Decrease of reactant concentration / initial concentration × 100;

<sup>b</sup> Uncertainties correspond to 95%-confidence intervals; <sup>c</sup>  $\epsilon_N$ - and AKIE<sub>N</sub>-values (Figure 3.1c) were derived using the Pitman estimator for combined data sets.

### 3.3.4 Influence of substituted aniline speciation on $\text{AKIE}_\text{N}$

Because the deprotonation of substituted anilines is associated with a normal  $^{15}\text{N}$ -equilibrium isotope effect,  $\text{EIE}_\text{N}$ , between 1.017 and 1.021,<sup>134</sup> we investigated the consequences of N-atom protonation on the observable N isotope fractionation trends during oxidation with selected *para*-substituted anilines in the pH-range 4.0–7.0. As shown in Table 3.1 (entries 4, 9–12) for *p*-CH<sub>3</sub>-aniline, the  $\text{AKIE}_\text{N}$  increased to almost unity at pH-values matching the  $\text{pK}_{\text{BH}^+}$  and isotope fractionation became normal once the protonated species ( $\text{BH}^+$ ) prevailed. Our data imply that  $^{14}\text{N}$ -isotopologues reacted faster at  $\text{pH} < \text{pK}_{\text{BH}^+}$  while they are outcompeted by  $^{15}\text{N}$ -isotopologues at higher solution pH. The same trend was found for *p*-OCH<sub>3</sub>-aniline (entries 7 and 13) and *p*-Cl-aniline (entries 8 and 14). Assuming that N atom oxidation can only occur from the neutral species, we propose that pH-dependent N isotope fractionation is due to a combined *normal*  $^{15}\text{N}$ -equilibrium isotope effects pertinent to the deprotonation of the substituted anilinium cation ( $\text{BH}^+$ , Equation 3.2) and the *inverse* apparent  $^{15}\text{N}$ -kinetic isotope effect associated with the oxidation of the neutral species (B, Equation 3.3) as described in Equation 3.6.

Fitting the data for *p*-CH<sub>3</sub>-aniline in Table 3.1 to Equation 3.6 adequately describes the trends of observable  $\text{AKIE}_\text{N}$  at different pH-values of the  $\text{MnO}_2$ -suspensions (Figure 3.3b). The calculated  $\text{AKIE}_\text{N}^\text{B}$  of 0.9933 agrees well with the observed  $\text{AKIE}_\text{N}$  measured at pH 7.0 (entry 4, Table 3.1). Deviations at pH-values below the  $\text{pK}_{\text{BH}^+}$  imply that the  $\text{EIE}_\text{N}^{\text{BH}^+}$  is smaller (1.015) than proposed previously but still within the experimental uncertainty of the  $\text{EIE}_\text{N}^{\text{BH}^+}$  derived for *p*-CH<sub>3</sub>-aniline ( $1.0199 \pm 0.0040$ <sup>134</sup>) supporting agreement of Equation 3.6 with experimental data. Our interpretation of the pH-dependent, observable  $\text{AKIE}_\text{N}$  is supported by the results from reference experiments regarding the electrochemical and homogeneous oxidation of aniline and *p*-CH<sub>3</sub>-aniline at pH 4.0 and 7.0. The trends of  $\text{AKIE}_\text{N}$  vs pH for oxidation at glassy carbon electrode surfaces and by  $\text{ABTS}^{\bullet-}$  were very similar to the ones observed in  $\text{MnO}_2$ -suspensions (Figure 3.3b, Table 3.1). These results confirm that at pH-values below the  $\text{pK}_{\text{BH}^+}$ , N isotope fractionation approaches the product of equilibrium and kinetic  $^{15}\text{N}$ -isotope effects (Equation 3.6), where the measured  $\text{AKIE}_\text{N}$  values are dominated by the normal EIE. As a final check, we evaluated the predicted KIEs for HAT from protonated anilines by active oxygen species  $\bullet\text{OH}$  /  $\bullet\text{OOH}$  (Table S3.1, entries 38–43). In all cases, N isotope effects were predicted to be inverse (Table S3.1), providing further evidence that the observed normal N isotope effects reflect acid/base partitioning prior to oxidation of the conjugate base.

### 3.4 Environmental Significance

Our study illustrates that oxidation of primary aromatic amino groups in organic contaminants is accompanied by a small and measurable N isotope fractionation thus enabling new avenues for the assessment of degradation reactions at N-containing functional groups. Because the  $pK_{BH^+}$  of many aromatic amines are in the range of pH-values encountered in many aquatic systems, the observable N isotope fractionation will be modulated substantially by the compound's acid/base equilibria. Isotope fractionation may even vanish under conditions where contributions from *normal*  $EIE_N$  associated with aromatic deprotonation and *inverse*  $AKIE_N$  of N atom oxidation cancel each other out. This variability of N isotope fractionation slightly complicates the application of CSIA in that the contaminant's  $pK_{BH^+}$  and solution pH have to be taken into account. The systematic trends of  $AKIE_N$ -values, on the other hand, provide a new line of evidence for the identification of contaminant degradation processes via reactions of primary aromatic amino groups.

Nitrogen isotope enrichment factors below 10‰ at the reactive position, as reported in this study, imply that  $\delta^{15}N$ -measurements should be carried out with small total uncertainties ( $< \pm 0.5\text{‰}$ ) and require that N isotope fractionation is not diluted by many non-reactive N atoms in a contaminant. The impact of substituent properties on  $AKIE_N$ -values suggest that contaminant-specific  $\epsilon_N$ -values will be required to assess their oxidation processes by CSIA. The compound-specific N isotope fractionation behavior contrasts earlier observations for the reduction of aromatic nitro groups,<sup>49,57</sup> which found  $AKIE_N$ -values that were largely independent of the compound's molecular structure. The substituent-dependence might, together with the influence of acid/base equilibria, prove indicative for the identification of N aryl oxidation processes. Further studies targeting N isotope fractionation in alternative contaminant transformation processes such as oxidative N-dealkylations and nucleophilic additions are warranted to evaluate the proposed trends of N isotope effects.

### Acknowledgement

This work was supported by the Swiss National Science Foundation (grant no. 200020-116447/1 to T.B.H.) and the U.S. National Science Foundation (CHE-0952054 to C.J.C). We thank Jakov Bolotin for experimental support, Michael Aeschbacher and Michael Sander for supporting the electrochemical experiments, Michael Plötze for assisting the

BET- and XRD-measurements, Brian Sinnet for his help with  $\zeta$ -potential measurements, Susanne Kern and Heinz Singer for assisting the LC-MS/MS-measurements and Maarten Nachtegaal and Markus Janousch for conducting the XANES-measurements. We acknowledge XD10A SuperXAS beamline of the SLS-PSI for the provision of beam time.

## Supporting Information to Chapter 3

## Chemicals

The chemicals used for this study were purchased from various manufacturers and used without further treatment. The aromatic amines used were aniline (99.5%, Fluka; Buchs SG, Switzerland), *p*-Cl-aniline (99%, Fluka), *o*-CH<sub>3</sub>-aniline (99.5%, Merck AG; Dietikon, Switzerland), *m*-CH<sub>3</sub>-aniline (99.5%, Aldrich; Steinheim, Germany), *p*-CH<sub>3</sub>-aniline (99%, Merck), *o*-OCH<sub>3</sub>-aniline (99%, Aldrich), *m*-OCH<sub>3</sub>-aniline (97%, Aldrich) and *p*-OCH<sub>3</sub>-aniline (99%, Aldrich). Further azobenzene (99%, Sigma-Aldrich; Seelze, Germany) was used. For stock solutions and product analysis the solvents used were methanol (HPLC grade, Scharlau, Barcelona, Spain) and ethyl acetate (99.8%, Riedel-de Haen, Germany). The buffers used were potassium phosphate (KH<sub>2</sub>PO<sub>4</sub>, 99%, Riedel-de Haen), sodium acetate (NaC<sub>2</sub>H<sub>3</sub>O<sub>2</sub>, 99.5%, Riedel-de Haen). Salts used included sodium chloride (99.5%, Fluka), potassium chloride (>99.5%, Fluka), sodium permanganate monohydrate (NaMnO<sub>4</sub>·H<sub>2</sub>O, 97%, Sigma-Aldrich), potassium iodide (99%, Sigma-Aldrich), manganese(II)chloride tetrahydrate (MnCl<sub>2</sub>·4H<sub>2</sub>O, analysis purity, Merck) and L(+)-ascorbic acid sodium salt (99%, Sigma-Aldrich). For electrochemical experiments 2,2'-azino-bis(3-ethylbenzthiazoline-6-sulfonic acid)diammonium salt (>99%, Fluka) was used. Further solutions were sodium thiosulfate titration solution (0.05M, 99.9%, Fluka), hydrochloric acid (32%, impureness: 0.0005%, Sigma-Aldrich), sodium hydroxide (32%, impureness: 0.0001%, Fluka) and nitric acid (Suprapur, Merck). Starch from wheat (Fluka) was used as color-indicator. The carrier gas for GC analysis was helium and high-purity argon was used for deoxygenation of aqueous solutions and methanol (99.999%, Carbagas; Rümlang, Switzerland). All aqueous solutions were prepared with nanopure water (18.2 MΩ · cm, Barnstead NANOpure Diamond Water Purification System).

## Non-reactive substituted anilines

*p*-CF<sub>3</sub>- and *p*-NO<sub>2</sub>-aniline did not show sufficient reactivity in MnO<sub>2</sub>-suspension. Electrochemical oxidation was limited by the applicable working electrode potentials, which did not exceed 0.96 V (SHE). Under these experimental conditions, only the oxidation of *p*-CH<sub>3</sub>-aniline could be carried out.



## Synthesis of $\text{MnO}_2$

$\text{MnO}_2$  particles were synthesized through oxidation of  $\text{Mn}^{2+}$  by  $\text{MnO}_4^-$  according to the method of Murray.<sup>101</sup> Briefly, for the synthesis of 1 L of 10 mM  $\text{MnO}_2$ -suspension, 40 mL 0.1 M  $\text{NaMnO}_4$  and 80 mL 0.1 M  $\text{NaOH}$  were diluted to 0.5 L with nanopure water. 60 mL of a 0.1 M  $\text{MnCl}_2$  solution were added dropwise under continuous stirring.  $\text{MnO}_2$ -particles were subsequently allowed to settle at the flask bottom and the supernatant was decanted. The suspension was washed with nanopure water until the conductivity of the supernatant was smaller than  $2 \mu\text{S}\cdot\text{cm}^{-1}$ . Finally the suspension was washed twice with the buffer solution used in subsequent kinetic experiments.

## X-ray absorption near edge structure (XANES) measurements

X-ray absorption near edge structure (XANES) measurements carried out for determining the manganese oxidation state(s) in  $\text{MnO}_2$  during the reaction, were performed at the SuperXAS beamline of the Swiss Light Source (Paul Scherrer Insitut, Villigen, Switzerland). The SLS storage ring was operated in top-up-mode at a current of 400 mA with 2.4 GeV electrons. The Si(111) double crystal monochromator (DCM) was detuned to 50% of the maximum intensity to reject higher order harmonics and was calibrated by setting the first inflection point in the absorption spectrum of a Mn-metal foil to 6539 eV. Spectra were measured at room temperature and in transmission mode. Reference spectra of  $\text{MnCl}_2\cdot 4\text{H}_2\text{O}$ ,  $\text{Mn}_2\text{O}_3$ ,  $\text{MnO}_2(\text{s})$  and  $\text{NaMnO}_4$  with a formal oxidation state of II, III, IV and VII respectively were prepared as pressed powder pellets after dilution with cellulose. The edge position of the reference spectra was determined from the first derivative and used to calibrate the oxidation state. To quantify the Mn redox-state at different time steps of the reaction *p*- $\text{OCH}_3$ -aniline (4.8 mM) was spiked to 10 mM  $\text{MnO}_2$ -suspension and samples were taken at given time intervals using a  $0.2 \mu\text{m}$  RC filter. The  $\text{MnO}_2$ -particles were directly measured on the filter on the beamline. The time resolution for one scan was one minute in continuous mode.

## <sup>15</sup>N-Kinetic isotope effect of cationic substituted aniline species

The kinetic scheme for interpreting N isotope fractionation of cationic substituted anilines includes proton exchange pre-equilibrium (Equation S3.1) and oxidation of neutral compound (Equation S3.2) and corresponding kinetic rate laws (Equations S3.3–S3.5). BH<sup>+</sup>, B, H<sup>+</sup>, and P represent the cationic substituted aniline, its neutral form, protons, and oxidation products, respectively.



$$\frac{d[\text{BH}^+]}{dt} = -k_1[\text{BH}^+] + k_2[\text{B}][\text{H}^+] \quad (\text{S3.3})$$

$$\frac{d[\text{B}]}{dt} = +k_1[\text{BH}^+] - (k_2[\text{H}^+] + k_3)[\text{B}] \quad (\text{S3.4})$$

$$\frac{d[\text{P}]}{dt} = +k_3[\text{B}] \quad (\text{S3.5})$$

Using the steady-state assumption for transient concentration of [B], the total rate cationic and neutral substituted aniline disappearance, which corresponds to the rate of product formation, is:

$$[\text{B}] = \frac{k_1[\text{BH}^+]}{k_2[\text{H}^+] + k_3} \quad (\text{S3.6})$$

$$\frac{d[\text{P}]}{dt} = \frac{k_1 k_3}{k_2[\text{H}^+] + k_3} [\text{BH}^+] \quad (\text{S3.7})$$

Equation S3.7 can be re-written for two N isotopologues as Equation S3.8. The first term on the right-hand side of Equation S3.8 corresponds to the apparent <sup>15</sup>N-kinetic isotope effects associated with the disappearance of cationic, substituted aniline species, AKIE<sub>N</sub><sup>BH<sup>+</sup></sup> (Equation S3.9).

$$\frac{d[^{14}\text{N}\text{P}]/dt}{d[^{15}\text{N}\text{P}]/dt} = \frac{{}^{14}\text{N}k_1 {}^{14}\text{N}k_3 / \left( {}^{14}\text{N}k_2[\text{H}^+] + {}^{14}\text{N}k_3 \right)}{{}^{15}\text{N}k_1 {}^{15}\text{N}k_3 / \left( {}^{15}\text{N}k_2[\text{H}^+] + {}^{15}\text{N}k_3 \right)} \times \frac{[^{14}\text{N}\text{BH}^+]}{[^{15}\text{N}\text{BH}^+]} \quad (\text{S3.8})$$

$$\text{AKIE}_{\text{N}}^{\text{BH}^+} = \frac{{}^{14}\text{N}k_1 {}^{14}\text{N}k_3 / \left( {}^{14}\text{N}k_2[\text{H}^+] + {}^{14}\text{N}k_3 \right)}{{}^{15}\text{N}k_1 {}^{15}\text{N}k_3 / \left( {}^{15}\text{N}k_2[\text{H}^+] + {}^{15}\text{N}k_3 \right)} \quad (\text{S3.9})$$

$$= \frac{{}^{14}\text{N}k_1}{{}^{15}\text{N}k_1} \times \frac{{}^{14}\text{N}k_3}{{}^{15}\text{N}k_3} \times \frac{\left( {}^{15}\text{N}k_2[\text{H}^+] + {}^{15}\text{N}k_3 \right)}{\left( {}^{14}\text{N}k_2[\text{H}^+] + {}^{14}\text{N}k_3 \right)} \times \frac{1/({}^{14}\text{N}k_2)}{1/({}^{14}\text{N}k_2)} \quad (\text{S3.10})$$

$$= \frac{{}^{14}\text{N}k_1}{{}^{15}\text{N}k_1} \times \frac{{}^{14}\text{N}k_3}{{}^{15}\text{N}k_3} \times \frac{\left( [\text{H}^+] {}^{15}\text{N}k_2 / {}^{14}\text{N}k_2 + {}^{15}\text{N}k_3 / {}^{14}\text{N}k_2 \right)}{\left( [\text{H}^+] + {}^{14}\text{N}k_3 / {}^{14}\text{N}k_2 \right)} \quad (\text{S3.11})$$

To obtain expressions for  $\text{AKIE}_{\text{N}}^{\text{BH}^+}$  at pH-values  $\leq 7.0$ , the following assumptions are made. (i) Proton exchange rate constants of substituted anilines are diffusion limited (i.e.,  $k_2 \approx 10^{10} \text{ M}^{-1}\text{s}^{-1}$ ).<sup>27</sup> (ii) Rate constants  $k_3$  of neutral species oxidation are obtained for *p*-OCH<sub>3</sub>- and *p*-Cl-aniline (most and least reactive compound) at pH >6.5 and >6.0, respectively (compare  $\text{pK}_{\text{BH}^+}$  in Table S3) from initial reaction rates. (iii) Typical measured values at the above mentioned pH-values are  $10^{-4} \text{ M}^{-1}\text{s}^{-1}$  for *p*-Cl-aniline while *p*-OCH<sub>3</sub>-aniline reacts 10<sup>2</sup>-times faster.<sup>72</sup> Therefore, ratios  $k_3/k_2$  are  $\leq 10^{-12} \text{ M}$  and one can safely assume that the following approximations are valid.

$$[\text{H}^+] \gg {}^{14}\text{N}k_3 / {}^{14}\text{N}k_2 \text{ and } [\text{H}^+] {}^{15}\text{N}k_2 / {}^{14}\text{N}k_2 \gg {}^{14}\text{N}k_3 / {}^{14}\text{N}k_2$$

The resulting expression for the modified Equation S3.11 is

$$\text{AKIE}_{\text{N}}^{\text{BH}^+} = \frac{{}^{14}\text{N}k_1}{{}^{15}\text{N}k_1} \times \frac{{}^{14}\text{N}k_3}{{}^{15}\text{N}k_3} \times \frac{\left( [\text{H}^+] {}^{15}\text{N}k_2 / {}^{14}\text{N}k_2 \right)}{([\text{H}^+])} \quad (\text{S3.12})$$

$$= \frac{{}^{14}\text{N}k_1}{{}^{15}\text{N}k_1} \times \frac{{}^{15}\text{N}k_2}{{}^{14}\text{N}k_2} \times \frac{{}^{14}\text{N}k_3}{{}^{15}\text{N}k_3} \quad (\text{S3.13})$$

The ratio of kinetic isotope effects for the forward and backward reaction in Equation S3.13 corresponds the <sup>15</sup>N-equilibrium isotope effect for the proton exchange (Equation S3.1) as determined recently.<sup>134</sup> The last term is the apparent <sup>15</sup>N-kinetic isotope effects associated with the oxidation of the neutral substituted aniline,  $\text{AKIE}_{\text{N}}^{\text{B}}$  (Equation S3.15).

$$\text{EIE}_\text{N}^{\text{BH}^+} = \frac{{}^{14}\text{N}k_1}{{}^{15}\text{N}k_1} \times \frac{{}^{15}\text{N}k_2}{{}^{14}\text{N}k_2} \quad (\text{S3.14})$$

$$\text{AKIE}_\text{N}^\text{B} = \frac{{}^{14}\text{N}k_3}{{}^{15}\text{N}k_3} \quad (\text{S3.15})$$

$$\text{AKIE}_\text{N}^{\text{BH}^+} = \text{EIE}_\text{N}^{\text{BH}^+} \times \text{AKIE}_\text{N}^\text{B} \quad (\text{S3.16})$$

## Computation of kinetic isotope effects

### Outer-sphere electron transfer reactions

In Marcus theory<sup>21,88</sup> the rate of an outer-sphere electron transfer may be expressed as

$$k_{\text{ET}} = Z \cdot e^{-\Delta G^*/RT} \quad (\text{S3.17})$$

where  $Z$  is a pre-exponential term,  $R$  is the universal gas constant,  $T$  is the temperature, and  $\Delta G^*$  is an activation free energy computed as

$$\Delta G^* = \frac{\lambda}{4} + \frac{\Delta G}{2} + \frac{(\Delta G)^2}{4\lambda} \quad (\text{S3.18})$$

where  $\lambda$  is the reorganization energy associated with the solvent coordinate (the effective reaction coordinate in Marcus theory) being equilibrated with the pre- vs. post-electron-transfer charge distribution, and  $\Delta G$  is the reaction driving force. The latter is the equilibrium free-energy change associated with the electron-transfer process. Thus, for instance, the reduction potential of *p*-CH<sub>3</sub>-aniline relative to the standard hydrogen electrode (SHE) has been measured to be 0.781 V.<sup>139</sup> In an electrochemical cell having an anode with a standard reduction potential of 0.800 V, the driving force for the ET reaction from *p*-CH<sub>3</sub>-aniline to the electrode would be 0.019 eV or 0.44 kcal/mol.

The Marcus theory rate constant is isotopically sensitive insofar as the driving force is a free energy change, and the molecular translational, rotational, and vibrational partition functions that contribute to the free energy at non-zero temperatures depend on isotopic composition. In particular, if Equation S3.18 above is used to define the driving force for the light isotope (the most abundant isotope for the carbon and nitrogen cases considered here), then the driving force for the heavy isotope may be computed as

$$\Delta G_\text{h}^* = \frac{\lambda}{4} + \frac{(\Delta G - RT \ln \alpha)}{2} + \frac{(\Delta G - RT \ln \alpha)^2}{4\lambda} \quad (\text{S3.19})$$

where  $\alpha$  is the ratio of reactant and product partition functions computed as

$$\alpha = \frac{{}^lQ_P \cdot {}^hQ_R}{{}^hQ_P \cdot {}^lQ_R} \quad (\text{S3.20})$$

where  $Q$  is a molecular partition function for the *light* (superscript  $l$ ) or *heavy* (superscript  $h$ ) isotopically substituted products (subscript P) or reactants (subscript R). For <sup>14</sup>N vs. <sup>15</sup>N substituted anilines as reactants and their corresponding radical cations as products, values of  $\alpha$  are typically about 0.011.

Operating under the assumption that the pre-exponential  $Z$  appearing in Equation S3.17 is not isotopically sensitive, the ET-KIE may be computed as

$$\text{ET} - \text{KIE} = \frac{k_l}{k_h} = e^{-(\Delta G_l^* - \Delta G_h^*)/RT} \quad (\text{S3.21})$$

We note that the above procedure essentially follows the development of Kavner et al.<sup>68</sup> However, Kavner et al.<sup>68</sup> present a derivation in which the pre-exponential  $Z$  is associated with a collision frequency that is dependent on the inverse square root of the molecular weight. Were this to be appropriate, Equation S3.21 above would need to be multiplied on the right-hand-side by the square root of the ratio of the molecular weights of the isotopomers, leading to the somewhat counterintuitive result that a large normal isotope effect would be observed in the case of a differential activation free energy of zero. The choice used in Kavner et al.<sup>68</sup> for the form of the pre-exponential might be appropriate within the context of gas-phase reaction dynamics, but Marcus theory in the condensed phase typically associates the reaction coordinate (and thus the pre-exponential) not with motion of the reacting species, but instead with motion along an effective solvent coordinate.<sup>104</sup> Within this formalism, the effective mass that appears in the pre-exponential is associated not with an actual mass, but instead with the magnitude of fluctuations of the solvent dielectric. This effective mass is not expected to be isotopically sensitive.

For the ET-KIEs presented here, all molecular partition functions were computed at the mPW/6-311+G(d) level. In the computation of free energies of activation,  $\lambda$  values of 100, 200, and 300 kJ/mol were surveyed (this spans a rather typical range for ET reactions running from small, metal ions as ET partners to large organics). For a driving force of 0, there is no sensitivity of the predicted KIE to  $\lambda$ . For driving forces of 0.3 eV, the predicted KIEs vary by only 1‰ over the entire range of  $\lambda$ . As the experimental situation covers only a fairly small range of driving forces, we may consider the choice of  $\lambda$  to be arbitrary; we employ a value of 100 kJ/mol. Driving forces were computed from the experimental standard reduction potentials reported for the anilines<sup>139</sup> and electrode

reduction potentials chosen to be consistent with experimental conditions.

## Hydrogen-atom transfer reactions

Rate constants were computed from the canonical transition-state theory (TST) expression<sup>21,146</sup>

$$k = \frac{k_{\text{B}}T}{h} \frac{Q^{\ddagger}}{Q_{\text{R}}} \frac{Q_{\text{R}}^{\circ}}{Q^{\ddagger,\circ}} e^{-\Delta V^{\ddagger}/RT} \quad (\text{S3.22})$$

where  $k_{\text{B}}$  is Boltzmann’s constant,  $T$  is temperature,  $h$  is Planck’s constant,  $Q$  is a partition function or product of partition functions for the TS structure ( $\ddagger$ ) or reactants (R),  $Q^{\circ}$  is a corresponding translational partition function having a value of unity but carrying the appropriate standard-state units,  $\Delta V^{\ddagger}$  is the zero-point including molar potential energy of activation, and R is the universal gas constant. Within canonical TST, the isotope effect may be computed as

$$\frac{k_{\text{l}}}{k_{\text{h}}} = \frac{Q_{\text{l}}^{\ddagger} \cdot Q_{\text{R,h}}}{Q_{\text{h}}^{\ddagger} \cdot Q_{\text{R,l}}} e^{-(\text{ZPVE}_{\text{light}}^{\ddagger} - \text{ZPVE}_{\text{heavy}}^{\ddagger})/RT} \quad (\text{S3.23})$$

where ZPVE is a zero-point vibrational energy and the analogy to Equations S3.19-S3.21 should be clear.

For the purposes of this paper, we optimized all reactants and TS structures at the mPW/6-311+G(2df,2p) level of theory and computed the necessary partition functions and zero-point vibrational energies for these structures. Reactants in this case included aniline and substituted anilines and their corresponding conjugate acids (i.e., protonated anilines) and the hydroxyl and hydroperoxyl radicals. We surveyed the sensitivity of the predicted KIEs to basis set. Removing the diffuse functions from the basis generally had an effect of less than 1%, although in a few instances larger variations (as much as 5%) were observed. Most TS structures were very early, reflecting the significant difference in forming OH bond strengths compared to breaking NH bond strengths.

## Software

All calculations were performed with the Gaussian 03<sup>39</sup> and 09<sup>40</sup> suites of electronic structure programs.

## Tables

### DFT-calculations

Table S3.1: Density functional theory (DFT) calculations of <sup>15</sup>N-Kinetic Isotope Effects for electron transfer (ET-KIE<sub>N</sub>) and hydrogen atom transfer (HAT-KIE<sub>N</sub>) from neutral and cationic substituted anilines to <sup>•</sup>OH and <sup>•</sup>OOH, respectively.

Entry	Compound	E <sub>h</sub> <sup>a)</sup>  (V vs. SHE)	ET-KIE <sub>N</sub>  (−)	HAT-KIE <sub>N</sub>	
				•OH (−)	•OOH (−)
Neutral substituted anilines					
25	Aniline	0.850	0.9943	0.9959	0.9963
26	<i>o</i> -CH <sub>3</sub> -Aniline	0.850	0.9945		
27	<i>m</i> -CH <sub>3</sub> -Aniline	0.850	0.9948		
28	<i>p</i> -CH <sub>3</sub> -Aniline	0.850	0.9948	0.9952	0.9972
29	<i>p</i> -CH <sub>3</sub> -Aniline	0.750	0.9943		
30	<i>p</i> -CH <sub>3</sub> -Aniline	0.950	0.9954		
31	<i>o</i> -OCH <sub>3</sub> -Aniline	0.850	0.9951		
32	<i>m</i> -OCH <sub>3</sub> -Aniline	0.850	0.9945		
33	<i>p</i> -OCH <sub>3</sub> -Aniline	0.850	0.9959	0.9950	0.9992
34	<i>m</i> -Cl-Aniline	0.850	0.9938		
35	<i>p</i> -Cl-Aniline	0.850	0.9944	0.9955	0.9965
36	<i>p</i> -OH-Aniline			0.9950	0.9989
37	<i>p</i> -NO <sub>2</sub> -Aniline			1.0008	0.9935
Cationic substituted anilines					
38	Aniline			0.9972	0.9910
39	<i>p</i> -OH-Aniline			0.9969	0.9929
40	<i>p</i> -OCH <sub>3</sub> -Aniline			0.9944	0.9935
41	<i>p</i> -CH <sub>3</sub> -Aniline			0.9991	0.9924
42	<i>p</i> -Cl-Aniline			1.0006	0.9920
43	<i>p</i> -NO <sub>2</sub> -Aniline			0.9959	0.9824

<sup>a)</sup> working electrode potentials for ET-KIE<sub>N</sub> calculations only, section 3.4.

Table S3.2: Difference in C–N bond length  $\Delta r$ , C–N stretching frequencies  $\Delta\nu$ , and Mayer bond order  $\Delta MBO$  (Bridgeman et al.<sup>14</sup>) between ground and transition state of aniline and anilinium cation during Hydrogen Atom Abstraction (HAT) by  $\bullet OH$  and  $\bullet OOH$  derived from DFT-calculations.

Compound	HAT Neutral species				HAT Cationic species							
	$\bullet\text{OH}$	$\Delta r$ [ang]	$\Delta\nu$ [cm $^{-1}$ ]	$\Delta\text{MBO}$ [-]	$\bullet\text{OOH}$	$\Delta r$ [ang]	$\Delta\nu$ [cm $^{-1}$ ]	$\Delta\text{MBO}$ [-]	$\bullet\text{OOH}$	$\Delta r$ [ang]	$\Delta\nu$ [cm $^{-1}$ ]	$\Delta\text{MBO}$ [-]
p-Cl-Aniline	-0.017	12	0.060	-0.037	32	0.116	-0.033	128	0.050	-0.060	111	0.090
p-H-Aniline	-0.012	6	0.062	-0.036	29	0.128	-0.038	71	0.040	-0.068	100	0.111
p-CH $_3$ -Aniline	-0.024	14	0.086	-0.041	39	0.117	-0.034	74	0.009	-0.061	115	0.101
p-OCH $_3$ -Aniline	-0.039	27	0.119	-0.045	50	0.125	-0.016	29	-0.012	-0.049	95	0.068



## Physico-chemical properties of substitutes anilines

Table S3.3: Names and selected physico-chemical properties of the investigated substituted anilines.  $E_{1/2}$  from Suatoni et al.<sup>139</sup>,  $\sigma$  and  $\sigma^+$  from March<sup>87</sup>.

Compound Name	MW [g/mol]	pK <sub>BH<sup>+</sup></sub> [-]	$E_{1/2}$ <sup>a)</sup> [V vs. SHE]	$\sigma$ [-]	$\sigma^+$ [-]
Aniline	93.1	4.63	0.625	0	-
<i>o</i> -CH <sub>3</sub> -Aniline	107.2	4.45	0.595	0.10 <sup>18,105</sup>	-
<i>m</i> -CH <sub>3</sub> -Aniline	107.2	4.45	0.606	-0.06	-0.10
<i>p</i> -CH <sub>3</sub> -Aniline	107.2	5.10	0.537	-0.14	-0.31
<i>o</i> -OCH <sub>3</sub> -Aniline	123.2	4.52	0.498	0.00 <sup>18,105</sup>	-
<i>m</i> -OCH <sub>3</sub> -Aniline	123.2	4.21	0.615	0.10	0.05
<i>p</i> -OCH <sub>3</sub> -Aniline	123.2	5.34	0.393	-0.28	-0.78
<i>p</i> -Cl-Aniline	126.6	3.98	0.675	0.24	0.11

a)  $\text{Ar-NH}_2^{\bullet+} + \text{e}^- \rightleftharpoons \text{Ar-NH}_2$

## Characterization of MnO<sub>2</sub>

Table S3.4: Surface area, Mn oxidation state, crystal structure, and point of zero charge pH<sub>IEP</sub> of MnO<sub>2</sub>.

Parameter	Value $\pm 1\sigma$	Method and Instrument
Surface area	$285 \pm 24.9 \text{ m}^2 \text{ g}^{-1}$	N <sub>2</sub> -BET <sup>15</sup> Micromimetics Gemini 2375 V5.01
Mn oxidation state	$3.88 \pm 0.3$	Iodometric titration <sup>47</sup>
Crystal structure	amorphous, Vernadite <sup>16,91</sup>	Powder X-ray diffraction Cu-K <sub><math>\alpha</math>1</sub> , $4^\circ < 2\Theta < 70^\circ$ Graphite Monochromator D8 Advance, Bruker AXS
pH <sub>IEP</sub>	$3.25 \pm 0.094$	micro-electrophoresis Zeta Size Nano-Series, Malvern Instruments

## Figures

### Reaction products identified by LC-MS/MS

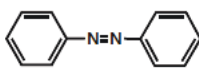
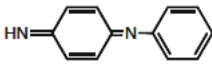
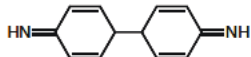
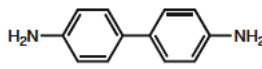
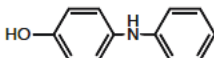
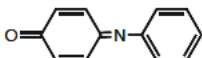
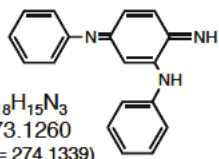
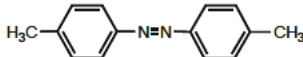
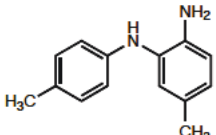
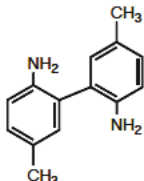
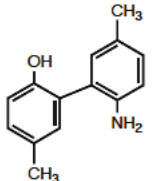
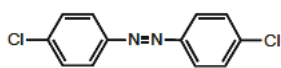
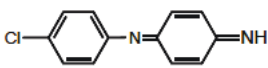
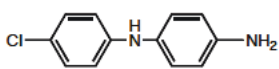
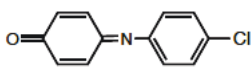
Aniline			
	$C_{12}H_{10}N_2$ 182.0838 ( $m/z = 183.0917$ )		$C_{12}H_{10}N_2$ 182.0838 ( $m/z = 183.0917$ )
	$C_{12}H_{12}N_2$ 184.0995 ( $m/z = 185.1073$ )		$C_{12}H_{12}N_2$ 184.0995 ( $m/z = 185.1073$ )
	$C_{12}H_{11}NO$ 185.0835 ( $m/z = 186.0913$ )		$C_{12}H_9NO$ 183.0679 ( $m/z = 184.0757$ )
			$C_{18}H_{15}N_3$ 273.1260 ( $m/z = 274.1339$ )
<i>p</i> -CH <sub>3</sub> -Aniline			
	$C_{14}H_{14}N_2$ 210.1152 ( $m/z = 211.1229$ )		$C_{14}H_{16}N_2$ 212.1308 ( $m/z = 213.1386$ )
	$C_{14}H_{16}N_2$ 212.1308 ( $m/z = 213.1386$ )		$C_{14}H_{15}NO$ 213.1148 ( $m/z = 214.1226$ )
<i>p</i> -Cl-Aniline			
	$C_{12}H_8N_2Cl_2$ 250.0059 ( $m/z = 251.0137$ )		$C_{12}H_9N_2Cl$ 216.0449 ( $m/z = 217.0527$ )
	$C_{12}H_{11}N_2Cl$ 218.0605 ( $m/z = 219.0684$ )		$C_{12}H_8NOCl$ 217.0289 ( $m/z = 218.0367$ )

Figure S3.1: Most probable molecular structures of reaction products of the aniline, *p*-CH<sub>3</sub>-aniline and *p*-Cl-aniline oxidation by MnO<sub>2</sub> as identified by LC-MS/MS (see main manuscript for detailed experimental procedures).

## Carbon isotope fractionation during aniline oxidation

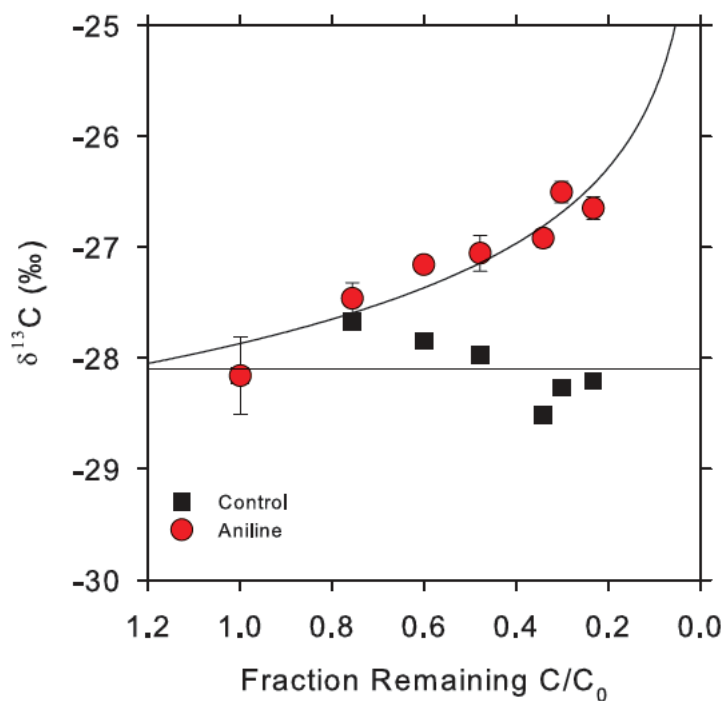


Figure S3.2:  $^{13}\text{C}$  isotope fractionation during oxidation of aniline by  $\text{MnO}_2$ . The concentration of the  $\text{MnO}_2$ -suspension was 7.5 mM in phosphate buffer at pH 7.0 and the initial aniline concentration 600  $\mu\text{M}$ . The fitted line corresponds to an C isotope enrichment factor,  $\epsilon_{\text{C}}$  of  $1.1 \pm 0.1\text{‰}$ .

## Reference experiments: Sorption of reactant and reaction products on $\text{MnO}_2$ -surface

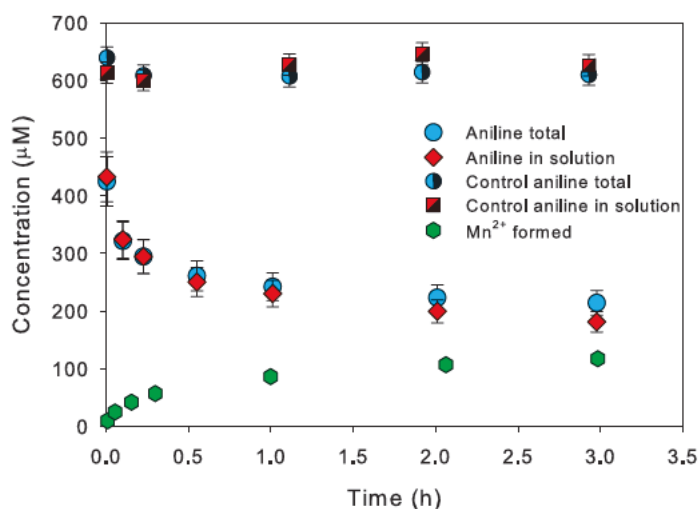


Figure S3.3: Total and dissolved aniline concentration during the oxidation with  $\text{MnO}_2$  at pH 5.5. Initial aniline concentration was  $600 \mu\text{M}$  and  $\text{MnO}_2$ -concentration was  $7.5 \text{ mM}$ . Increasing  $\text{Mn}^{2+}$ -concentration due to reductive dissolution by the aniline.

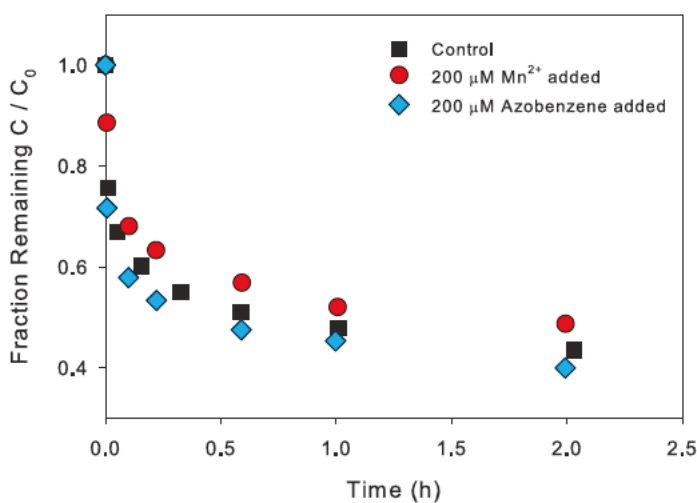


Figure S3.4: Effect of additionally spiked  $\text{Mn}^{2+}$  and azobenzene to the disappearance kinetics of aniline during the oxidation by  $\text{MnO}_2$ . Initial  $\text{MnO}_2$ -concentration was  $7.5 \text{ mM}$ , aniline concentration was  $400 \mu\text{M}$ , which corresponds to  $200 \mu\text{M}$  of  $\text{Mn}^{2+}$ - and azobenzene formation equivalents.

## Characterization of $\text{MnO}_2$ synthesized and used in this study: XRD and $\text{pH}_{\text{IEP}}$

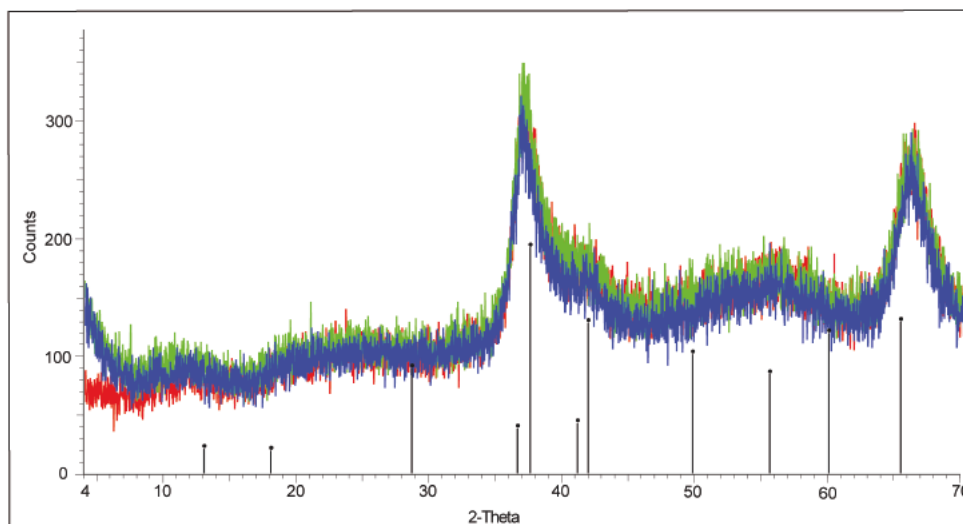


Figure S3.5: X-ray diffractogram of  $\text{MnO}_2$ . The three colors correspond to three different  $\text{MnO}_2$ -batches. The black lines represent theoretical spectra of Vernadite.

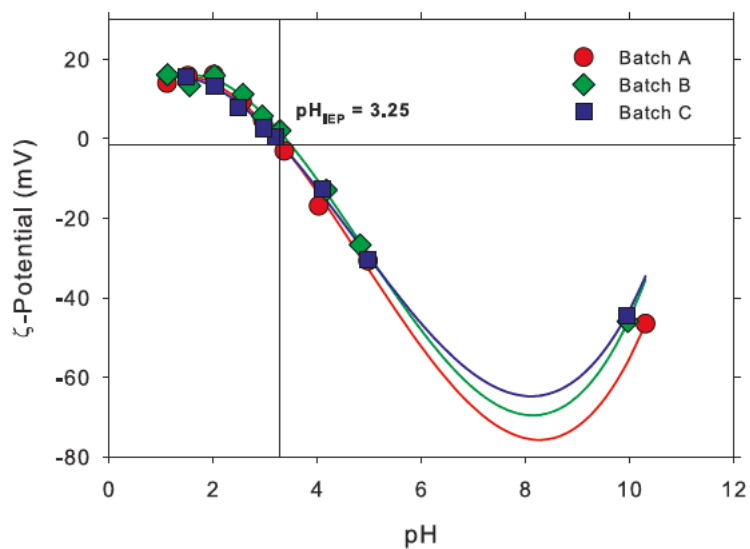


Figure S3.6:  $\zeta$ -Potential as a function of pH for three different  $\text{MnO}_2$ -batches prepared in nanopure water. The pH-values were adjusted with 1M HCl and 1M NaOH. The final amount of HCl or NaOH in the suspension did not exceed 0.01 Vol-%. The data points are fitted by a cubic polynomial to interpolate the zero point of charge of the synthesized  $\text{MnO}_2$ -suspension.



## Chapter 4

# Carbon, Hydrogen, and Nitrogen Isotope Fractionation Associated with Oxidative Transformation of Substituted Aromatic *N*-Alkyl Amines

M. Skarpeli-Liati, S. G. Pati, J. Bolotin, S. N. Eustis, and T. B. Hofstetter. Carbon, Hydrogen, and Nitrogen Isotope Fractionation Associated with Oxidative Transformation of Substituted Aromatic *N*-Alkyl Amines. *Environ. Sci. Technol.*, 46, 7189-7198, 2012

## Abstract

We investigated the mechanisms and isotope effects associated with the *N*-dealkylation and N-atom oxidation of substituted *N*-methyl- and *N,N*-dimethyl-anilines to identify isotope fractionation trends for the assessment of oxidations of aromatic *N*-alkyl moieties by compound-specific isotope analysis (CSIA). In laboratory batch model systems, we determined the C, H, and N isotope enrichment factors for the oxidation by MnO<sub>2</sub> and horseradish peroxidase (HRP), derived apparent <sup>13</sup>C-, <sup>2</sup>H-, and <sup>15</sup>N-kinetic isotope effects (AKIEs), and characterized reaction products. The N-atom oxidation pathway leading to radical coupling products typically exhibited inverse <sup>15</sup>N-AKIEs (up to 0.991) and only minor <sup>13</sup>C- and <sup>2</sup>H-AKIEs. Oxidative *N*-dealkylation, in contrast, was subject to large normal <sup>13</sup>C- and <sup>2</sup>H-AKIEs (up to 1.019 and 3.1, respectively) and small <sup>15</sup>N-AKIEs. Subtle changes of the compound's electronic properties due to different types of aromatic and/or *N*-alkyl substituent resulted in changes of reaction mechanisms, rate-limiting step(s), and thus isotope fractionation trends. The complex sequence of electron and proton transfers during the oxidative transformation of substituted aromatic *N*-alkyl amines suggests highly compound- and mechanism-dependent isotope effects precluding extrapolations to other organic micropollutants reacting along the same degradation pathways.

## 4.1 Introduction

A significant number of organic micropollutants exhibit aromatic *N*-alkyl moieties that may be the site of initial attack when transformed by abiotic and biotic processes in the environment as has been found for antibacterial agents<sup>109,110,159</sup> and pesticides.<sup>33,161</sup> However, these processes take place at very different rates through photochemical as well as mineral- and enzyme-catalyzed reactions and they proceed via alternative pathways to a variety of products.<sup>17,46,50,147</sup> Quantifying the exposure of these micropollutants and their transformation products in the environment is therefore difficult and the assessment of their impact on humans and the environment very challenging.<sup>127,128</sup>

We have recently shown that compound-specific isotope analysis<sup>28,53,58</sup> (CSIA) offers new avenues for assessing the oxidative degradation of substituted *primary* aromatic amines.<sup>134,135</sup> Nitrogen isotope signatures varied systematically depending on the changes of N-atom bonding as a consequence of kinetic or equilibrium isotope effects. One-electron oxidation of substituted anilines at MnO<sub>2</sub>-surfaces is subject to an *inverse*



apparent  $^{15}\text{N}$ -kinetic isotope effect,  $\text{AKIE}_\text{N}$ , that is heavy,  $^{15}\text{N}$ -containing isotopologues reacted faster than compounds with  $^{14}\text{N}$ . This effect was proposed to be indicative of the formation of partial imine-type  $\text{N}=\text{C}$  bonds in aminium radical intermediates,<sup>75,76,99,135</sup> which react to a variety of radical coupling products after N-atom oxidation (Figure 4.1). In addition, the observable N isotope fractionation associated with N-atom oxidation can be modulated at neutral to acidic pH-values by a *normal*  $^{15}\text{N}$ -equilibrium isotope effect,  $\text{EIE}_\text{N}$ , originating from the slightly increased acidity of  $^{14}\text{N}$ -containing substituted anilines.

These observations suggest that oxidative transformations of aromatic *N*-alkyl amines might also be associated with isotope effects that are potentially indicative of their pathway of degradation. In addition to the N-atom oxidation observed with substituted anilines, secondary and tertiary aromatic *N*-alkyl amines are also subject to oxidative *N*-dealkylation in mineral- and enzyme-catalyzed reactions (Figure 4.1).<sup>46,69,147,148,151,159</sup> Because these two pathways result in cleavages of C–N and C–H bonds, a combined analysis of C, H, and N isotope fractionation could provide new means for the identification of these transformation pathways. The mechanisms of aromatic *N*-alkyl amine oxidation, however, are very complex because they involve a series of electron,  $\text{H}^+$ , and H atom transfer steps that can take place in competing reactions (Figure 4.1). It is therefore unclear whether CSIA of substituted aromatic *N*-alkyl amines results in pathway-dependent, indicative isotope fractionation trends. Indeed, highly compound-dependent  $^2\text{H}$ -KIE profiles have been invoked to elucidate the mechanism of enzymatic oxidative *N*-dealkylation via competing initial H atom and single electron transfer.<sup>24,46,67</sup> Beyond the studies of cytochrome- and peroxidase-catalyzed oxidations of selected  $^2\text{H}$ -labelled, substituted *N,N*-dimethylanilines,<sup>46,80,98,107</sup> however, nothing is known about the isotope effects of C and N and the potential fractionation of C, H, and N isotopes at natural abundance isotope distributions.

The objective of the present work was to study the mechanisms of N-atom oxidation and oxidative *N*-dealkylation of substituted aromatic *N*-alkyl amines, to identify isotope fractionation trends pertinent to each transformation pathway, and to assess their *apparent* kinetic isotope effects. To this end, we studied the C, H, and N isotope fractionation associated with the oxidation of a series of ring-substituted *N*-methyl- and *N,N*-dimethylanilines by  $\text{MnO}_2$  and horseradish peroxidase (HRP) in laboratory model systems. Both systems have been used previously to mimic important oxidants in soils and aquatic environments<sup>72,78,109,131,151,159</sup> and it was shown that the oxidation of primary aromatic amines by  $\text{MnO}_2$  and that of tertiary aromatic amines by HRP proceed via ini-

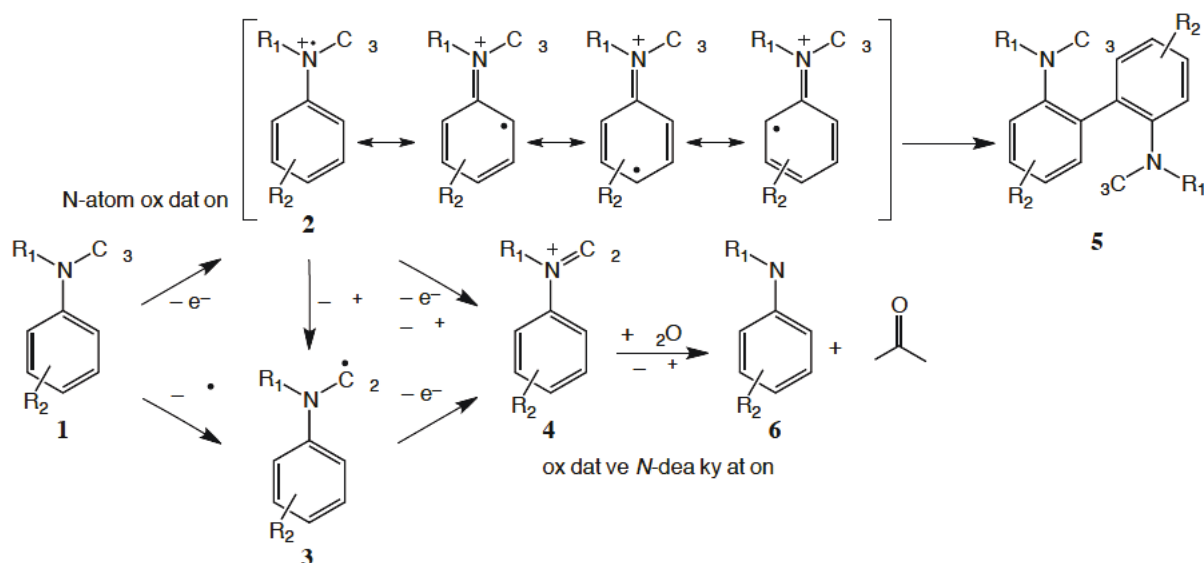


Figure 4.1: Proposed reaction scheme for the oxidative transformation of substituted aromatic *N*-alkyl amines by  $\text{MnO}_2$ <sup>135,159</sup> and  $\text{HRP}/\text{H}_2\text{O}_2$ .<sup>45,107</sup> 1: aromatic *N*-alkyl amine, 2: aminium radical, 3: C-centered radical, 4: iminium cation, 5: radical coupling product, 6: product of *N*-dealkylation reaction (substituted *N*-MA or aniline).

tial one-electron transfer<sup>45,72,78,107,135</sup> (Figure 4.1, reaction 1  $\rightarrow$  2). Multielement isotope fractionation trends and apparent  $^{13}\text{C}$ -,  $^2\text{H}$ -, and  $^{15}\text{N}$ -kinetic isotope effects (AKIEs) were studied systematically for *p*-Cl-, *p*-H-, *p*-CH<sub>3</sub>-, and *p*-OCH<sub>3</sub>-substituted *N*-methyl- and *N,N*-dimethylanilines (i) to identify isotope-sensitive elementary reaction step(s) and (ii) to understand the impact of structural modifications in the substrate on reaction pathways and isotope fractionation.<sup>152,153</sup> The interpretation of isotopic analyses of substituted aromatic *N*-alkyl amines by GC/IRMS was supported by quantitative and qualitative product analysis performed by GC/MS and LC-MS/MS, respectively, as well as computations of selected thermodynamic properties of the substrates and radical intermediates. Finally, we discuss whether the observed AKIE-values and multi-element isotope fractionation trends ( $\delta^{15}\text{N}$  vs.  $\delta^{13}\text{C}$  and  $\delta^2\text{H}$  vs.  $\delta^{13}\text{C}$ ) are valid generally for oxidations of aromatic *N*-alkyl amines and can thus be used to rationalize the isotope fractionation behavior of aquatic micropollutants exhibiting the same reactive functional groups.

## 4.2 Experimental Section

A complete list of all chemicals used including purities and suppliers can be found in the Supporting Information (SI).  $\text{MnO}_2$  particles were synthesized as described by Murray<sup>101</sup> through oxidation of  $\text{Mn}^{2+}$  by  $\text{MnO}_4^-$  following the procedure described by<sup>135</sup> and characterized accordingly.

### 4.2.1 Oxidation experiments in $\text{MnO}_2$ -suspensions

All oxidation experiments with substituted *N*-methylanilines (*N*-MAs) and *N,N*-dimethylanilines (*N,N*-DMAs) in  $\text{MnO}_2$ -suspensions were performed according to recently established procedures<sup>135</sup> under oxic conditions at room temperature. An experiment typically consisted of a series of 7 to 9 separate 10 mL batch reactors, in which the substrate reacted to different extents or 2 to 4 larger (100 mL) batch reactors, from which samples were withdrawn at different time intervals.<sup>49,135,142</sup> Blanks were set up in an identical matter except for the addition of oxidant to exclude losses due to phase transfer processes. Batch reactors contained  $\text{MnO}_2$ -suspensions buffered in 10 mM phosphate buffer at pH 7.0, NaCl (final ionic strength 0.02 M), and a PTFE-coated magnetic stir bar.  $\text{MnO}_2$  concentrations were varied between 1.5 and 5 mM to avoid conversion of more than 50% of the substrate within the first minute of the experiment and to attain at least 60% turnover within 8 days. Reactions were initiated by the addition of methanolic stock solutions of the substituted aromatic *N*-methyl amines. Initial concentrations were 600  $\mu\text{M}$  except for *p*-Cl-*N,N*-DMA (300  $\mu\text{M}$ ) due to its lower aqueous solubility. Isotope fractionation artifacts from dissolution of the reactant from methanol can be ruled out based on previous experience, where the identical approach was used to study even faster (redox) reactions.<sup>49,57</sup> Aqueous samples were withdrawn at predefined time intervals with a gastight glass syringe and the reaction was stopped by filtration through a 0.22  $\mu\text{m}$  hydrophilic PTFE-filter.

Because the disappearance of *p*- $\text{OCH}_3$ -*N*-MA in  $\text{MnO}_2$ -suspensions occurred within seconds (Figure S4.2) and was thus too fast to be sampled using the above procedure, reactors containing the identical initial *p*- $\text{OCH}_3$ -*N*-MA concentration were spiked with variable amounts of  $\text{MnO}_2$ -suspension to achieve different degrees of conversion following a previously established procedure<sup>135</sup>. After the reaction was completed, the reactors were shaken on a vortex shaker and the solution was filtered to ensure identical treatment as in other experiments with  $\text{MnO}_2$ -suspensions. Filtered solutions were stored in amber glass vials in the dark at 4°C until measurements of the concentration, isotope analysis

by solid-phase microextraction GC/IRMS, and further characterization of reaction products. Samples from blank experiments were treated identically and revealed that neither substrate concentration nor C, N, and H isotope signatures changed in the absence of the oxidant (Figure S4.2).

### 4.2.2 Oxidation experiments with horseradish peroxidase

Enzymatic oxidation of substituted *N*-MAs and *N,N*-DMAs by horseradish peroxidase (HRP) was carried out using the approach described above for  $\text{MnO}_2$ -suspensions including three types of reference experiments (without HRP, without  $\text{H}_2\text{O}_2$ , and without HRP and  $\text{H}_2\text{O}_2$ ) to check for side reactions and losses due to phase transfer processes. Batch reactors contained variable amounts of HRP and  $\text{H}_2\text{O}_2$  in buffered solution (10 mM  $\text{KH}_2\text{PO}_4$ , pH 7.0) of 18 mL total volume. Initial reactant concentrations were identical to those used in experiments with  $\text{MnO}_2$ . Experiments were set up to maximize reactant conversion under conditions for substrate-saturated enzymes<sup>69</sup> as shown in Figure S4.4. In general, higher enzyme to  $\text{H}_2\text{O}_2$ -ratios led to faster and more complete substrate transformation. Experimental conditions are listed in Table S4.2.

The reactions were initiated by the addition of a defined amount of  $\text{H}_2\text{O}_2$  (0.6 - 4.5 mM) to the reactors containing HRP (0.5 - 15 nM) and the substituted aromatic *N*-methyl amine.  $\text{H}_2\text{O}_2$  and HRP concentrations were chosen to enable adequate sampling of the aromatic amine transformation. To prevent photochemical transformation of  $\text{H}_2\text{O}_2$ , all reactors were wrapped in aluminum foil. The oxidation of the aromatic amines was stopped by extracting the substrate into 18 mL of methylene chloride through vigorous shaking for 1 minute. For concentration measurements of reactant and potential *N*-dealkylation products, 1 mL of the methylene chloride-extract was used immediately for GC/MS-analysis. The remainder of the extract was stored in amber glass vials at  $-20^\circ\text{C}$  until isotopic analysis. Samples from blank experiments were treated identically and showed no concentration decrease of the substrates (Figure S4.4) nor change in their C, N, and H isotope signatures (data not shown).

For the identification of possible reaction products, the oxidation experiments were repeated under the identical experimental conditions, except for using only one batch reactor for each substituted aromatic *N*-alkyl amine. For concentration measurements by GC/MS, 500  $\mu\text{L}$  of aqueous solution was extracted into 500  $\mu\text{L}$  ethyl acetate by vigorous shaking on a vortex shaker at defined time points. After complete reactant conversion, aliquots were stored at  $-20^\circ\text{C}$  in the dark prior to analysis by LC-MS/MS.

### 4.2.3 Analytical methods

#### Chemical analyses

Quantification of the reactants and *N*-dealkylation products was carried out on a GC/MS (Ultra Trace GC and DSQII, Thermo Electron Corporation) upon on-column injection using the identical instrumental setup and settings described in previous work.<sup>134</sup> Substituted *N,N*-DMAs, *N*-MAs, and anilines in aqueous buffer solution were extracted into ethyl acetate or methylene chloride containing an internal standard (*p*-nitrotoluene). Extraction efficiencies from aqueous solution into the organic solvent were found to vary between 99-109% for ethyl acetate and 95-110% for methylene chloride.

Qualitative product analysis for the identification of polar compounds as well as di- and trimers from radical coupling reactions was performed by liquid chromatography coupled to an LTQ (Linear Trap Quadrupole) Orbitrap mass spectrometry (Thermo Electron Corporation) with electrospray ionization (LC-MS/MS) as reported previously.<sup>70,135</sup> Filtered aliquots from oxidation experiment with MnO<sub>2</sub> and HRP batch experiments were purified by solid phase extraction. Methanol/water eluates (1:4 v/v) were analyzed by LC-MS/MS using a solvent gradient from 90/10% to 5/95% H<sub>2</sub>O/MeOH on an Xbridge C-18 column (Waters, 2.1×50 mm, 3.5 μm particle size). MS/MS spectra were recorded according to a target list containing the exact masses of expected reaction products. Based on the exact molecular mass and fragmentation pattern of each detected product the most probable structures were postulated; these are shown in Figure S4.6.

#### Stable Isotope Ratio Measurements

Stable C, H, and N isotope signatures ( $\delta^{13}\text{C}$ ,  $\delta^2\text{H}$ ,  $\delta^{15}\text{N}$ ) of substituted *N*-MAs and *N,N*-DMAs were measured by GC/IRMS (gas chromatography isotope ratio mass spectrometry) with a combustion interface using the procedure and instrumental setup described previously.<sup>134,135</sup> For experiments with MnO<sub>2</sub> suspensions, solid-phase microextraction (SPME, 65 μm PDMS/DVB, Supelco) was used for extraction and pre-concentration of the analytes from aqueous solutions (45 min at 40°C). pH-values of the samples was adjusted to avoid isotope fractionation by SPME as documented in Skarpeli-Liati et al.<sup>134</sup> and verified through the C, H, and N isotope analyses of calibrated in-house standards by SPME-GC/IRMS. For isotopic analyses of methylene chloride-extracts from experiments with HRP/H<sub>2</sub>O<sub>2</sub>, the following treatment was used prior to on-column injections into the GC: residual water in the organic phase was removed with anhydrous Na<sub>2</sub>SO<sub>4</sub> and filtration through a 0.22 μm hydrophilic PTFE-filter. Subsequently, methylene chloride

was evaporated under a stream of N<sub>2</sub> to attain concentration ranges suitable for isotopic analysis.

To minimize analytical uncertainty due to instrument non-linearity, all samples were diluted to concentrations yielding constant peak amplitudes (4-5 V for <sup>13</sup>C- and <sup>2</sup>H-, and 1-2 V for <sup>15</sup>N-analysis). C, H, and N isotopic signatures are reported as arithmetic mean of triplicate measurements ( $\pm 1\sigma$ ) in per mil (‰) relative to Vienna PeeDee Belemnite ( $\delta^{13}\text{C}_{\text{VPDB}}$ ), Vienna Standard Mean Ocean Water ( $\delta^2\text{H}_{\text{VSMOW}}$ ), and air ( $\delta^{15}\text{N}_{\text{air}}$ ), respectively. Calibrated in-house standards (aniline for  $\delta^{13}\text{C}$  and  $\delta^{15}\text{N}$ ; 2-nitrotoluene for  $\delta^2\text{H}$ ) of known  $\delta^{13}\text{C}$ -,  $\delta^2\text{H}$ -, and  $\delta^{15}\text{N}$ -values were used in standard bracketing procedures<sup>134</sup> to ensure accuracy of the isotopic measurements.

#### 4.2.4 Data evaluation

Because secondary substituted aromatic *N*-alkyl amines exhibit one H atom that is exchangeable with H<sup>+</sup> from aqueous media, the average H isotope signature of non-exchangeable H atoms bound to C,  $\delta^2\text{H}_{\text{C-H}}$ , was derived as follows. We assumed that  $\delta^2\text{H}$  of exchangeable H atoms corresponds to the H isotope signature of the water ( $\delta^2\text{H}_{\text{H}_2\text{O}}$ ), which was measured by cavity ring-down spectroscopy ( $-71 \pm 0.5\text{‰}$ ). The latter was subtracted from the  $\delta^2\text{H}$ -values measured in substituted *N*-MAs ( $\delta^2\text{H}_{\text{measured}}^{N-\text{MA}}$ ) to obtain  $\delta^2\text{H}_{\text{C-H}}$  as shown in Equation 4.1.

$$\delta^2\text{H}_{\text{C-H}} = \frac{1}{n_{\text{H}} - x_{\text{H}}} (n_{\text{H}} \cdot \delta^2\text{H}_{\text{measured}}^{N-\text{MA}} - x_{\text{H}} \cdot \delta^2\text{H}_{\text{H}_2\text{O}}) \quad (4.1)$$

where  $n_{\text{H}}$  is the number of H atoms and  $x_{\text{H}}$  are the exchangeable ones.

Bulk isotopic enrichment factors,  $\epsilon$ , were quantified from linear regression analysis of  $\delta^{13}\text{C}$ -,  $\delta^2\text{H}$ -, and  $\delta^{15}\text{N}$ -values, respectively, versus the fractional amount of reactant conversion as shown in Equation 4.2.

$$\ln \left( \frac{\delta^h\text{E} + 1}{\delta^h\text{E}_0 + 1} \right) = \epsilon_{\text{E}} \cdot \ln \left( \frac{C}{C_0} \right) \quad (4.2)$$

where  $\delta^h\text{E}_0$  and  $\delta^h\text{E}$  stand for the initial isotope signature of element E and its value measured during the reaction and  $C/C_0$  is the fraction of remaining reactant. Data from replicate experiments were combined using the Pitman estimator<sup>129</sup> as shown previously.<sup>135,143</sup>

Information about the position-specific, apparent kinetic isotope effects, AKIE, was obtained according to the procedure proposed by Elsner<sup>28</sup> neglecting contributions from



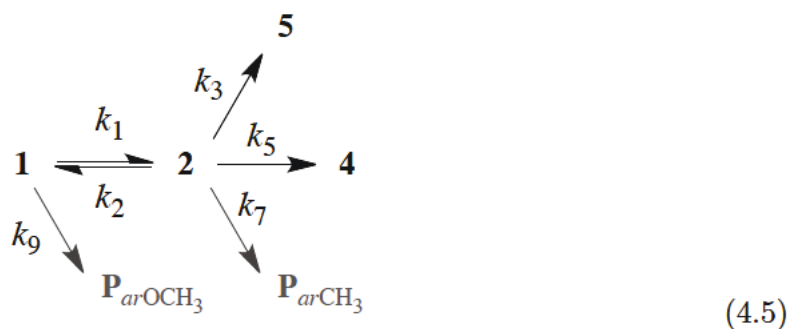
secondary isotope effects and assuming that isotope ratios change only at reactive atoms and are invariant at non-reactive ones. Position-specific enrichment factors,  $\epsilon_{\text{E,rp}}$ , were calculated to correct for non-reactive atoms as in Equation 4.3), where  $n$  is the number of isotopic atoms of an element, and  $x$  the number of these atoms at the reactive position, and  $\Delta\delta^h\text{E}$  is the increase or decrease of isotope signature relative to its initial value  $\delta^h\text{E}_0$ .

$$\ln\left(\frac{\delta^h\text{E}_0 + n/x \cdot \Delta\delta^h\text{E} + 1}{\delta^h\text{E}_0 + 1}\right) = \epsilon_{\text{E,rp}} \cdot \ln\left(\frac{C}{C_0}\right) \quad (4.3)$$

Apparent kinetic isotope effects,  $\text{AKIE}_{\text{ES}}$ , were determined from  $\epsilon_{\text{E,rp}}$ -value taking into account corrections for sites subject to intramolecular isotopic competition,  $z$ , in Equation 4.4. Notice that because  $z$  equals  $x$ , AKIE-calculations are insensitive to the number of (hypothesized) reactive sites of the same element thus complicating mechanistic interpretation of cases, in which different functional groups participate in the (isotopic) reaction.

$$\text{AKIE}_{\text{E}} = \frac{1}{1 + z \cdot \epsilon_{\text{E,rp}}} \quad (4.4)$$

Interpretation of *observable* isotope effects as AKIE-values was made in terms of up to four partially competing (multistep) reactions according to Equation 4.5 and procedures outlined in detail in the Supporting Information SI. To this end, AKIEs for (i) N-atom oxidations were assumed to reflect the initial oxidation step ( $1 \rightarrow 2$ ) while those for (ii) oxidative *N*-dealkylation and (iii) oxidation of aromatic  $\text{CH}_3$ -side chains include contributions of equilibrium ( $1 \rightleftharpoons 2$ ) and kinetic ( $2 \rightarrow 4$  or  $2 \rightarrow \text{P}_{\text{arCH}_3}$ ) isotope effect as well as potential masking by commitment factors from the rates of aminium radical oxidation ( $k_5, k_7$ ) vs. its backward reaction ( $k_2$ ). (iv) Oxidation of  $\text{OCH}_3$ -side chains ( $1 \rightarrow \text{P}_{\text{arOCH}_3}$ ) competes with N-atom oxidation of *p*- $\text{OCH}_3$ -*N,N*-DMA. A compilation of AKIE-contribution from the different reaction pathways for every substrate is shown in Table S4.1.



Two-dimensional isotope fractionation trends for *N*-MAs and *N,N*-DMAs with either of the two oxidants ( $\text{MnO}_2$  and HRP) were calculated from the linear regression analysis of the isotope signatures of N vs. C ( $\delta^{15}\text{N}$  vs.  $\delta^{13}\text{C}$ ) and H vs. C ( $\delta^2\text{H}$  vs.  $\delta^{13}\text{C}$ ) as shown in Equation 4.6 and 4.7. These slopes correspond to the ratio of bulk enrichment factors  $\epsilon_{\text{E}}$  as follows.

$$\frac{\Delta\delta^{15}\text{N}}{\Delta\delta^{13}\text{C}} \approx \frac{\epsilon_{\text{N}}}{\epsilon_{\text{C}}} \quad (4.6)$$

$$\frac{\Delta\delta^2\text{H}}{\Delta\delta^{13}\text{C}} \approx \frac{\epsilon_{\text{H}}}{\epsilon_{\text{C}}} \quad (4.7)$$

Two-dimensional isotope signature trends were used to compare the isotope fractionation trends pertinent to the oxidation of substituted aromatic *N*-alkyl amines exhibiting identical *n*, *x*, and *z* by the two different oxidants.

## 4.2.5 Computational Methods

To gain insights into the relative reactivity of substituted radical cation intermediates **2** (Figure 4.1) towards *N*-dealkylation via the iminium cation **4** and oxidation of *p*- $\text{CH}_3$  and *p*- $\text{OCH}_3$  substituents, we calculated bond dissociation enthalpies (BDE) of various bonds in the reactant **1** and intermediate **2** as outlined in Table S4.6 and Figure S4.7. The spin density values (Table S4.5) were calculated to assess the degree of radical localization within the substituted aromatic *N*-amine structures.

All calculations were performed using the Gaussian 09 suite of programs.<sup>38</sup> Accurate thermodynamic energies were computed using the CBS-QB3 method of Petersson and co-workers.<sup>106,116</sup> The Integral Equation Formalism - Polarizable Continuum Model (IEF-PCM) implicit solvation model was employed in all calculations to account for effects of hydration upon the energies and structures of the molecules under study.<sup>144,145</sup> Testing alternative solvent models' accuracy may be of interest, but is outside of the scope of this study. To calculate the Mulliken spin density values a minimum basis set Mulliken population analysis was performed.<sup>100</sup> This method uses a small, atom-centered basis set to determine the net spin associated with a given atom within a molecule.



## 4.3 Results and Discussion

### 4.3.1 Isotope fractionation associated with the oxidative transformation of *para*-substituted *N*-methylanilines by MnO<sub>2</sub>

Oxidation of *para*-substituted *N*-methylanilines (*N*-MAs) in MnO<sub>2</sub>-suspensions showed biphasic reaction kinetics. Fast initial transformation was followed by a decrease in transformation rate, as observed previously for the reaction of substituted anilines and phenols with MnO<sub>2</sub>.<sup>72,78,135,136</sup> The relative reactivity of the *para*-substituted *N*-MAs increased in the order  $p\text{-H} < p\text{-Cl} < p\text{-CH}_3 < p\text{-OCH}_3$  and thus did not strictly follow the order anticipated from electron-donating properties of the aromatic substituent. The latter was observed for oxidations of substituted primary aromatic amines<sup>72,78</sup> and would have favored the faster oxidation of *N*-MA over *p*-Cl-*N*-MA. The identity of substituted *N*-MA transformation products also contrast observations made for the oxidation of primary aromatic amines in that *N*-dealkylation products (**6** in Figure 4.1, Table 4.1, Figure S4.6) were detected in addition to the expected, typical radical coupling products (**5** in Figure 4.1).

The C, H, and N isotope fractionation observed for the oxidation of *para*-substituted *N*-MAs exhibited diverse, substituent-dependent behavior. The distinctly different two-dimensional isotope fractionation trends  $\delta^{15}\text{N}$  vs.  $\delta^{13}\text{C}$  and  $\delta^2\text{H}$  vs.  $\delta^{13}\text{C}$  (Figure 4.2) suggest that the reaction mechanism of the oxidative transformation of the four compounds by MnO<sub>2</sub> were not identical. Negative correlations of  $\Delta\delta^{15}\text{N}/\Delta\delta^{13}\text{C}$ -values (Table S4.3) imply mechanisms with predominant *inverse* N isotope fractionation and normal (secondary) isotope effects for C. Alternative routes involving reactive C–H bonds can be invoked from the positive  $\Delta\delta^2\text{H}/\Delta\delta^{13}\text{C}$ . Oxidation of *p*-OCH<sub>3</sub>-*N*-MA was accompanied by a depletion of <sup>15</sup>N in the reactant corresponding to an *inverse* bulk enrichment factor,  $\epsilon_{\text{N}}$  of  $3.7 \pm 0.8\text{‰}$  (entry 4, Table 4.1) while no significant C and H isotope enrichment was observed (Figure 4.2, panels a and b). *p*-Cl-*N*-MA transformation displayed the opposite isotope fractionation trend, that is *normal* C and H isotope fractionation ( $\epsilon_{\text{C}} = -1.9 \pm 0.2\text{‰}$ ,  $\epsilon_{\text{H}} = -73 \pm 23\text{‰}$ , entry 2, Table 4.1) and no discernible trend of N isotope fractionation. The oxidation of *N*-MA and *p*-CH<sub>3</sub>-*N*-MA always showed C, H, and N isotope fractionation and  $\epsilon$ -values between those delineated by *p*-OCH<sub>3</sub>-*N*-MA and *p*-Cl-*N*-MA, respectively.

According to our previous work on the oxidation of substituted anilines by MnO<sub>2</sub>,<sup>135</sup> inverse N isotope fractionation is indicative for partial imine-bonding at the N atom dur-

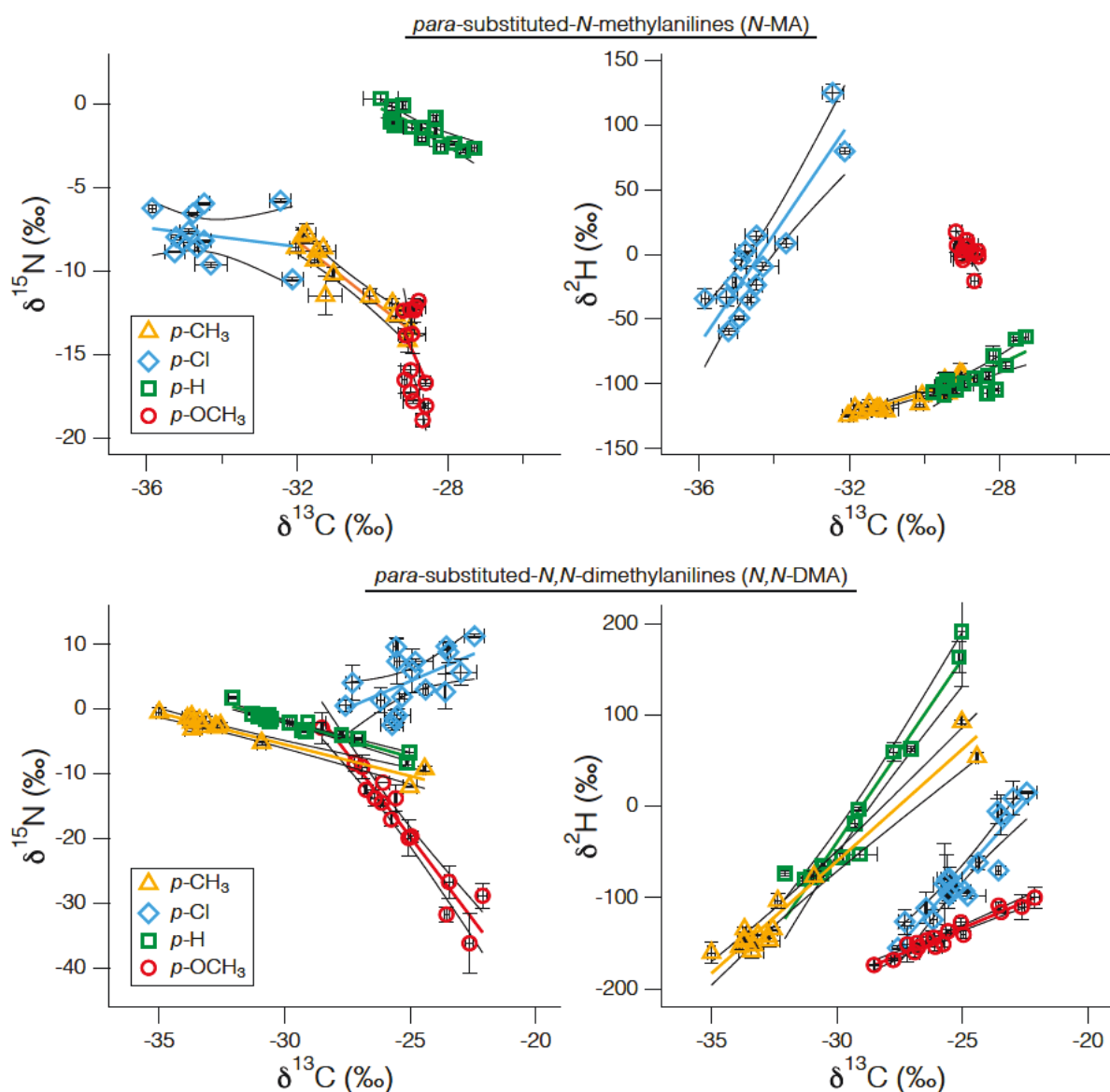


Figure 4.2: Multidimensional isotope analysis illustrating the changes of  $\delta^{15}\text{N}$  vs.  $\delta^{13}\text{C}$  and  $\delta^2\text{H}$  vs.  $\delta^{13}\text{C}$  of *para*-substituted *N*-methyl- (panels a and b) and *N,N*-dimethylanilines (panels c and d) during oxidative transformation by  $\text{MnO}_2$ .

ing one-electron oxidation and concomitant formation of an aminium radical-type intermediate in the rate-limiting step of the reaction. The  $\text{AKIE}_\text{N}$ -value of  $0.9964 \pm 0.0008$  for *p*-OCH<sub>3</sub>-*N*-MA suggests that this compound indeed reacts predominantly via the N-atom oxidation pathway ( $1 \rightarrow 2$  in Figure 4.1). Notice that all experiments were carried out at pH 7.0 and this  $\text{AKIE}_\text{N}$ -value might be slightly more inverse (by 0.0007) owing to small contributions of the normal  $\text{EIE}_\text{N}$  associated with the deprotonation of the conjugate acid.

The difference, however, is small and within the experimental uncertainty of the  $\text{AKIE}_\text{N}$  (see procedure in <sup>135</sup> and  $\text{pK}_\text{a}$ -values in Table S4.2) and does not alter the interpretation of the results. For the transformation of *p*-OCH<sub>3</sub>-*N*-MA, we almost exclusively observe radical coupling products (**5**) and only a minor fraction of *N*-dealkylated compound (<2.5% of initial concentration, Table 4.1, entry 4) that would point to further transformation of intermediate **2** at MnO<sub>2</sub>-surfaces. These observations imply that the stabilization of the aminium radical intermediates by the electron-donating OCH<sub>3</sub>-substituent not only facilitates N-atom oxidation but also the formation of radical coupling products via the reaction pathway **1** → **2** → **5**. The lack of observable C and H isotope fractionation corroborates our interpretation that only a negligible share of OCH<sub>3</sub>-substituted compound **2** undergoes *N*-dealkylation and that the AKIE-values shown in Table 4.1 are characteristic for the N-atom oxidation pathway (primary <sup>15</sup>N-AKIE and no significant secondary <sup>13</sup>C- and <sup>2</sup>H-AKIEs, see SI for details).

Almost completely opposite findings were made for the C, H, and N isotope fractionation during oxidation of *p*-Cl-*N*-MA (Figure 4.3). While the  $\text{AKIE}_\text{N}$ -value would not be statistically different from unity, primary <sup>13</sup>C- and <sup>2</sup>H-AKIEs of  $1.0138 \pm 0.0017$  and  $2.12 \pm 0.55$  (Table 4.1, entry 2), respectively, point to the cleavage of a C–H bond in the rate-limiting step of the *N*-dealkylation reaction. The lack of observable radical coupling products suggests that *p*-Cl-*N*-MA reacts either via H atom abstraction (Figure 4.1, **1** → **3**) or via consecutive electron and proton transfers (**1** → **2** → **4**) to *p*-Cl-aniline (**4** → **6**, 22% of the initial substrate concentration, Table 4.1).

Multi-element isotope fractionation patterns of *N*-MA and *p*-CH<sub>3</sub>-*N*-MA are both very similar (Figure 4.2, Table 4.1 and S4.3). The corresponding C, H, and N isotope enrichment factors are within the boundaries for reactions proceeding predominantly via the N-atom oxidation pathway to radical coupling products (*p*-OCH<sub>3</sub>-*N*-MA, **1** → **2** → **5**) and *N*-dealkylation (*p*-Cl-*N*-MA, **1** → **2** → **4** → **6**). Inverse <sup>15</sup>N-AKIE from partial imine bond formation (**1** → **2**) and normal <sup>2</sup>H- and <sup>13</sup>C-AKIEs due to C–H bond cleavage (**2** → **4**) suggest that both pathways were operational and contributed as isotope sensitive reaction steps (see section S3 in the SI for details on the allocation of AKIE-values to the two pathways). This interpretation is corroborated by the observation of reaction products for both reaction pathways (Table 4.1 and Figure S4.6).

Theoretical calculations of the bond dissociation enthalpies (BDE, Table S4.4) of the C<sub>α</sub>–H bond for the substituted *N*-MAs and the radical cation intermediates (**2** in Figure 4.1) and N-centered Mulliken spin densities (Table S4.5) further support the above interpretation. C<sub>α</sub>–H BDEs are substantially lower in radical intermediates than in the

reactants, implying that C $_{\alpha}$ -H bonds are much more likely to be cleaved after an initial electron transfer (**1**  $\rightarrow$  **2**). Moreover, C $_{\alpha}$ -H BDEs of compound **2** decrease in the order  $p\text{-OCH}_3 > p\text{-CH}_3 > p\text{-Cl} \approx p\text{-H}$  suggesting that the cleavage of the C $_{\alpha}$ -H bond is thermodynamically more favorable for  $p\text{-H}$ - and  $p\text{-Cl}$ -substituted radical species than for the  $p\text{-CH}_3$ - and  $p\text{-OCH}_3$ -substituted ones. This sequence is in excellent agreement with the larger share of  $N$ -dealkylation products found for  $N\text{-MA}$  and  $p\text{-Cl-}N\text{-MA}$ . (Table 4.1, entries 1-4). The series of N-centered Mulliken spin densities (Table S4.5), which express the excess spin present on the amino N atom of the  $N\text{-MA}$  radical cation intermediates,<sup>22</sup> correlate with the trends in relative reactivity of substituted  $N\text{-MAs}$  and also support the measured product distribution. The degree of radical localization on the amino N atom decreased in the order  $p\text{-H} > p\text{-Cl} > p\text{-CH}_3 > p\text{-OCH}_3$ . This observation implies that highly localized N-centered radicals might be responsible for the decrease in reactivity.

### 4.3.2 Isotope fractionation associated with the oxidative transformation of substituted $N,N$ -dimethylanilines by MnO<sub>2</sub>

With the investigation of *para*-substituted  $N,N$ -dimethylanilines ( $N,N$ -DMAs), we explored the impact of an additional  $N$ -methyl group on the C, H, and N isotope fractionation trends in identical experimental systems containing MnO<sub>2</sub>. As illustrated in Figure 4.2 and Table 4.1, similar trends for N-atom oxidation vs. C-H bond cleavage were observed. Contaminant disappearance kinetics were biphasic and the relative reactivity increased in the order  $p\text{-H} < p\text{-Cl} < p\text{-CH}_3 < p\text{-OCH}_3$ . Multi-element isotope fractionation patterns (Figure S4.5), however, were not fully identical with observations made for *para*-substituted  $N\text{-MAs}$  owing to the additional C and H atoms of the  $N$ -methyl group of  $N,N$ -DMAs. Only the oxidation of  $N,N$ -DMA by MnO<sub>2</sub> resembled that of  $N\text{-MA}$  and showed the same qualitative product distribution and almost identical isotope fractionation and <sup>13</sup>C-, <sup>2</sup>H-, and <sup>15</sup>N-AKIE-values as  $N\text{-MA}$  within experimental error (Table 4.1 and S4.3, Figure 4.3).

In the case of  $p\text{-Cl-}N,N\text{-DMA}$ , <sup>13</sup>C-, <sup>2</sup>H-AKIE-values were similar to those of  $p\text{-Cl-}N\text{-MA}$ . Furthermore, a high share of  $N$ -dealkylation products ( $p\text{-Cl-}N\text{-MA}$  and  $p\text{-Cl-aniline}$ ) was detected (71%, Table 4.1, entry 6) but no radical coupling products. The normal AKIE<sub>N</sub> of  $p\text{-Cl-}N,N\text{-DMA}$  ( $1.0023 \pm 0.0017$ ) is consistent with the assumption that partial imine bond formation in the aminium intermediate **2** is not involved in the isotope-sensitive step of oxidative  $N$ -dealkylations. Instead, this observation suggests that  $p\text{-Cl-}N,N\text{-DMA}$  could have reacted via initial H atom abstraction to intermediate

**3**, in which bond strength to N does not increase (**1**  $\rightarrow$  **3**  $\rightarrow$  **4**  $\rightarrow$  **6**). Alternatively, the observed fractionation could imply a shift in the rate-limiting step of the reaction, assuming that the cleavage of the C $_{\alpha}$ -H bond (**2**  $\rightarrow$  **4**) exhibits a normal secondary N isotope effect. Given that inverse AKIE<sub>N</sub>-values were found for the MnO<sub>2</sub>-catalyzed oxidation of all *N*-MAs and *N,N*-DMAs except for Cl-substituted ones, as well as for a series of substituted anilines,<sup>135</sup> we infer that MnO<sub>2</sub> reacts via one-electron transfer with aromatic amines rather than via H atom abstraction. Therefore, we hypothesize that the normal AKIE<sub>N</sub> of *p*-Cl-*N,N*-DMA more likely reflects the isotope effects pertinent to pre-equilibrium kinetics involving the rate-limiting C $_{\alpha}$ -H bond cleavage<sup>72,78,159</sup> (see Equation S4.7). Further evidence that the reaction is initiated by an electron transfer and not by H atom abstraction from the N-methyl group is obtained from theoretical calculations of the BDEs of the C $_{\alpha}$ -H bond for the reactant and the radical cation intermediates (Table S4.4). C $_{\alpha}$ -H BDEs of the substituted *N,N*-DMA radical species are substantially smaller than for the corresponding reactants implying that the cleavage of the C $_{\alpha}$ -H bond is energetically more favorable after an initial electron transfer from the aminium radicals (**2** in Figure 4.1).

Oxidation of *p*-CH<sub>3</sub>-*N,N*-DMA was accompanied by notably large C and H isotope fractionation presumably due to additional reactions at the *aromatic* CH<sub>3</sub>-substituent.  $\epsilon_C$ - and  $\Delta\delta^2\text{H}/\Delta\delta^{13}\text{C}$ -values increased compared to *p*-CH<sub>3</sub>-*N*-MA despite isotopic dilution by the additional methyl group (Table S4.3). Tentative AKIE<sub>C</sub>-values of  $1.0215 \pm 0.0012$  (Table 4.1, entry 7a) also significantly exceed those of other *N,N*-DMAs, corroborating the assumption of additional reactive C-H bonds. In fact, product analyses confirmed the presence of *p*-dimethylaminobenzyl alcohol and coupling products thereof (Figure S4.6). AKIE-values therefore reflect a weighted average of isotope effects associated with several reactions taking place at competing sites in the reactive intermediates (see Equation 4.5 and Equation S4.13). Further confirmation for the contribution of side chain oxidation reaction of *p*-CH<sub>3</sub>-*N,N*-DMA was obtained from experiments with *ortho*- and *meta*-substituted CH<sub>3</sub>-*N,N*-DMAs (Table 4.1, entries 7a-c). All CH<sub>3</sub>-*N,N*-DMAs showed identical C, H, and N isotope fractionation within experimental error, that is, the isotope effects were not sensitive to the position of the aromatic substituent. Our previous work on the oxidation of substituted anilines by MnO<sub>2</sub>, however, showed that isotope effects for reactions at the N atom are not affected by *meta*-substitution, because the latter exerts no electronic effects on the radical stabilization.<sup>135</sup> The absence of this effect is evidence for isotope fractionation at a reactive site that is not sensitive to the position of aromatic substituent.

The  $\epsilon_N$ -value, for the oxidation of *p*-OCH<sub>3</sub>-*N,N*-DMA was the most inverse one observed in this study ( $+9.6 \pm 1.6\%$ , Table 4.1, entry 8) despite small contributions from the normal EIE<sub>N</sub> associated with N atom deprotonation from the conjugate acid (see previous discussion for *p*-OCH<sub>3</sub>-*N*-MA). The AKIE<sub>N</sub> of  $0.9910 \pm 0.0012$  (Table 4.1, entry 8) again implies a reaction pathway **1** → **2** → **5** (Figure 4.1), in which the formation of partial imine bonds (**1** → **2**) is the isotope-sensitive elementary step. The share of *N*-dealkylation product was equally minor for both *p*-OCH<sub>3</sub>-*N*-MA and -*N,N*-DMA (Table 4.1, entries 4 and 8), as expected for a reaction leading predominantly to radical coupling products. C and H isotope fractionation of *p*-OCH<sub>3</sub>-*N,N*-DMA reflects primarily side chain oxidation of the *p*-OCH<sub>3</sub>-group. In contrast to *p*-OCH<sub>3</sub>-*N*-MA, for which  $\epsilon_C$  and  $\epsilon_H$  were statistically indifferent from zero (Table 4.1, entry 4), we observed significant C and H isotope fractionation for *p*-OCH<sub>3</sub>-*N*-MA ( $\Delta\delta^2H/\Delta\delta^{13}C$ -value of  $12 \pm 0.8$ ; Table S4.3, entry 8), so that <sup>13</sup>C- and <sup>2</sup>H-AKIEs were attributed primarily to -OCH<sub>3</sub>-group oxidations (SI). Evidence for *p*-OCH<sub>3</sub>-group oxidation could only be obtained from the detection of radical coupling products with -OH instead of -OCH<sub>3</sub>-substituents (Figure S4.6). Note that product analysis ruled out the presence of *p*-OH-*N,N*-DMA in the reactors. Because C and H isotope fractionation cannot be explained by reactions along the radical coupling pathway, we speculate that the phenol-type intermediates might have been oxidized further with MnO<sub>2</sub> as reported earlier by others.<sup>136</sup>

The computed BDEs of the C–H and O–C bonds of the *p*-CH<sub>3</sub>- and *p*-OCH<sub>3</sub>-substituent, respectively, for reactant and radical cations further support this interpretation of side chain oxidations (Table S4.4). Lower BDEs for the O–C bond of the *p*-OCH<sub>3</sub>-substituent compared to the C<sub>α</sub>–H bond of the N-methyl group of *p*-OCH<sub>3</sub>-*N,N*-DMA indicate that *O*-dealkylation is thermodynamically more favorable than *N*-dealkylation, in agreement with the identified reaction products (Table 4.1 and Figure S4.6). In contrast, BDEs of the C–H bonds of the *p*-CH<sub>3</sub>-substituent and C<sub>α</sub>–H bond of the N-methyl group of *p*-CH<sub>3</sub>-*N,N*-DMA suggest that side chain oxidation is more likely to occur from species **2** after one-electron oxidation of the reactant.

### 4.3.3 Isotope fractionation associated with the enzymatic oxidation by horseradish peroxidase

Combined C, H, and N isotope fractionation trends obtained during HRP-catalyzed oxidation of *para*-substituted *N*-MAs and *N,N*-DMAs are shown in Figure S4.5 and the corresponding isotope enrichment factors and AKIE values are listed in Table 4.1. Oxida-



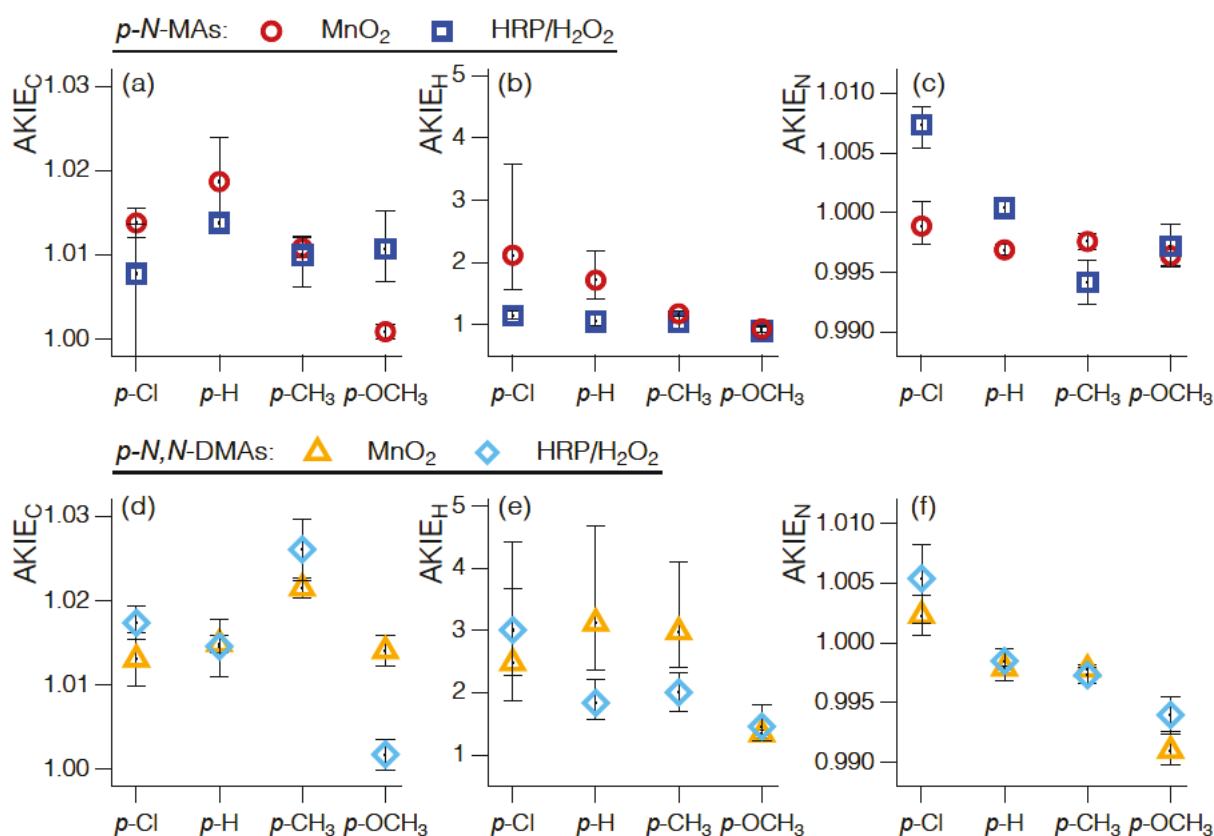


Figure 4.3:  $^{13}\text{C}$ -,  $^2\text{H}$ -, and  $^{15}\text{N}$ -Apparent kinetic isotope effects (AKIE) associated with oxidative transformation of *p*-Cl, *p*-H, *p*-CH<sub>3</sub>, and *p*-OCH<sub>3</sub>-*N*-methyl, and *N,N*-dimethylanilines by MnO<sub>2</sub> and HRP.

tion of *para*-substituted *N*-MAs exhibited less pronounced isotope fractionation compared to the reaction of the same compounds in MnO<sub>2</sub>-suspensions, and  $\epsilon$ -values were generally smaller. H isotope fractionation was almost insignificant, that is 95% confidence intervals approached the size of  $\epsilon_{\text{H}}$ -values. Moreover, C isotope fractionation did not show any systematic trend with *para*-substitution. The same observation was made for N isotope fractionation, where  $\epsilon_{\text{N}}$ -values of *p*-CH<sub>3</sub>-*N*-MA ( $5.8 \pm 1.8\text{‰}$ ) were more inverse than for *p*-OCH<sub>3</sub>-*N*-MA ( $2.9 \pm 1.7\text{‰}$ ) and significantly normal for *p*-Cl-*N*-MA ( $-7.4 \pm 1.5\text{‰}$ , Table 4.1, entries 10-12). *N*-dealkylation and radical coupling products were found in all cases (see compilation of tentative di- and trimer structures in the Figure S4.6) but the share of substituted anilines formed did not exceed 7% of the initial substrate concentration (*p*-Cl-*N*-MA, Table 4.1) in agreement with the frequent observation of radical coupling products in reactions of peroxidases.<sup>45</sup>

Although oxidation of substituted aromatic *N*-alkyl amines by both HRP and MnO<sub>2</sub> is reported to occur via initial electron transfer to form aminium radical species as

common intermediates,<sup>45,65,78,135,147</sup> subsequent product dismutation can also represent the non-enzymatic rate-determining step in case of HRP.<sup>45,107</sup> Because the  $\text{AKIE}_N$  for *p*-Cl-*N*-MA is normal, as found in experiments with  $\text{MnO}_2$ , we suggest this to imply that the second electron and proton transfer from the aminium intermediate **2** leading to compound **4** (Figure 4.1) was responsible for the observed isotope fractionation. This rate-limiting step and the corresponding  $\text{AKIE}_N$  are presumably typical for HRP-catalyzed *N*-dealkylations with substituted *N*-MAs as substrates see Table S4.1 and Equation S4.7).

The HRP-catalyzed oxidation of *para*-substituted *N,N*-DMAs exhibited multi-element isotope fractionation and isotope effect trends that were very similar to those for the oxidation of the same compounds by  $\text{MnO}_2$  as indicated by the correlations of  $\delta^{15}\text{N}$  vs.  $\delta^{13}\text{C}$  and  $\delta^2\text{H}$  vs.  $\delta^{13}\text{C}$ , respectively (Figure 4.2, 4.3 and S4.5c/d). This observation suggests that the oxidation mechanisms follow the three principal trends found in experiments with  $\text{MnO}_2$ -suspensions. *p*- $\text{OCH}_3$ -*N,N*-DMA reacts predominantly via N-atom oxidation and the share of *N*-dealkylation products (*p*- $\text{OCH}_3$ -*N*-MA and *p*- $\text{OCH}_3$ -aniline) was below 2.4% of the initial substrate mass (Table 4.1). Consequently,  $\text{AKIE}_N$  was inverse ( $0.9940 \pm 0.0015$ ). Small C and H isotope fractionation was due to minor contributions from *O*-dealkylation invoked from the detection of the corresponding products (incl. *p*-dimethylaminophenol, Figure S6) and the corresponding  $^{13}\text{C}$ - and  $^2\text{H}$ -AKIEs likely reflect side-chain oxidation reactions. *p*-Cl-*N,N*-DMA oxidation caused significant C and H isotope fractionation and the  $\epsilon_{\text{C}}$ - and  $\epsilon_{\text{H}}$ -values were in the range of those found for the oxidation by  $\text{MnO}_2$  (compare entries no. 6 and 14 in Table 4.1). Furthermore, *p*-Cl-*N,N*-DMA oxidation led to the corresponding *N*-dealkylation products (>55%, Table 4.1) without the formation of radical coupling products. The normal  $\text{AKIE}_N$  is consistent with the above interpretation for *p*-Cl-*N*-MA that HRP-catalyzed oxidation of compounds with electron-withdrawing substituents occurs via oxidative *N*-dealkylation as found at mineral surfaces, so that the second electron and proton transfer (**2**  $\rightarrow$  **4**) becomes the isotopic and rate-limiting step. Isotope fractionation and product formation trends of *p*- $\text{CH}_3$ -*N,N*-DMA and *N,N*-DMA oxidation follow a combination of the observed trends. Similar to oxidation by  $\text{MnO}_2$ , C and H isotope fractionation of *p*- $\text{CH}_3$ -*N,N*-DMA is affected by oxidation of the *p*- $\text{CH}_3$ -group to the corresponding *p*-dimethylaminobenzyl alcohol (Figure S4.6) so that AKIE-values reflect the ensemble of competing reaction pathways (Equation S4.13).



Table 4.1: Reaction product analyses and C, H, and N isotope fractionation associated with oxidation of substituted *N*-methyl- (*N*-MA) and *N,N*-dimethylanilines (*N,N*-DMA) by MnO<sub>2</sub> and horseradish peroxidase HRP/H<sub>2</sub>O<sub>2</sub>. Detection of radical coupling products, fraction of *N*-dealkylation products, bulk compound C, H, and N isotope enrichment factors,  $\epsilon_E$ , and corresponding apparent kinetic isotope effects, AKIE<sub>E</sub>.<sup>a</sup>

Entry	Compound	Reactant conversion (%)	Radical coupling products (-)	<i>N</i> -MA (%)	<i>N</i> -dealkylation to aniline (%)	$\epsilon_C$ <sup>b</sup> (‰)	$\epsilon_H$ (‰)	$\epsilon_N$ (‰)	AKIE <sub>C</sub> <sup>c</sup> (-)	AKIE <sub>H</sub> (-)	AKIE <sub>N</sub> (-)
<b>MnO<sub>2</sub>-suspensions</b>											
1	<i>N</i> -MA	74	yes	-	30.6	-2.6 (0.8, 0.7)	-48.1 (14.4, 14.4)	3.1 (0.5, 0.5)	1.0187 (0.0058, 0.0053)	1.72 (0.30, 0.46)	0.9969 (0.0004, 0.0005)
2	<i>p</i> -Cl- <i>N</i> -MA	80	no	-	22 <sup>d</sup>	-1.9 (0.2, 0.2)	-72.5 (23.1, 26.8)	1.1 (1.5, 2.1)	1.0138 (0.0017, 0.0017)	2.12 (0.55, 1.46)	n.a. <sup>e</sup>
3	<i>p</i> -CH <sub>3</sub> - <i>N</i> -MA	98	yes	-	1.7	-1.3 (0.1, 0.2)	-14.6 (3.1, 3.0)	2.4 (0.7, 0.7)	1.0108 (0.0011, 0.0013)	1.18 (0.04, 0.04)	0.9976 (0.0007, 0.0007)
4	<i>p</i> -OCH <sub>3</sub> - <i>N</i> -MA	71	yes	-	2.5	-0.1 (0.1, 0.1)	5.5 (6.3, 4.9)	3.7 (0.8, 0.8)	n.a.	n.a.	0.9964 (0.0008, 0.0008)
5	<i>N,N</i> -DMA	100	yes	33.9	2.2	-1.8 (0.1, 0.1)	-66.6 (10.2, 10.7)	2.1 (0.2, 0.2)	1.0149 (0.0011, 0.0011)	3.12 (0.76, 1.57)	0.9979 (0.0002, 0.0002)
6	<i>p</i> -Cl- <i>N,N</i> -DMA	100	no	59.7	11.0	-1.6 (0.4, 0.4)	-63.5 (13.4, 13.5)	-2.3 (1.7, 1.7)	1.0131 (0.0032, 0.0032)	2.48 (0.61, 1.20)	1.0023 (0.0017, 0.0017)
7a	<i>p</i> -CH <sub>3</sub> - <i>N,N</i> -DMA	90	yes	10.5	1.7	-2.3 (0.1, 0.1)	-57.7 (7.6, 8.5)	2.2 (0.6, 0.4)	1.0215 (0.0012, 0.0012)	2.98 (0.58, 1.12)	0.9978 (0.0006, 0.0004)
7b	<i>o</i> -CH <sub>3</sub> - <i>N,N</i> -DMA	85	yes <sup>f</sup>	yes <sup>f</sup>	n.d. <sup>g</sup>	-2.2 (0.2, 0.2)	-69.2 (14.2, 14.3)	1.6 (0.7, 0.6)	1.0200 (0.0015, 0.0015)	7.10 (3.17, <sup>h</sup> )	0.9984 (0.0007, 0.0006)
7c	<i>m</i> -CH <sub>3</sub> - <i>N,N</i> -DMA	100	yes	yes	n.d.	-2.4 (0.2, 0.2)	-50.5 (11.2, 11.3)	2.4 (0.4, 0.4)	1.0222 (0.0016, 0.0017)	2.55 (0.63, 1.29)	0.9976 (0.0004, 0.0004)
8	<i>p</i> -OCH <sub>3</sub> - <i>N,N</i> -DMA	100	yes	1.8	2.3	-1.5 (0.2, 0.2)	-20.6 (3.1, 3.1)	9.6 (1.2, 1.6)	1.0141 <sup>i</sup> (0.0018, 0.0018)	1.34 <sup>i</sup> (0.07, 0.07)	0.9910 (0.0012, 0.0016)
<b>Horseradish peroxidase (HRP) / H<sub>2</sub>O<sub>2</sub></b>											
9	<i>N</i> -MA	56	yes	-	2.4	-1.9 (0.1, 0.1)	-6 (8, 10)	-0.4 (0.7, 0.9)	1.0138 (0.0006, 0.0006)	n.a.	1.0004 (0.0007, 0.0009)
10	<i>p</i> -Cl- <i>N</i> -MA	78	yes	-	7.1	-1.1 (3.3, 0.8)	-16 (6, 7)	-7.4 (2.5, 1.5)	1.0078 (0.0228, 0.0059)	1.15 (0.06, 0.07)	1.0074 (0.0020, 0.0015)
11	<i>p</i> -CH <sub>3</sub> - <i>N</i> -MA	51	yes	-	2.3	-1.2 (0.5, 0.3)	-4 (10, 8)	5.8 (1.8, 1.8)	1.0100 (0.0037, 0.0022)	n.a.	0.9942 (0.0018, 0.0018)
12	<i>p</i> -OCH <sub>3</sub> - <i>N</i> -MA	97	yes	-	1.1	-1.3 (0.5, 0.5)	11 (10, 7)	2.9 (1.7, 1.8)	1.0107 (0.0039, 0.0045)	n.a.	0.9972 (0.0017, 0.0018)
13	<i>N,N</i> -DMA	66	yes	44.2	1.5	-1.8 (0.4, 0.4)	-43 (8, 8)	1.5 (1.7, 1.0)	1.0146 (0.0036, 0.0032)	1.84 (0.26, 0.38)	0.9985 (0.0017, 0.0010)
14	<i>p</i> -Cl- <i>N,N</i> -DMA	83	no	52.9	2.3	-2.1 (0.2, 0.2)	-69 (11, 11)	-5.4 (3.7, 2.9)	1.0174 (0.0020, 0.0020)	3.01 (0.73, 1.41)	1.0054 (0.0037, 0.0029)
15	<i>p</i> -CH <sub>3</sub> - <i>N,N</i> -DMA	85	yes	13.4	1.4	-2.8 (0.4, 0.4)	-41 (9, 6)	2.7 (0.7, 0.7)	1.0261 (0.0037, 0.0036)	2.01 (0.30, 0.32)	0.9973 (0.0007, 0.0007)
16	<i>p</i> -OCH <sub>3</sub> - <i>N,N</i> -DMA	79	yes	1.2	1.2	-0.2 (0.2, 0.2)	-24 (10, 10)	6.0 (1.6, 1.5)	1.0018 <sup>i</sup> (0.0018, 0.0017)	1.46 <sup>i</sup> (0.24, 0.35)	0.9940 (0.0016, 0.0015)

<sup>a</sup>Uncertainties of  $\epsilon_E$ - and AKIE<sub>E</sub>-values are reported as upper and lower 95% confidence intervals and shown in parentheses; <sup>b</sup> derived from linear regression using Equation 4.2;

<sup>c</sup> AKIE<sub>E</sub>s calculated according to Equation 4.4; <sup>d</sup> carbinolamine detected, see Figure S4.6; <sup>e</sup> n.a. = not applicable, experimental error too high;

<sup>f</sup> Product was not quantified but identified by LC-MS/MS; <sup>g</sup> n.d. = not determined; <sup>h</sup> Because of high uncertainty the upper confidence interval is not applicable;  $\epsilon_{rp}$  = -899 (185,

186); <sup>i</sup> values reflect oxidation of OCH<sub>3</sub>-side chains only.



## 4.4 Environmental Significance

This study reveals the complexity of the reaction mechanism and isotope effects associated with the oxidative transformation of substituted aromatic *N*-alkyl amines. Isotope fractionation patterns for C, H, and N and the corresponding AKIE-values enable one to delineate reactions pathways proceeding via *N*-dealkylation vs. N-atom oxidation, respectively, despite dilution of isotope fractionation by up to 9 C and 13 H atoms. The observed trends are highly compound-specific, however, and even subtle changes in electronic properties from the presence or absence of different types of aromatic and/or *N*-alkyl substituent can result in changes of reaction mechanisms, rate-limiting step(s) and thus isotope fractionation behavior. Moreover, regardless of the fact that reactions are initiated at a N-containing functional group, they are not necessarily accompanied by characteristic trends of N isotope fractionation.

Our findings suggest that even if three elements are evaluated simultaneously for isotope fractionation, an extrapolation of the AKIEs to other contaminants reacting through oxidation of the *N*-alkyl moiety (e.g., fluoroquinolones,<sup>159</sup> triazines<sup>131</sup>) is challenging. This task requires one to assess the impact of complex structural features on the reactivity of the *N*-alkyl moiety very thoroughly and on a compound-by-compound basis. Further isotope fractionation studies of alternative routes of aromatic *N*-alkyl amine degradation, including nucleophilic additions of the amino functional group to electrophilic sites of natural organic matter, are warranted for a comprehensive isotopic evaluation of the transformation processes of this class of aquatic micropollutants.

## Acknowledgement

This work was supported by the Swiss National Science Foundation (grants no. 200020-116447/1 and 200020-134720/1 to T.B.H.). We thank René Schwarzenbach, Kristopher McNeill, and A. Lynn Roberts for helpful discussions.



# Supporting Information to Chapter 4

## Chemicals

The chemicals used for this study were purchased from various manufacturers and used without further treatment. Pure compounds were aniline (99.5%), *N*-methylaniline (98%), *N,N*-dimethylaniline (99.5%), *p*-chloroaniline (99%), *p*-nitrotoluene (98%) from Fluka (Buchs SG, Switzerland), and *N,N*-dimethyl-*o*-toluidine (99%), *N,N*-dimethyl-*m*-toluidine (97%), *N,N*-dimethyl-*p*-toluidine (99%), *N*-methyl-*p*-toluidine (98%), *p*-chloro-*N*-methylaniline (94%), *p*-methoxy-*N*-methylaniline (98%), *p*-methoxy-aniline (99%), and *o*-nitrotoluene (99%) from Aldrich (Buchs SG, Switzerland). Furthermore *p*-(methylamino)phenol was purchased from Sigma-Aldrich (Buchs SG, Switzerland), *p*-methylaniline (99.5%) from Merck (Dietikon, Switzerland), *p*-chloro-*N,N*-dimethylaniline (98%), and *p*-methoxy-*N,N*-dimethylaniline (98%) from the Capot Chemical Company (Hangzhou, Zhejiang, China), *p*-dimethylaminobenzyl alcohol (97%) from ABCR GmbH & Co. KG (Karlsruhe, Germany), and *p*-(dimethylamino)phenol from Specs (Delft, The Netherlands).

Stock solutions were prepared in methanol (HPLC grade) from Acros Organics (Geel, Belgium). Methanol (HPLC Grade) and water (HPLC grade, Acros Organics) were used for HPLC and LC-MS/MS analysis. Additional solvents were ethyl acetate (99.5%, Fluka), and methylene chloride (99.5%, Merck). Further solutions were hydrochloric acid (32%, impureness: 0.0001%, Merck) and sodium hydroxide (32%, impureness: 0.0001%, Fluka), formic acid (98-100%, for analysis, Merck) and hydrogen peroxide (32%, for analysis, Fluka).

Salts used included sodium chloride (99.5%, Fluka), potassium phosphate (99%, Sigma, Buchs SG, Switzerland), sodium permanganate monohydrate (97%, Sigma-Aldrich), manganese(II) chloride tetrahydrate (analysis purity, Merck), and sodium sulphate anhydrous (99%, Merck). Horse-radish peroxidase (Type IV, 256 units / mg solid (using pyrogallol), RZ  $\sim$  3.1, Sigma-Aldrich) was purchased as a salt-free powder. All aqueous solutions were prepared in nanopure water (18.2 M $\Omega$ ·cm, Barnstead NANOpure Diamond Water Purification System).

The carrier gas for GC and GC/IRMS analysis was helium (He, 99.999%) and GC/IRMS-measurements required N<sub>2</sub> (99.999%), CO<sub>2</sub> (99.999%), and H<sub>2</sub> (99.999%) as reference gases. In addition O<sub>2</sub> (99.9995%), and synthetic air (20  $\pm$  1% O<sub>2</sub> in N<sub>2</sub> (99.9995%)) from Carbagas (Rümlang, Switzerland) were used.

## Computational methods: Supplemental benchmarking

To determine if the CBS-QB3 method properly described general thermodynamic parameters for the system in question, gas phase CBS-QB3 calculations on *N*-methyl- and *N,N*-dimethylaniline were performed. The CBS-QB3 procedure is a compound method which is designed to produce very accurate thermodynamic parameters. The procedure involves: (a) geometry optimization to a local (global) minimum structure (b) calculation of the molecular frequencies and corresponding zero point energies (with scaling factors determined by benchmarking) (c) determination of highly accurate electronic energies by extrapolating the results of successively more accurate methods to the asymptotic end representing an infinite basis set and full configuration interaction treatment. Interested readers are directed to<sup>116</sup> for a thorough review of the method.

All calculations were performed in the absence of solvent because there are highly accurate gas phase values available in the literature. This serves as a fundamental test of the method's ability to model redox chemistry and thus the accuracy of the underlying theory employed for the remaining processes studied in this work. The Ionization energies (IE) shown in Table S4.6 show that the theory performs quite well for this limited test set (error < 1%). The accuracy of the integral equation formalism - polarizable continuum model (IEF-PCM) method has been shown to be quite accurate, but it has not yet been well benchmarked for aqueous phase redox chemistry.

## Assumptions for interpretation of apparent kinetic isotope effects (AKIE)

Interpretation of *observed* isotope effects as apparent kinetic isotope effects (AKIEs) was made in terms of up to four partially competing multistep reactions according to Figure S4.1. The numbers correspond to the compounds in Scheme 1 of the main manuscript and are shown here in a simplified reaction scheme for (i) N-atom oxidation (**1** → **2** → **5**), (ii) oxidative *N*-dealkylation (**1** ⇌ **2** → **4**), and (iii) oxidation of *aromatic* CH<sub>3</sub>-groups (**1** ⇌ **2** → **P<sub>arCH<sub>3</sub></sub>**) and (iv) OCH<sub>3</sub>-groups (**1** → **P<sub>arOCH<sub>3</sub></sub>**). Notice that reactions (iii) and (iv) is an unintended side reaction that are not shown in Scheme 1.

Apparent kinetic isotope effects reported in Table 4.1 of the main manuscript may thus reflect *combinations* of isotope effects for the different pathways. The most likely and most predominant contributions are summarized in Table S4.1 based on the magnitude of measured C, H, and N isotope fractionation and product identification studies (molecular

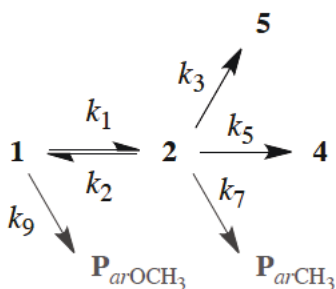


Figure S4.1: Reaction kinetics assumed for interpretation of AKIE-values. Numbers correspond to compounds in Figure 4.1,  $P_{arCH_3}$  and  $P_{arOCH_3}$  stand for products from oxidation of *aromatic*  $CH_3$ - and  $OCH_3$ -side chains, respectively. Rate constants are numbered according to conventions proposed by Cook and Cleland<sup>20</sup>.

structures of identified reaction products 4, 5,  $P_{arCH_3}$ , and  $P_{arOCH_3}$  are shown in Figure Figure S4.6). As illustrated in detail below, the AKIEs of the multistep reaction shown in Figure S4.1 can be further complicated through equilibrium isotope effect contributions and masking by different commitment factors.

1. The most typical AKIE-values for N-atom oxidation ( $AKIE^{N-ox}$ ) were found for reactions of *p*- $OCH_3$ -*N*-MA with  $MnO_2$  and HRP/ $H_2O_2$  (entries 4 and 12 in Table S4.1) as well as for *p*- $OCH_3$ -*N,N*-DMA transformation by  $MnO_2$  (only  $^{15}N$ - $AKIE^{N-ox}$ ). In the absence of any competing reaction,  $AKIE^{N-ox}$  reflect a one-step process and are primary effects for N while those for C and H are secondary.
2. Characteristic AKIE-values for oxidative *N*-dealkylation ( $AKIE^{N-dealk}$ ) were found for *p*-Cl-*N*-MAs and *p*-Cl-*N,N*-DMAs regardless of the type of oxidant (entries 2, 6, 10, 14 in Table S4.1). In the absence of any competing reaction,  $AKIE^{N-dealk}$  are primary effects for C and H and secondary for N and reflect a two-step reaction. Therefore,  $AKIE^{N-dealk}$  may be subject to equilibrium isotope effect contribution and masking through forward commitment factors.
3. AKIE-values listed for the oxidation of *N*-MA (entries 1 and 9) and *N,N*-DMA (entries 5 and 13) by either oxidant and oxidation of *p*- $CH_3$ -*N*-MA by HRP/ $H_2O_2$  (entry 11) are weighted averages of two distinct, isotope fractionating reactions. Primary isotope effects during N-atom oxidation ( $AKIE^{N-ox}$ ) and oxidative *N*-dealkylation ( $AKIE^{N-dealk}$ ), however, predominantly affect different atoms, that is N during N-atom oxidation and C, H during oxidative *N*-dealkylation. As first approximation,  $^{15}N$ -AKIEs can be allocated to N-atom oxidation while  $^{13}C$ - and  $^2H$ -AKIEs



are pertinent to oxidative *N*-dealkylation even if both reactions take place in parallel.  $\text{AKIE}^{\text{N-dealk}}$  may be subject to equilibrium isotope effect contribution and masking through forward commitment factors.

4. Compounds with aromatic  $\text{CH}_3$ - and  $\text{OCH}_3$ -substituents additionally underwent side-chain oxidation reactions. On the basis of the BDE-calculations, we hypothesize that these reactions occur differently at the two substituents.
  - (a) Oxidative *O*-dealkylation of the  $\text{OCH}_3$ -group competes with N-atom oxidation.  $^{13}\text{C}$ - and  $^2\text{H}$ -AKIE are indicative for this reaction ( $\text{AKIE}^{\text{arOx}}$ ) because no significant C and H isotope fractionation occurs during N-atom oxidation.  $^{15}\text{N}$ -AKIEs, on the other hand, largely stand for N-atom oxidation ( $\text{AKIE}^{\text{N-ox}}$ ). AKIE-values for entries 8, and 16 reflect a combination of N-atom oxidation ( $\text{AKIE}^{\text{N-ox}}$ ) and AKIEs from the oxidation of the  $\text{OCH}_3$ -group in the substrate (Table S4.1).
  - (b) Oxidation of aromatic  $\text{CH}_3$ -groups, in contrast, is postulated to take place only after formation of the aminium radical **2**. Consequently, AKIE-values for entries 3, 7a-c, and 15 reflect a combination of N-atom oxidation ( $\text{AKIE}^{\text{N-ox}}$ ) and competing *N*-dealkylation and side-chain oxidation ( $\text{AKIE}_{\text{comp}}$ ), respectively (Table S4.1). The expression for  $\text{AKIE}_{\text{comp}}$  is derived in the section below.

## Isotope effects associated with the N-atom oxidation pathway

As reported previously,<sup>135</sup> the AKIE-values for N atom oxidations of aromatic amines reflect the initial electron transfer step to the aminium radical, while no contributions of the fast radical coupling process to isotope fractionation have been found. Assuming  $k_3 \gg k_1$  and  $k_3 \gg k_2$ , the corresponding  $\text{AKIE}^{\text{N-ox}}$  thus reflects the kinetic isotope effect on  $k_1$  ( $\text{KIE}_1$ ).

$$\text{AKIE}^{\text{N-ox}} = \text{KIE}_1 = \frac{k_1^l}{k_1^h} \quad (\text{S4.1})$$

Apparent kinetic isotope effects arising from N-atom oxidation can, in principle, be implied for every substrate and reaction, in which radical coupling products were detected (Figure S4.6). Such AKIEs are primary only for N, while those for C and H are

secondary and neglected here. The substituted aromatic *N*-alkyl amines, whose isotope fractionation behavior involves N-atom oxidation are listed in Table S4.1.

## Isotope effects associated with the oxidative *N*-dealkylation pathway

In contrast, oxidative *N*-dealkylation (ii) is a two-step reaction and its  $\text{AKIE}^{\text{N-dealk}}$  is derived using the steady-state approximation for pathway  $\mathbf{1} \rightleftharpoons \mathbf{2} \rightarrow \mathbf{4}$  (Figure S4.1), where  $k_1$  and  $k_2$  are the rate constants of the electron transfers and  $k_5$  stands for the second electron and  $\text{H}^+$ -transfer reactions leading to the highly reactive iminium cation ( $\mathbf{4}$ ). The derivation of the reaction rate and  $\text{AKIE}^{\text{N-dealk}}$  follows. Superscripts  $l$  and  $h$  denote light and heavy isotopologs, respectively,  $\text{EIE}_1$  is the ratio of  $\text{KIE}_1 / \text{KIE}_2$ .

$$\frac{d[\mathbf{1}]}{dt} = -\frac{k_1 \cdot k_5}{k_2 + k_5} [\mathbf{1}] \quad (\text{S4.2})$$

$$\frac{d[\mathbf{1}]^l}{d[\mathbf{1}]^h} = \frac{k_1^l \cdot k_5^l (k_2^h + k_5^h)}{k_1^h \cdot k_5^h (k_2^l + k_5^l)} \frac{[\mathbf{1}]^l}{[\mathbf{1}]^h} \quad (\text{S4.3})$$

$$\text{AKIE}^{\text{N-dealk}} = \text{KIE}_1 \cdot \text{KIE}_5 \frac{(1/\text{KIE}_2 + k_5^h/k_2^l)}{(1 + k_5^l/k_2^l)} \quad (\text{S4.4})$$

$$= \text{KIE}_1 \cdot \text{KIE}_5 \frac{(1/\text{KIE}_2 + k_5^h/k_5^l \cdot k_5^l/k_2^l)}{(1 + k_5^l/k_2^l)} \quad (\text{S4.5})$$

$$= \text{KIE}_1 \cdot \text{KIE}_5 \frac{(1/\text{KIE}_2 + 1/\text{KIE}_5 \cdot k_5^l/k_2^l)}{(1 + k_5^l/k_2^l)} \quad (\text{S4.6})$$

$$\text{AKIE}^{\text{N-dealk}} = \frac{\text{EIE}_1 \cdot \text{KIE}_5 + \text{KIE}_1 \cdot k_5/k_2}{1 + k_5/k_2} \quad (\text{S4.7})$$

Interpretation of AKIEs pertinent to oxidative *N*-dealkylation pathway involves assumptions about contributions of equilibrium isotope effect,  $\text{EIE}_1$ , of the initial electron transfer ( $\mathbf{1} \rightleftharpoons \mathbf{2}$ ) and masking by the forward commitment to catalysis by  $k_5/k_2$ . The AKIE-values for C and H are most indicative for the cleavage of the  $\text{C}_\alpha\text{-H}$  bond reflected in  $\text{KIE}_5$  if commitment is negligible ( $\ll 1$ ) and  $\text{EIE}_1$  approaches unity. The latter can be justified by the assumption that the secondary C and H  $\text{KIE}_1$  associated with  $\mathbf{1} \rightarrow \mathbf{2}$  are cancelled by similar secondary C and H  $\text{KIE}_2$  of the backward reaction. There is, however, no information about the possible values  $k_5/k_2$ .

Table S4.1: Predominant contributions of C, H, and N isotope fractionation to AKIE-values associated with oxidation of substituted *N*-methyl- (*N*-MA) and *N,N*-dimethylanilines (*N,N*-DMA) by MnO<sub>2</sub> and horseradish peroxidase HRP/H<sub>2</sub>O<sub>2</sub>.<sup>a</sup>

Entry	Compound	AKIE <sup>N-ox</sup>	AKIE <sup>N-dealk</sup>	AKIE <sup>arOx</sup>	AKIE <sub>comp</sub>
<b>MnO<sub>2</sub>-suspensions</b>					
1	<i>N</i> -MA	x	x		
2	<i>p</i> -Cl- <i>N</i> -MA		x		
3	<i>p</i> -CH <sub>3</sub> - <i>N</i> -MA	x			x
4	<i>p</i> -OCH <sub>3</sub> - <i>N</i> -MA	x			
5	<i>N,N</i> -DMA	x	x		
6	<i>p</i> -Cl- <i>N,N</i> -DMA		x		
7a	<i>p</i> -CH <sub>3</sub> - <i>N,N</i> -DMA	x			x
7b	<i>o</i> -CH <sub>3</sub> - <i>N,N</i> -DMA	x			x
7c	<i>m</i> -CH <sub>3</sub> - <i>N,N</i> -DMA	x			x
8	<i>p</i> -OCH <sub>3</sub> - <i>N,N</i> -DMA	x		x	
<b>Horseradish peroxidase (HRP) / H<sub>2</sub>O<sub>2</sub></b>					
9	<i>N</i> -MA	x	x		
10	<i>p</i> -Cl- <i>N</i> -MA		x		
11	<i>p</i> -CH <sub>3</sub> - <i>N</i> -MA	x	x		
12	<i>p</i> -OCH <sub>3</sub> - <i>N</i> -MA	x			
13	<i>N,N</i> -DMA	x	x		
14	<i>p</i> -Cl- <i>N,N</i> -DMA		x		
15	<i>p</i> -CH <sub>3</sub> - <i>N,N</i> -DMA	x			x
16	<i>p</i> -OCH <sub>3</sub> - <i>N,N</i> -DMA	x		x	

[a] AKIE definitions are: AKIE<sup>N-ox</sup> = N atom oxidation, AKIE<sup>N-dealk</sup> = N-dealkylation, AKIE<sup>arOx</sup> = oxidation of OCH<sub>3</sub> side chains of compound **1**, AKIE<sub>comp</sub> = oxidative *N*-dealkylation in CH<sub>3</sub>-substituted *N*-MAs and *N,N*-DMAs in competition with oxidation of CH<sub>3</sub>-side chains from compound **2**.

## Isotope effects associated with competing oxidative *N*-dealkylation and aromatic CH<sub>3</sub> side-chain oxidation

For some of the investigated compounds, side-chain oxidation of aromatic CH<sub>3</sub>-groups contribute to the observed isotope fractionation. Because oxidative *N*-dealkylation and side-chain oxidations were assumed to share the same reactive intermediate **2**, the overall AKIE-value is a weighted average of AKIE-values (AKIE<sub>comp</sub>) for each pathway (**2** → **4** vs. **2** → **P**<sub>arCH<sub>3</sub></sub>). The final expression for AKIE<sub>comp</sub> illustrates that quantification of the branching ratio,  $\theta$ , and possible commitment factors ( $c_f$ ) is necessary to apportion the observed isotope effects to the different, competing pathways. This task is, however, beyond the scope of the present study.

$$\frac{d[\mathbf{1}]}{dt} = -\frac{k_1 \cdot k_5 + k_1 \cdot k_7}{k_2 + k_5 + k_7} [\mathbf{1}] \quad (\text{S4.8})$$

$$\frac{d[\mathbf{1}]^l}{d[\mathbf{1}]^h} = \frac{k_1^l (k_5^l + k_7^l)}{k_1^h (k_5^h + k_7^h)} \frac{(k_2^h + k_5^h + k_7^h)}{(k_2^l + k_5^l + k_7^l)} \frac{[\mathbf{1}]^l}{[\mathbf{1}]^h} \quad (\text{S4.9})$$

$$\text{AKIE}_{\text{comp}} = \text{KIE}_1 \frac{\text{KIE}_5 + \text{KIE}_5 \cdot k_7^l/k_5^l}{1 + \text{KIE}_5/\text{KIE}_7 \cdot k_7^l/k_5^l} \frac{(1/\text{KIE}_2 + 1/\text{KIE}_5 \cdot k_5^l/k_2^l + 1/\text{KIE}_7 \cdot k_7^l/k_2^l)}{(1 + k_5^l/k_2^l + k_7^l/k_2^l)} \quad (\text{S4.10})$$

$$= \frac{\text{KIE}_5 (k_5^l + k_7^l) / k_5^l \cdot \text{KIE}_7 \cdot k_5^l}{k_5^l \cdot \text{KIE}_7 + k_7^l \cdot \text{KIE}_5} \frac{(\text{EIE}_1 + \text{KIE}_1/\text{KIE}_5 \cdot k_5^l/k_2^l + \text{KIE}_1/\text{KIE}_7 \cdot k_7^l/k_2^l)}{(1 + k_5^l/k_2^l + k_7^l/k_2^l)} \quad (\text{S4.11})$$

$$= \frac{\text{KIE}_5 \cdot \text{KIE}_7}{\frac{k_5^l}{(k_5^l + k_7^l)} \text{KIE}_7 + \frac{k_7^l}{(k_5^l + k_7^l)} \text{KIE}_5} \frac{\text{EIE}_1 + \text{KIE}_1 \frac{(k_5^l + k_7^l)}{k_2^l} \left( \frac{k_5^l}{(k_5^l + k_7^l) \text{KIE}_5} + \frac{k_7^l}{(k_5^l + k_7^l) \text{KIE}_7} \right)}{\left( 1 + \frac{k_5^l + k_7^l}{k_2^l} \right)} \quad (\text{S4.12})$$

$$\text{AKIE}_{\text{comp}} = \frac{1}{1 + c_f} \left( \frac{\text{EIE}_1 \cdot \text{KIE}_5 \cdot \text{KIE}_7}{\theta \cdot \text{KIE}_7 + (1 - \theta) \cdot \text{KIE}_5} + \text{KIE}_1 \cdot c_f \right) \quad (\text{S4.13})$$

with

$$\theta = \frac{k_5^l}{k_5^l + k_7^l} \approx \frac{k_5}{k_5 + k_7}$$

$$c_f = \frac{k_5^l + k_7^l}{k_2^l} \approx \frac{k_5 + k_7}{k_2}$$

## Tables

**Selected physico-chemical properties of substituted *N*-alkylated aromatic amines**

Table S4.2: Names, abbreviations, molecular weight,  $pK_a$ -values, Hammett  $\sigma$  constant of the aromatic substituent of the investigated substituted *N*-methyl- and *N,N*-dimethylanilines and experimental conditions:  $MnO_2$ -, horseradish peroxidase (HRP) and  $H_2O_2$ -concentrations.

Entry <sup>a</sup>	Compound name (IUPAC)	Abbreviation	MW [g/mol]	$pK_a^b$ [-]	$\sigma^{87}$ [-]	$MnO_2$ [mM]	Experimental conditions HRP/ $H_2O_2$ [nM / mM]
1 / 9	<i>N</i> -methylaniline	<i>N</i> -MA	107.2	4.68	0.00	3	15 / 4.5
2 / 10	4-chloro- <i>N</i> -methylaniline	<i>p</i> -Cl- <i>N</i> -MA	141.6	4.35	0.23	3	5 / 1.5
3 / 11	4-methyl- <i>N</i> -methylaniline	<i>p</i> -CH <sub>3</sub> - <i>N</i> -MA	121.2	5.12	-0.17	1.5	0.5 / 0.75
4 / 12	4-methoxy- <i>N</i> -methylaniline	<i>p</i> -OCH <sub>3</sub> - <i>N</i> -MA	137.2	5.72	-0.28	- <sup>c</sup>	0.5 / 0.75
5 / 13	<i>N,N</i> -dimethylaniline	<i>N,N</i> -DMA	121.2	5.12 <sup>126</sup>	0.00	5	10 / 3
6 / 14	4-chloro- <i>N,N</i> -dimethylaniline	<i>p</i> -Cl- <i>N,N</i> -DMA	155.6	4.25	0.23	1.5	2.5 / 0.75
7a / 15	4-methyl-CH <sub>3</sub> - <i>N,N</i> -dimethylaniline	<i>p</i> -CH <sub>3</sub> - <i>N,N</i> -DMA	135.2	5.46	-0.17	3	2 / 0.6
7b	2-methyl- <i>N,N</i> -dimethylaniline	<i>o</i> -CH <sub>3</sub> - <i>N,N</i> -DMA	135.2	5.61	0.10 <sup>18</sup>	5	
7c	3-methyl- <i>N,N</i> -dimethylaniline	<i>m</i> -CH <sub>3</sub> - <i>N,N</i> -DMA	135.2	5.57	-0.07	3	
8 / 16	4-methoxy- <i>N,N</i> -dimethylaniline	<i>p</i> -OCH <sub>3</sub> - <i>N,N</i> -DMA	151.2	5.55	-0.28	2	1.1 / 0.75

<sup>a</sup> Entries 1-8 refer to experiments with  $MnO_2$  and entries 9-16 to those with HRP/ $H_2O_2$ , compare Table 1 in the main manuscript;

<sup>b</sup> Values calculated with MarvinSketch, Version 5.2.3 from ChemAxon<sup>90</sup>; <sup>c</sup> Different  $MnO_2$ -amounts added.

## Multi-element isotope analysis for the oxidation by $\text{MnO}_2$ and $\text{HRP}/\text{H}_2\text{O}_2$

Table S4.3: Multi-element isotope fractionation analysis for the evaluation of oxidative transformation of substituted *N*-methyl- and *N,N*-dimethylanilines by  $\text{MnO}_2$  and  $\text{HRP}/\text{H}_2\text{O}_2$ : linear regression slopes of the isotopic signatures  $\Delta\delta^{15}\text{N}/\Delta\delta^{13}\text{C}$  and  $\Delta\delta^2\text{H}/\Delta\delta^{13}\text{C}$  are compared to the ratios of the bulk enrichment factors  $\epsilon_{\text{N}}/\epsilon_{\text{C}}$  and  $\epsilon_{\text{H}}/\epsilon_{\text{C}}$ .

Entry	Compound	$\Delta\delta^{15}\text{N}/\Delta\delta^{13}\text{C}$	$\epsilon_{\text{N}}/\epsilon_{\text{C}}$	$\Delta\delta^2\text{H}/\Delta\delta^{13}\text{C}$	$\epsilon_{\text{H}}/\epsilon_{\text{C}}$
<b>Substituted <i>N</i>-methylanilines (<i>N</i>-MA)</b>					
$\text{MnO}_2$					
1	<i>N</i> -MA	$-1.1 \pm 0.2$	$-1.2 \pm 0.2$	$14 \pm 3.0$	$19 \pm 4.4$
2	<i>p</i> -Cl- <i>N</i> -MA	n.a. <sup>a</sup>		$43 \pm 6.3$	$38 \pm 6.3$
3	<i>p</i> -CH <sub>3</sub> - <i>N</i> -MA	$-1.8 \pm 0.2$	$-1.8 \pm 0.2$	$9.4 \pm 1.1$	$11 \pm 1.3$
4	<i>p</i> -OCH <sub>3</sub> - <i>N</i> -MA	n.a. <sup>a</sup>		n.a. <sup>a</sup>	
$\text{HRP} / \text{H}_2\text{O}_2$					
9	<i>N</i> -MA	$1.0 \pm 0.4$	$0.2 \pm 0.4$	$2.9 \pm 1.9$	$3.2 \pm 2.0$
10	<i>p</i> -Cl- <i>N</i> -MA	n.a. <sup>a</sup>		n.a. <sup>a</sup>	
11	<i>p</i> -CH <sub>3</sub> - <i>N</i> -MA	$-1.5 \pm 1.2$	$-4.8 \pm 1.8$	$-5.3 \pm 4.4$	$3.3 \pm 6.2$
12	<i>p</i> -OCH <sub>3</sub> - <i>N</i> -MA	$-1.8 \pm 0.4$	$-2.2 \pm 0.7$	$-9.4 \pm 1.7$	$-8.5 \pm 2.4$
<b>Substituted <i>N,N</i>-dimethylanilines (<i>N,N</i>-DMA)</b>					
$\text{MnO}_2$					
5	<i>N,N</i> -DMA	$-1.1 \pm 0.1$	$-1.2 \pm 0.1$	$40 \pm 2.9$	$37 \pm 2.7$
6	<i>p</i> -Cl- <i>N,N</i> -DMA	$1.4 \pm 0.6$	$1.4 \pm 0.7$	$31 \pm 3.2$	$40 \pm 5.6$
7a	<i>p</i> -CH <sub>3</sub> - <i>N,N</i> -DMA	$-1.0 \pm 0.1$	$-1.0 \pm 0.1$	$25 \pm 1.4$	$25 \pm 1.8$
7b	<i>o</i> -CH <sub>3</sub> - <i>N,N</i> -DMA	$-0.5 \pm 0.2$	$-0.7 \pm 0.2$	$33 \pm 3.5$	$31 \pm 3.8$
7c	<i>m</i> -CH <sub>3</sub> - <i>N,N</i> -DMA	$-0.9 \pm 0.1$	$-1.0 \pm 0.1$	$22 \pm 2.4$	$21 \pm 2.7$
8	<i>p</i> -OCH <sub>3</sub> - <i>N,N</i> -DMA	$-5.1 \pm 0.4$	$-6.4 \pm 0.5$	$12 \pm 0.8$	$14 \pm 1.3$
$\text{HRP} / \text{H}_2\text{O}_2$					
13	<i>N,N</i> -DMA	$-1.2 \pm 0.4$	$-0.8 \pm 0.3$	$23 \pm 3.3$	$24 \pm 3.9$
14	<i>p</i> -Cl- <i>N,N</i> -DMA	$1.8 \pm 0.5$	$2.6 \pm 0.6$	$19 \pm 3.7$	$33 \pm 3.8$
15	<i>p</i> -CH <sub>3</sub> - <i>N,N</i> -DMA	$-1.1 \pm 0.1$	$-1.0 \pm 0.2$	$14 \pm 0.7$	$15 \pm 2.1$
16	<i>p</i> -OCH <sub>3</sub> - <i>N,N</i> -DMA	n.a. <sup>a</sup>		n.a. <sup>a</sup>	

<sup>a</sup> n.a. = not applicable because of lack of significant isotope fractionation for one of the elements considered. These numbers would have exhibited uncertainties in the same orders of magnitude as the calculated parameters.

## Bond dissociation enthalpies (BDE) for neutral substituted aromatic *N*-alkyl amines and the corresponding radical cations

Table S4.4: Bond dissociation enthalpies (BDE) for neutral substituted aromatic *N*-alkyl amines and the corresponding radical cations, compounds **1** and **2** in Scheme 1 of the main manuscript.

Bond broken	Bond ID <sup>a</sup>	R <sub>1</sub>	R <sub>2</sub>	Leaving group	BDE cpd 1 (kcal/mol)	BDE cpd 2 (kcal/mol)
C <sub>α</sub> (H <sub>2</sub> )–H	I	H	Cl	H•	93.6	52.6
		H	H	H•	93.1	51.9
		H	CH <sub>3</sub>	H•	92.4	53.8
		H	OCH <sub>3</sub>	H•	90.9	56.9
		CH <sub>3</sub>	Cl	H•	91.3	49.5
		CH <sub>3</sub>	H	H•	91.3	49.0
		CH <sub>3</sub>	CH <sub>3</sub>	H•	91.7	50.9
		CH <sub>3</sub>	OCH <sub>3</sub>	H•	91.7	53.7
<i>p</i> -C(H <sub>2</sub> )–H	II	H	CH <sub>3</sub>	H•	88.5	61.0
		CH <sub>3</sub>	CH <sub>3</sub>	H•	89.0	62.7
<i>p</i> -O–CH <sub>3</sub>	III	H	OCH <sub>3</sub>	CH <sub>3</sub> •	50.7	46.1
		CH <sub>3</sub>	OCH <sub>3</sub>	CH <sub>3</sub> •	52.0	45.4
<i>p</i> -OC(H <sub>2</sub> )–H	IV	H	OCH <sub>3</sub>	H•	96.6	85.0
		CH <sub>3</sub>	OCH <sub>3</sub>	H•	98.3	86.5

<sup>a</sup> The bonds for which the BDEs are calculated are highlighted in Figure S4.7.



## Mulliken spin densities

Table S4.5: Minimum basis set Mulliken atom-centered spin density values obtained for the radical cation intermediate **2** in Scheme 1 of the main manuscript. *o*-C and *m*-C values represent the mean of two centers.

<b>R<sub>1</sub></b>	<b>R<sub>2</sub></b>	<b>MBS Spin Density</b>				
		N	<i>o</i> -C	<i>m</i> -C	<i>p</i> -C	R <sub>2</sub> fragment
H	H	0.456	0.254	0.147	0.387	0.058
H	Cl	0.434	0.234	0.137	0.350	-0.016
H	CH <sub>3</sub>	0.421	0.222	0.120	0.374	0.015
H	OCH <sub>3</sub>	0.372	0.156	0.050	0.252	0.129
CH <sub>3</sub>	H	0.528	0.250	0.145	0.345	0.048
CH <sub>3</sub>	Cl	0.507	0.237	0.140	0.317	-0.014
CH <sub>3</sub>	CH <sub>3</sub>	0.489	0.226	0.125	0.341	0.012
CH <sub>3</sub>	OCH <sub>3</sub>	0.426	0.166	0.061	0.241	0.116

## Supplemental benchmarking

Table S4.6: Benchmarking CBS-QB3 method against known gas-phase ionization energies (IE) ( $\Delta H_{2\rightarrow 1}$  in Scheme 1 of the main manuscript.)

<b>Compound name</b>	<b>IE (experimental)<sup>81</sup></b>	<b>IE (theory)</b>	<b><math>\Delta</math>IE</b>
	[kcal / mol]	[kcal / mol]	[kcal / mol]
<i>N</i> -methylaniline	168.8 $\pm$ 0.5	170.3	1.5
<i>N,N</i> -dimethylaniline	164.2 $\pm$ 0.5	165.4	1.2

## Figures

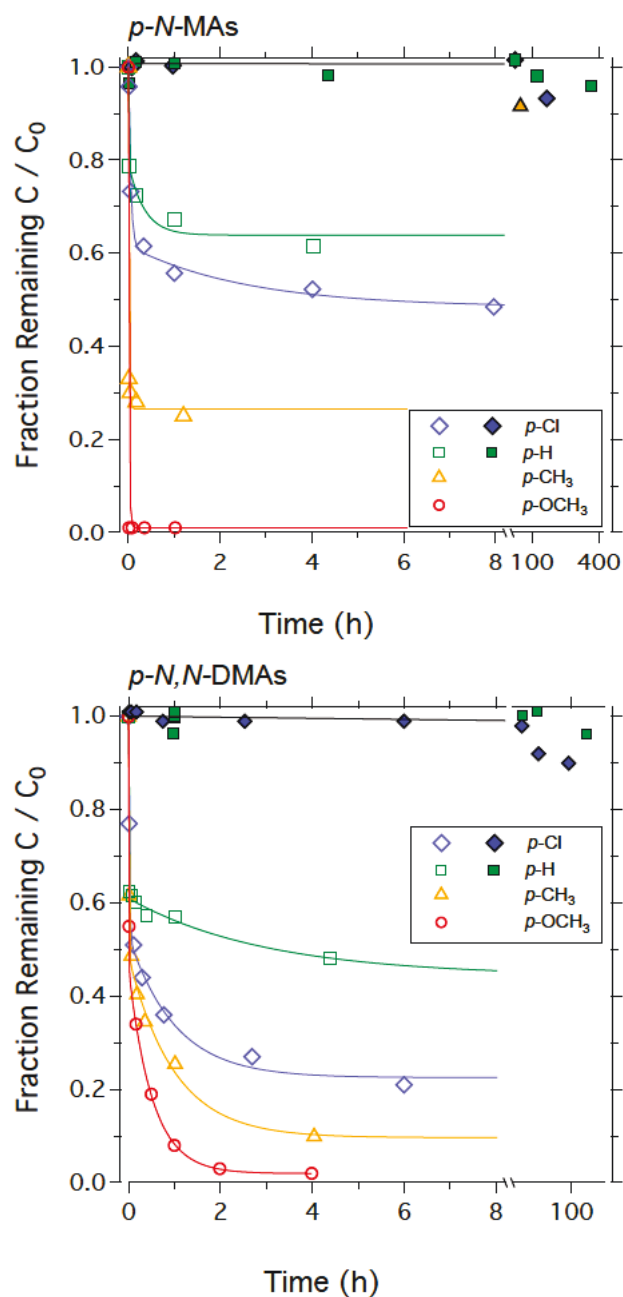
Oxidative transformation kinetics with  $\text{MnO}_2$ 

Figure S4.2: Reaction kinetics of *para*-substituted *N*-methyl- (top) and *N,N*-dimethylanilines (bottom) in 3mM  $\text{MnO}_2$ -suspension. Filled symbols denote long-term blank experiments, which are shown only for *p*-Cl- and *p*-H-*N*-MAs and *N,N*-DMAs, respectively.

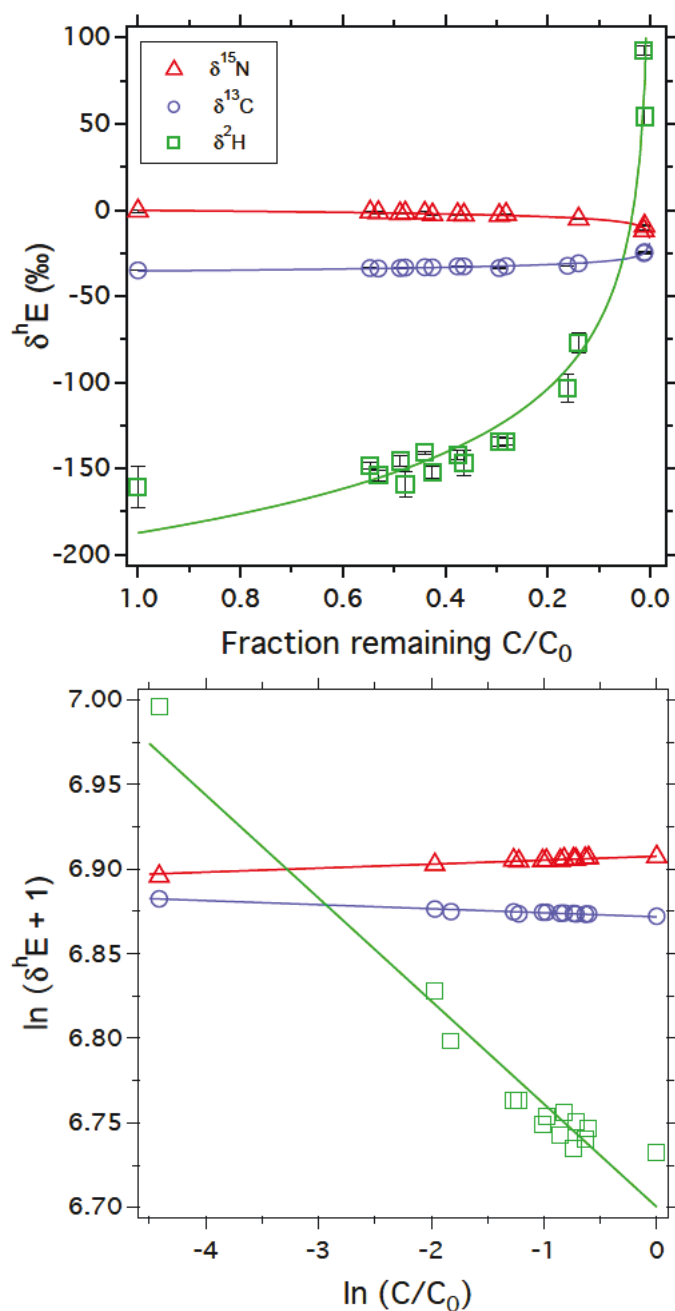
C, H, and N isotope fractionation during oxidation by  $\text{MnO}_2$ 

Figure S4.3: C, H, and N isotope fractionation measured in the bulk reactant during oxidation of *p*-CH<sub>3</sub>-*N,N*-dimethylaniline in 3 mM  $\text{MnO}_2$ -suspension (top) and linearized isotope fractionation according to equation 2 in the main manuscript (bottom). Blank experiments (not shown) did not reveal any isotope fractionation.

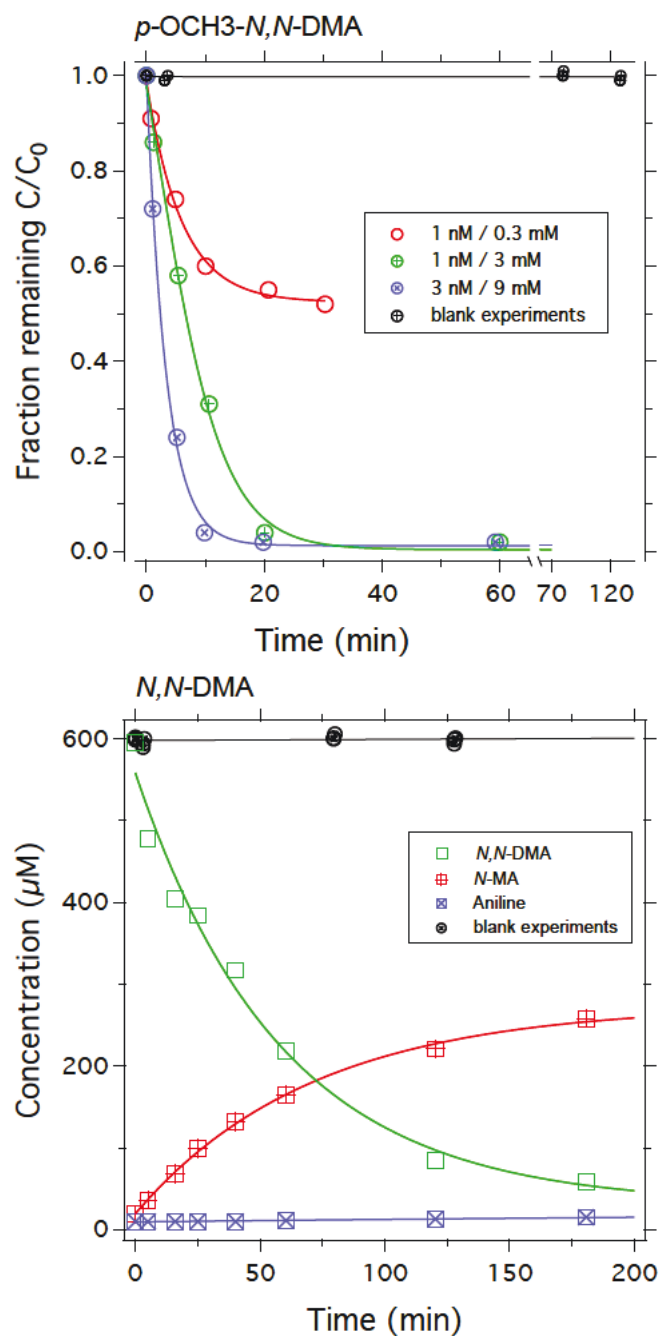
Oxidative transformation kinetics with HRP/H<sub>2</sub>O<sub>2</sub>

Figure S4.4: Reaction kinetics of *p*-OCH<sub>3</sub>-*N,N*-DMA with different HRP (nM)/H<sub>2</sub>O<sub>2</sub> (mM) concentration ratios (top) and transformation of *N,N*-DMA to *N*-MA and aniline with 10 nM HRP/3 mM H<sub>2</sub>O<sub>2</sub> (bottom). Blank experiments were performed in the absence of HRP, H<sub>2</sub>O<sub>2</sub>, or both.

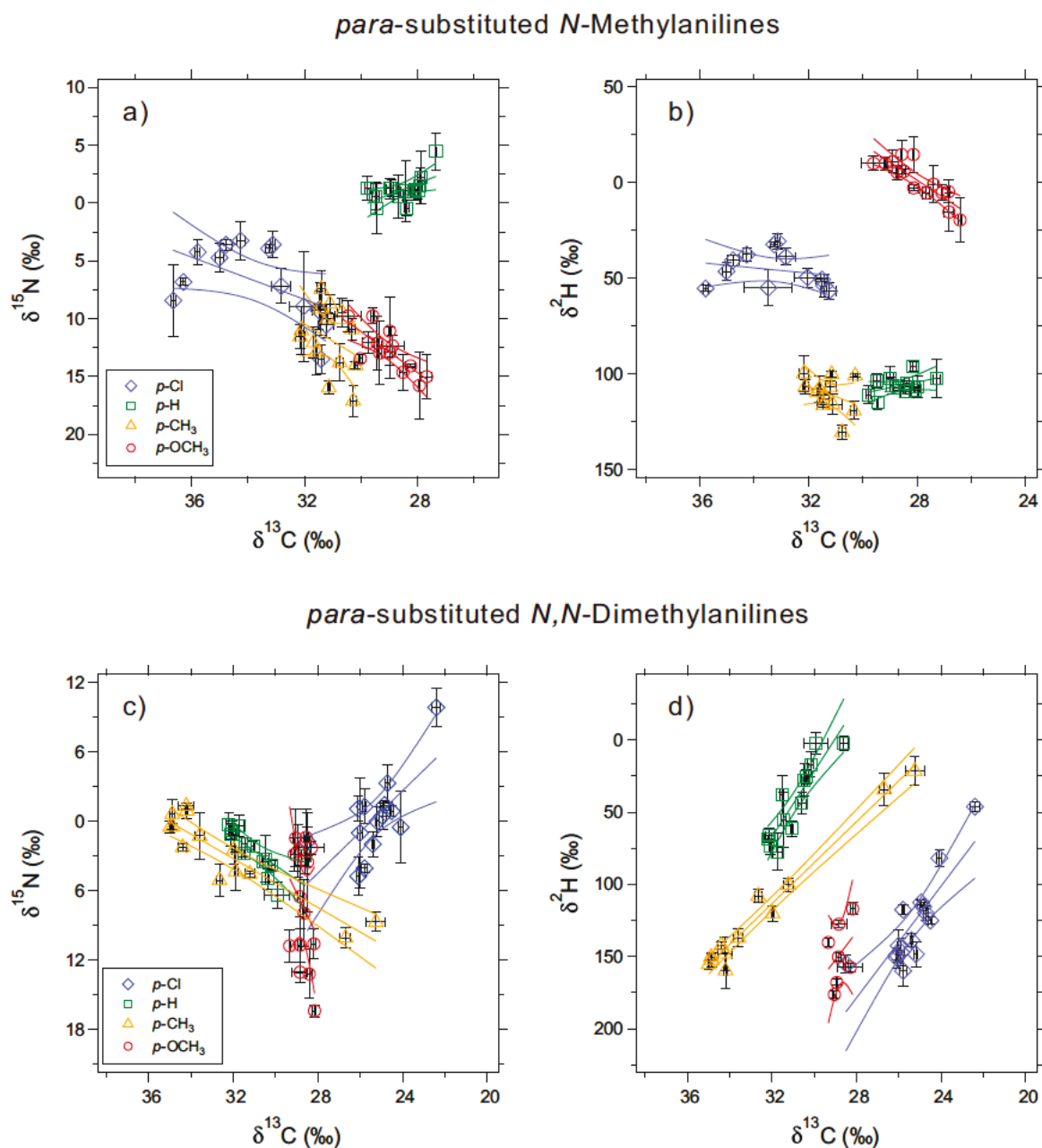
Multidimensional isotope analysis for the oxidation by HRP/H<sub>2</sub>O<sub>2</sub>

Figure S4.5: Multidimensional isotope plots illustrating the changes of  $\delta^{15}\text{N}$  vs.  $\delta^{13}\text{C}$  and  $\delta^2\text{H}$  vs.  $\delta^{13}\text{C}$  of *para*-substituted *N*-methyl- (panels a and b) and *N,N*-dimethylanilines (panels c and d) during oxidative transformation by HRP/H<sub>2</sub>O<sub>2</sub>.

## Product analysis

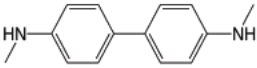
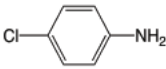
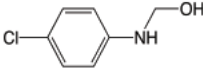
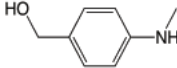
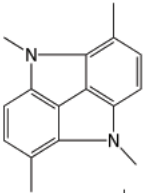
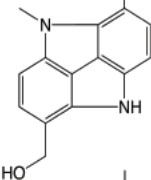
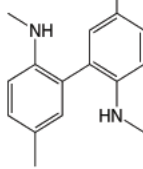
Oxidation by MnO <sub>2</sub>			
Detected mass m / z	Molecular formula	Most probable molecular structure	Remarks
Reactant: <i>N</i> -MA			
212 138	C <sub>14</sub> H <sub>16</sub> N <sub>2</sub>		
Reactant: <i>p</i> -C- <i>N</i> -MA			
128 026	C <sub>6</sub> H <sub>6</sub> NC		
158 037	C <sub>7</sub> H <sub>8</sub> NC		Intermediate of <i>N</i> -dealkylation
Reactant: <i>p</i> -CH <sub>3</sub> - <i>N</i> -MA			
138 091	C <sub>8</sub> H <sub>11</sub> ON		Based on MS/MS fragmentation pattern (-CH <sub>3</sub> -OH) Standard not available
237 138	C <sub>16</sub> H <sub>16</sub> N <sub>2</sub>		
239 117	C <sub>15</sub> H <sub>14</sub> ON <sub>2</sub>		
241 169	C <sub>16</sub> H <sub>20</sub> N <sub>2</sub>		

Figure S4.6: Most probable molecular structures of reaction products detected by LC-MS/MS during oxidation of substituted *N*-methyl- and *N,N*-dimethylanilines by MnO<sub>2</sub> and HRP/H<sub>2</sub>O<sub>2</sub>.

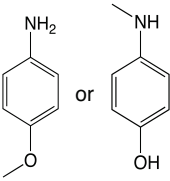
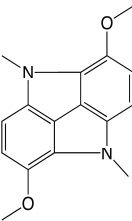
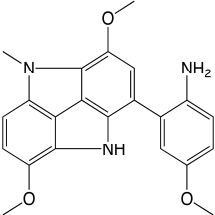
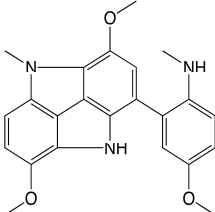
Detected mass m / z	Molecular formula	Most probable molecular structure	Remarks
329 181	C <sub>22</sub> H <sub>21</sub> N <sub>3</sub>		Trimer structure
Reactant: <i>p</i> -OCH <sub>3</sub> - <i>N</i> -MA			
124 075	C <sub>7</sub> H <sub>9</sub> ON		Not clear structure MS/MS: -CH <sub>3</sub> - elimination Standard not available
269 128	C <sub>16</sub> H <sub>16</sub> O <sub>2</sub> N <sub>2</sub>		
376 166	C <sub>22</sub> H <sub>21</sub> O <sub>3</sub> N <sub>3</sub>		Not clear whether -CH <sub>3</sub> - groups are attached to the N or the O atom
390 181	C <sub>23</sub> H <sub>23</sub> O <sub>3</sub> N <sub>3</sub>		Not clear whether -CH <sub>3</sub> - groups are attached to the N or the O atom

Figure S4.6 (continued): Most probable molecular structures of reaction products detected by LC-MS/MS during oxidation of substituted *N*-methyl- and *N,N*-dimethylanilines by MnO<sub>2</sub> and HRP/H<sub>2</sub>O<sub>2</sub>.

Detected mass m / z	Molecular formula	Most probable molecular structure	Remarks
Reactant: <i>N,N</i> -DMA			
227 154	C <sub>15</sub> H <sub>18</sub> N <sub>2</sub>		
241 169	C <sub>16</sub> H <sub>20</sub> N <sub>2</sub>		
Reactant: <i>p</i> -C - <i>N,N</i> -DMA			
128 026	C <sub>6</sub> H <sub>6</sub> NC		
142 042	C <sub>7</sub> H <sub>8</sub> NC		
172 052	C <sub>8</sub> H <sub>10</sub> ONC		Intermediate of <i>N</i> -dealkylation
Reactant: <i>p</i> -CH <sub>3</sub> - <i>N,N</i> -DMA			
138 091	C <sub>8</sub> H <sub>11</sub> ON		Structure not clear based on MS/MS spectrum
152 107	C <sub>9</sub> H <sub>13</sub> ON		Confirmed by means of a standard

Figure S4.6 (continued): Most probable molecular structures of reaction products detected by LC-MS/MS during oxidation of substituted *N*-methyl- and *N,N*-dimethylanilines by MnO<sub>2</sub> and HRP/H<sub>2</sub>O<sub>2</sub>.



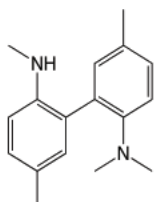
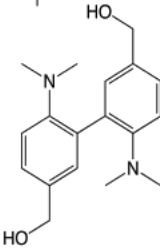
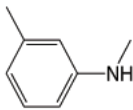
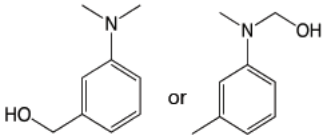
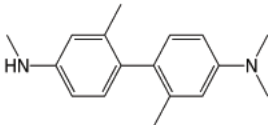
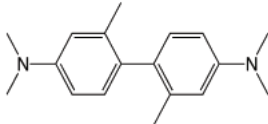
Detected mass m / z	Molecular formula	Most probable molecular structure	Remarks
255 184	$C_{17}H_{22}N_2$		
301 191	$C_{18}H_{24}O_2N_2$		
Reactant: <i>m</i> -CH <sub>3</sub> - <i>N,N</i> -DMA			
122 096	$C_8H_{11}N$		
152 107	$C_9H_{13}ON$		
255 186	$C_{17}H_{22}N_2$		
269 201	$C_{18}H_{24}N_2$		

Figure S4.6 (continued): Most probable molecular structures of reaction products detected by LC-MS/MS during oxidation of substituted *N*-methyl- and *N,N*-dimethylanilines by  $MnO_2$  and HRP/ $H_2O_2$ .

Detected mass m / z	Molecular formula	Most probable molecular structure	Remarks
Reactant: <i>o</i> -CH <sub>3</sub> - <i>N,N</i> -DMA			
122 096	C <sub>8</sub> H <sub>11</sub> N		
255 186	C <sub>17</sub> H <sub>22</sub> N <sub>2</sub>		
269 201	C <sub>18</sub> H <sub>24</sub> N <sub>2</sub>		
Reactant: <i>p</i> -OCH <sub>3</sub> - <i>N,N</i> -DMA			
124 076	C <sub>7</sub> H <sub>9</sub> ON		
138 091	C <sub>8</sub> H <sub>11</sub> ON		Phenolic structure was excluded by means of a standard based on the retention time
257 128	C <sub>15</sub> H <sub>16</sub> O <sub>2</sub> N <sub>2</sub>		
285 159	C <sub>17</sub> H <sub>20</sub> O <sub>2</sub> N <sub>2</sub>		
479 170	C <sub>28</sub> H <sub>22</sub> O <sub>4</sub> N <sub>4</sub>		Tetramer structure

Figure S4.6 (continued): Most probable molecular structures of reaction products detected by LC-MS/MS during oxidation of substituted *N*-methyl- and *N,N*-dimethylanilines by MnO<sub>2</sub> and HRP/H<sub>2</sub>O<sub>2</sub>.

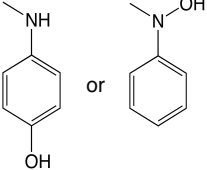
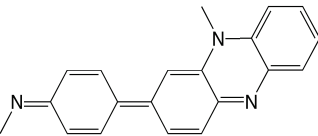
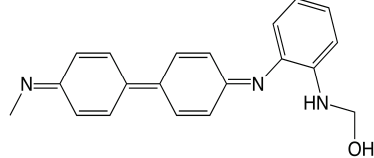
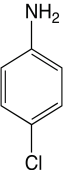
Oxidation by HRP / H <sub>2</sub> O <sub>2</sub>			
Detected mass m / z	Molecular formula	Most probable molecular structure	Remarks
Reactant: <i>N</i> -MA			
124 076	C <sub>7</sub> H <sub>9</sub> ON		Carbino amine structure not probable due to CH <sub>3</sub> -fragment in MS/MS spectrum
300 149	C <sub>20</sub> H <sub>17</sub> N <sub>3</sub>		
318 160	C <sub>20</sub> H <sub>20</sub> ON <sub>3</sub>		
391 191	C <sub>26</sub> H <sub>22</sub> N <sub>4</sub>		Tetramer structure
Reactant: <i>p</i> -C - <i>N</i> -MA			
128 026	C <sub>6</sub> H <sub>6</sub> NC		

Figure S4.6 (continued): Most probable molecular structures of reaction products detected by LC-MS/MS during oxidation of substituted *N*-methyl- and *N,N*-dimethylanilines by MnO<sub>2</sub> and HRP/H<sub>2</sub>O<sub>2</sub>.

Detected mass m / z	Molecular formula	Most probable molecular structure	Remarks
281.061	$C_{14}H_{14}N_2Cl_2$		
Reactant: <i>p</i> -CH <sub>3</sub> - <i>N</i> -MA			
138.091	$C_8H_{11}ON$		Structure not clear: CH <sub>3</sub> - and OH-fragments in MS/MS spectrum standard not available
237.139	$C_{16}H_{16}N_2$		
241.169	$C_{16}H_{20}N_2$		
328.181	$C_{22}H_{21}N_3$		

Figure S4.6 (continued): Most probable molecular structures of reaction products detected by LC-MS/MS during oxidation of substituted *N*-methyl- and *N,N*-dimethylanilines by  $MnO_2$  and HRP/ $H_2O_2$ .

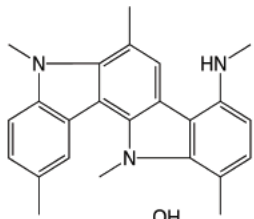
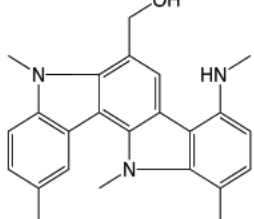
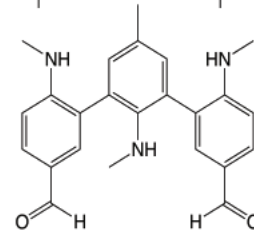
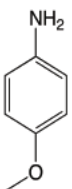
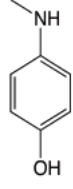
Detected mass m / z	Molecular formula	Most probable molecular structure	Remarks
356 212	C <sub>24</sub> H <sub>25</sub> N <sub>3</sub>		
372 207	C <sub>24</sub> H <sub>25</sub> ON <sub>3</sub>		
388 202	C <sub>24</sub> H <sub>25</sub> O <sub>2</sub> N <sub>3</sub>		
477 251	C <sub>27</sub> H <sub>32</sub> O <sub>4</sub> N <sub>4</sub>		Tetramer structure
Reactant: <i>p</i> -OCH <sub>3</sub> - <i>N</i> -MA			
124 076	C <sub>7</sub> H <sub>9</sub> ON	 or 	

Figure S4.6 (continued): Most probable molecular structures of reaction products detected by LC-MS/MS during oxidation of substituted *N*-methyl- and *N,N*-dimethylanilines by MnO<sub>2</sub> and HRP/H<sub>2</sub>O<sub>2</sub>.

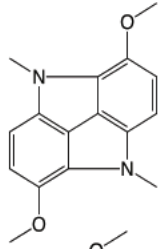
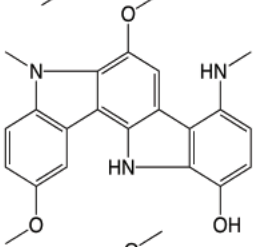
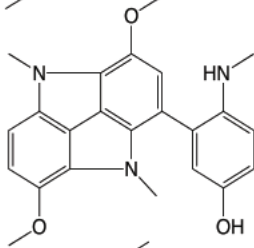
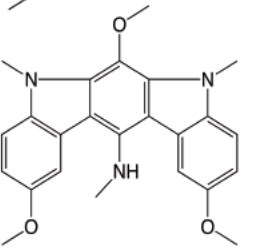
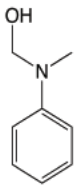
Detected mass m / z	Molecular formula	Most probable molecular structure	Remarks
269 128	$C_{16}H_{16}O_2N_2$		
376 166	$C_{22}H_{21}O_3N_3$		
390 181	$C_{23}H_{23}O_3N_3$		Not clear whether the CH <sub>3</sub> -group is attached to the N or the O atom
404 197	$C_{24}H_{25}O_3N_3$		Not clear whether the CH <sub>3</sub> -group is attached to the N or the O atom
Reactant: <i>N,N</i> -DMA			
138 091	$C_8H_{11}ON$		Intermediate of <i>N</i> -dealkylation

Figure S4.6 (continued): Most probable molecular structures of reaction products detected by LC-MS/MS during oxidation of substituted *N*-methyl- and *N,N*-dimethylanilines by  $MnO_2$  and HRP/ $H_2O_2$ .

Detected mass m / z	Molecular formula	Most probable molecular structure	Remarks
227 155	C <sub>15</sub> H <sub>18</sub> N <sub>2</sub>		
241 169	C <sub>16</sub> H <sub>20</sub> N <sub>2</sub>		
Reactant: <i>p</i> -C - <i>N,N</i> -DMA			
128 026	C <sub>6</sub> H <sub>6</sub> NC		
142 042	C <sub>7</sub> H <sub>8</sub> NC		
172 052	C <sub>8</sub> H <sub>10</sub> ONC		Intermediate of <i>N</i> -dealkylation
Reactant: <i>p</i> -CH <sub>3</sub> - <i>N,N</i> -DMA			
122 096	C <sub>8</sub> H <sub>11</sub> N		
138 091	C <sub>8</sub> H <sub>11</sub> ON		Structure not clear based on MS/MS spectrum
152 107	C <sub>9</sub> H <sub>13</sub> ON		Confirmed by means of a standard

Figure S4.6 (continued): Most probable molecular structures of reaction products detected by LC-MS/MS during oxidation of substituted *N*-methyl- and *N,N*-dimethylanilines by MnO<sub>2</sub> and HRP/H<sub>2</sub>O<sub>2</sub>.

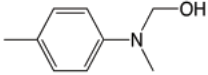
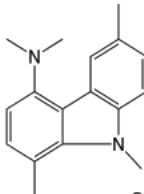
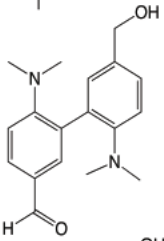
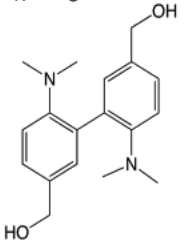
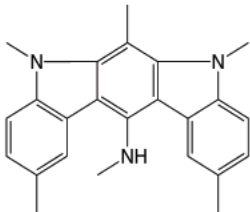
Detected mass m / z	Molecular formula	Most probable molecular structure	Remarks
152 107	$C_9H_{13}ON$		
253 170	$C_{17}H_{20}N_2$		
298 175	$C_{18}H_{22}O_2N_2$		
301 191	$C_{18}H_{24}O_2N_2$		
356 212	$C_{24}H_{25}N_3$		
388 239	$C_{25}H_{29}ON_3$		Trimer structure
409 166	$C_{25}H_{20}O_2N_4$		Tetramer structure

Figure S4.6 (continued): Most probable molecular structures of reaction products detected by LC-MS/MS during oxidation of substituted *N*-methyl- and *N,N*-dimethylanilines by  $MnO_2$  and HRP/ $H_2O_2$ .



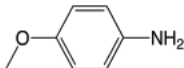
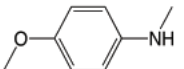
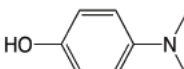
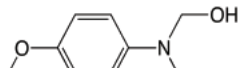
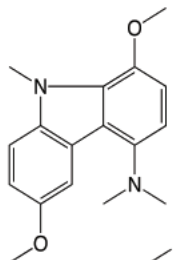
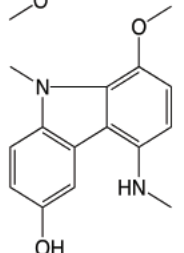
Detected mass m / z	Molecular formula	Most probable molecular structure	Remarks
Reactant: <i>p</i> -OCH <sub>3</sub> - <i>N,N</i> -DMA			
124 076	C <sub>7</sub> H <sub>9</sub> ON		
138 091	C <sub>8</sub> H <sub>11</sub> ON		
138 091	C <sub>8</sub> H <sub>11</sub> ON		Confirmed by means of a standard
168 101	C <sub>9</sub> H <sub>13</sub> O <sub>2</sub> N		
285 160	C <sub>17</sub> H <sub>20</sub> O <sub>2</sub> N <sub>2</sub>		
257 128	C <sub>15</sub> H <sub>16</sub> O <sub>2</sub> N <sub>2</sub>		Not clear whether the CH <sub>3</sub> -group is attached to the N or the O atom
349 178	C <sub>21</sub> H <sub>22</sub> O <sub>2</sub> N <sub>3</sub>		Trimer structure
379 165	C <sub>22</sub> H <sub>22</sub> O <sub>4</sub> N <sub>2</sub>		Trimer structure

Figure S4.6 (continued): Most probable molecular structures of reaction products detected by LC-MS/MS during oxidation of substituted *N*-methyl- and *N,N*-dimethylanilines by MnO<sub>2</sub> and HRP/H<sub>2</sub>O<sub>2</sub>.

## Bond dissociation enthalpy scheme

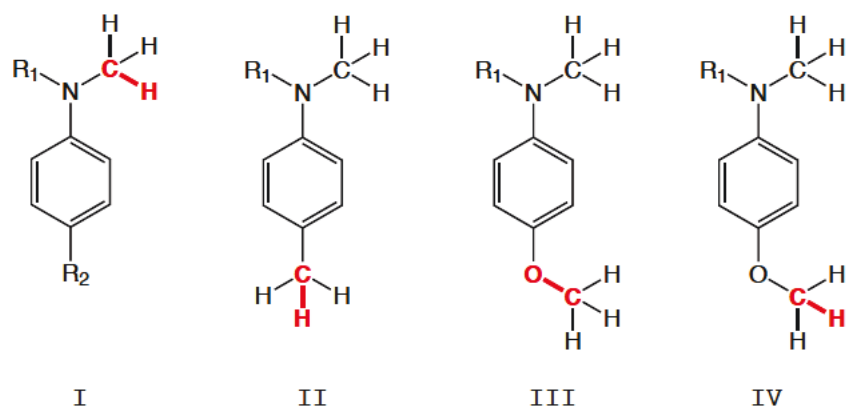


Figure S4.7: Naming scheme: The bond dissociation enthalpies (BDEs) listed for each molecule in Table Table S4.4 (neutral substituted aromatic *N*-alkyl amines and the corresponding radical cation) correspond to the bonds in bold and red. I:  $\text{NC}_\alpha\text{H}_2\text{-H}$ , II:  $p\text{-CH}_2\text{-H}$ , III:  $p\text{-O-CH}_3$ , IV:  $p\text{-OCH}_2\text{-H}$

## Chapter 5

# Conclusions and Outlook

## 5.1 Assessing oxidative transformations by CSIA

The goal of this PhD was to explore the C, H, and N isotope fractionation trends during transformation of aromatic *N*-alkyl amines via N atom oxidation and *N*-dealkylation in order to evaluate the potential of CSIA to track these transformation processes in the environment. To this end, we determined the magnitude and variability of  $^{13}\text{C}$ -,  $^2\text{H}$ -, and  $^{15}\text{N}$ -AKIEs pertinent to these two reaction pathways and investigated their reaction mechanisms. Our results also allow us to draw first conclusions regarding the application of CSIA to other important reaction pathways of aromatic amines in the environment, that is direct and indirect photolysis, nucleophilic addition to electrophilic sites of natural organic matter and enzymatic dioxygenation. These issues are discussed in detail in the present chapter.

C, H, and N isotope fractionation associated with N-atom oxidation and oxidative *N*-dealkylation of substituted aromatic *N*-alkyl amines showed complex trends depending on the type and position of the aromatic substituent as well as the degree of *N*-methylation. Extrapolations of C, H, and N fractionation trends to environmental situations can thus be made only for compounds studied in the present thesis and other substituted aromatic amines. This is the case for many intermediates used in the manufacture of agrochemicals, pharmaceuticals, dyes, and polymers, e.g. *m*-aminophenol, *N,N*-dimethyl-*m*-aminophenol, nitroanilines, and chloroanilines, which can be released into the environment through spills, accidents, industrial waste water effluents or agriculture.<sup>122</sup>

Oxidation of primary aromatic amines could be assessed by determining  $^{15}\text{N}$  fractionation over time or distance from the pollution source. Because  $\text{AKIE}_{\text{N}}$ -values approach unity with increasing electron acceptor properties of the aromatic substituent, further investigation is required for compounds carrying stronger electron acceptors than -Cl to check whether transformation via N atom oxidation leads to measurable N isotope fractionation. Since C bulk enrichment factors were very small,  $\epsilon_{\text{C,bulk}} = -1.1\text{‰}$ , unambiguous identification of the oxidation reaction by means of  $^{13}\text{C}$ -CSIA is related to several analytical challenges. Measuring C and H isotope fractionation might be more important for secondary and tertiary aromatic *N*-alkyl amines substituted with weak electron donors or electron acceptors. Substitution with a strong electron donor, such as  $-\text{OCH}_3$ , might cause C, and H isotope fractionation to vanish. In that case, determining  $^{15}\text{N}$  depletion in the reactant can be indicative of the oxidation reaction. Extrapolation of our findings to assess isotope fractionation patterns during oxidative transformation of larger,

structurally more complex contaminant molecules containing aromatic amino groups is not feasible. Instead, a compound-by-compound assessment is required if emerging micropollutants such as fluoroquinolone and sulfonamide antibacterial agents as well as acetanilide herbicides become accessible to CSIA. The establishment of appropriate analytical methods for the precise and accurate determination of the isotopic composition of these polar compounds using LC/IRMS should therefore be subject of future research.

Our results further indicate that assessment of oxidative transformation of aromatic *N*-alkyl amines in field situations by means of CSIA is associated with several analytical challenges. In the case that  $^{15}\text{N}$ -CSIA is applied under acidic conditions, the  $\text{EIE}_{\text{N}}$  associated with N atom deprotonation can compromise the accuracy of  $\delta^{15}\text{N}$  measurements. At pH smaller than the compound's  $\text{pK}_{\text{a}}$ ,  $\delta^{15}\text{N}$ -values can deviate by up to  $-20\text{‰}$  from reference values. In order to measure accurate  $^{15}\text{N}$  signatures the solution pH should be adjusted to  $\text{pH}=\text{pK}_{\text{a}}+2$  prior to isotope measurements. At  $\text{pH} < \text{pK}_{\text{a}}$  protonated and neutral species react simultaneously and the observable  $\text{AKIE}_{\text{N}}$  approaches then the product of  $\text{EIE}_{\text{N}}$  and  $\text{AKIE}_{\text{N,ox}}$ .

Many of the bulk enrichment factors determined in this work exhibited very small magnitudes. Observable  $^{15}\text{N}$  fractionation during oxidation of all investigated aromatic *N*-alkyl amines ranged between  $\epsilon_{\text{N,bulk}}=1.1$  and  $9.1\text{‰}$ . The largest  $\epsilon_{\text{C,bulk}}$  observed during oxidative *N*-dealkylation of secondary and tertiary aromatic amines was  $-2.8\text{‰}$  corresponding to C isotope signature changes  $\Delta\delta^{13}\text{C}$  of approximately  $10\text{‰}$  after 85% reactant conversion. For many substrates  $\epsilon_{\text{H,bulk}}$  was smaller than  $10\text{‰}$ , where  $\Delta\delta^2\text{H}$  was  $\simeq 20\text{‰}$  at 97% conversion. Measuring small isotope fractionations with the required precision ( $\pm 0.5\text{‰}$  for C,  $\pm 10\text{‰}$  for H, and  $\pm 1\text{‰}$  for N) that allows for unambiguous identification of the occurring reaction represents an analytical challenge. It requires higher reactant conversion, especially in case of isotopic dilution, and can be associated with high statistical uncertainties. High conversion implies lower reactant concentration in the samples and therefore larger sample sizes, efficient extraction and enrichment techniques and analytical methods and instrumentation for precise measurements must be available.

Furthermore, as anilines can enter the environment either directly or as a result of reductive transformation of nitroaromatic compounds (NACs), the source of contamination, i.e. primary contamination vs. transformation product, is not always clear. Aniline formation via NAC reduction can occur under anaerobic iron or sulfate reducing conditions. Anilines can be transported through the various redox-zones,<sup>126</sup> to environments where they can be oxidized to azobenzene or other radical coupling products. In case of a NACs plume at steady-state, evidence of the aniline's contamination source could be

provided by  $^{15}\text{N}$ -CSIA based on current knowledge of the N isotope fractionation associated with NACs reduction and aniline oxidation. N isotope fractionation associated with NACs reduction by Fe(II) sorbed to goethite<sup>48</sup> and Fe(II) in clay minerals<sup>57</sup> is normal ( $\epsilon_{\text{N,bulk}}$  ranged between  $-30$  and  $-40\text{‰}$ ). Aniline oxidation by  $\text{MnO}_2$  causes inverse  $^{15}\text{N}$  fractionation ( $\epsilon_{\text{N,bulk}}$  ranges between  $1$  and  $9\text{‰}$ ), resulting in  $^{14}\text{N}$  enrichment in aniline. Evaluating the change of the aniline's N isotope signature  $\Delta\delta^{15}\text{N}$  over time or distance at sites, where both input of contaminant and its degradation can occur is however difficult and the interpretation of the isotope fractionation challenging. Moreover, reduction of azo-dyes<sup>154</sup> under anaerobic conditions can lead to aniline formation but no knowledge of N isotope fractionation associated with the reductive cleavage of the azo group is yet available.

Finally, it is unclear whether the C, H, and N isotope fractionation trends observed during HRP-catalyzed *N*-dealkylation are also indicative for the *N*-dealkylation catalyzed by cytochrome P450 enzymes. Numerous studies suggest that the two heme-enzymes react to the same products via different pathways involving different intermediates.<sup>45,46,107</sup> Whereas reaction with HRP is reported to proceed via initial single electron transfer (SET), P450 enzymes react via hydrogen atom abstraction (HAT). Isotope effects associated with P450-catalyzed *N*-dealkylation remain unexplored. Therefore, applying CSIA and determining  $^{13}\text{C}$ -,  $^2\text{H}$ -, and  $^{15}\text{N}$ -AKIEs will provide important information regarding differences in reaction mechanisms between the two enzymes, i.e. SET vs. HAT.

## 5.2 Implications for other reaction pathways based on mechanistic considerations

As illustrated in Figure 1.1 aromatic *N*-alkyl amines can be also degraded via other reaction pathways that remain unexplored regarding C, H, and N isotope fractionation trends. Based on the knowledge obtained from the present work and the postulated reaction mechanisms in the literature, possible isotope fractionation scenarios are postulated below for photochemical reactions, enzymatic dioxygenation and nucleophilic additions to electrophilic sites of NOM.

In surface waters aromatic amines can be subject to light-induced degradation via direct and indirect photolysis. Given the different reaction mechanisms and different reactive sites within the aniline molecules for the two pathways, CSIA could be successfully applied to distinguish between the two potentially competing reactions. Transformation of anilines via indirect photolysis by carbonate radicals  $\text{CO}_3^{\bullet-}$  and excited triplet states of natural organic matter proceeds via one electron oxidation to form N centered aminium radicals.<sup>17</sup> This reaction pathway is probably associated with very similar N isotope fractionation trends as observed for the N atom oxidation pathway in Chapter 3. Transformation via direct photolysis is expected to cause observable C but negligible N isotope fractionation, as only the C atoms of the aromatic ring are directly involved in the reaction. The mechanism postulated for substituted haloanilines involves photohydrolysis, i.e. elimination of the halide and  $\text{H}_2\text{O}$  attack to carbene species.<sup>43</sup>

Microbial dioxygenation of anilines has been subject of multiple studies, which revealed that it occurs via formation of catechol species and subsequent cleavage of the aromatic ring.<sup>4,41,158,162</sup> Although several isotopic studies to elucidate the mechanism of microbial dioxygenation of benzenes<sup>34,44</sup> and nitrobenzenes<sup>59</sup> have been performed, the isotope effects associated with aniline dioxygenation remain unexplored. Preliminary results of aniline biodegradation by the *Burkholderia* sp. strain JS667 revealed relatively large inverse N isotope fractionation,  $\epsilon_{\text{N,bulk}} \simeq 13\text{‰}$ , and very small normal  $^{13}\text{C}$  fractionation,  $\epsilon_{\text{C,bulk}} \simeq -0.6\text{‰}$ , associated with the formation of cis-dihydrodiol species.<sup>54</sup> These results illustrate that microbial dioxygenation is associated with distinct different  $^{15}\text{N}$  and  $^{13}\text{C}$  fractionation trends than observed for abiotic N atom oxidation (Chapter 3).

Isotope effects associated with nucleophilic addition of anilines to electrophilic sites of natural organic matter should be subject of future research. Depending on the mechanism that governs chemical incorporation to NOM different isotope fractionation trends can be expected. Irreversible binding via oxidative coupling to sediment bound radicals,

which occurs via initial electron abstraction by  $\text{MnO}_2$  or HRP,<sup>19</sup> would cause similar N and C isotope effects as observed during N atom oxidation (Chapter 3). Significant  $^{15}\text{N}$  fractionation is expected during fast, reversible 1,2- as well as during slower, irreversible 1,4-nucleophilic addition to quinone moieties of the NOM, which leads to formation of labile amine-carbonyl adducts and anilinoquinones, respectively.<sup>141,155,156</sup> During the latter addition to quinone groups, which are reported to be the major substrate sites for nucleophilic addition in NOM,<sup>141</sup> N isotope fractionation could be masked because the availability of electrophilic sites for irreversible binding in NOM can be limited and mass transfer processes, i.e. access to these sites, can become rate-determining.<sup>156</sup>

Even though this thesis only established isotope fractionation patterns for two of the possible degradation pathways, it shows that N atom oxidation and *N*-delkylation of substituted aromatic *N*-alkyl amines are associated with variable and complex C, H, and N isotope fractionation trends and implies that compound-by-compound assessment is inevitable even for molecules of simple molecular structure. Even multielement isotope analysis exhibits certain limitations in case of complex reaction mechanisms with multiple elementary reaction steps. Exploring C, H, and N isotope effects associated with photodegradation, microbial dioxygenation and nucleophilic addition to NOM should be the subject of future research in order to obtain a more comprehensive picture regarding applicability of CSIA to assess the fate of aromatic amines in the environment.



# Literature

- [1] C. Adamo and V. Barone. Exchange functionals with improved long-range behavior and adiabatic connection methods without adjustable parameters: The mPW and mPW1PW models. *J. Chem. Phys.*, 108(2):664–675, 1998.
- [2] C. Aeppli, T. B. Hofstetter, H. I. F. Amaral, R. Kipfer, R. P. Schwarzenbach, and M. Berg. Quantifying in situ transformation rates of chlorinated ethenes by combining compound-specific stable isotope analysis, groundwater dating, and carbon isotope mass balances. *Environ. Sci. Technol.*, 44(10):3705–3711, 2010.
- [3] M. Aeschbacher, M. Sander, and R. P. Schwarzenbach. Novel electrochemical approach to assess the redox properties of humic substances. *Environ. Sci. Technol.*, 44(1):87–93, 2010.
- [4] E. L. Ang, J. P. Obbard, and H. M. Zhao. Directed evolution of aniline dioxygenase for enhanced bioremediation of aromatic amines. *Appl. Microbiol. Biotechnol.*, 81(6):1063–1070, 2009.
- [5] R. Bartha and D. Pramer. Pesticide transformation to aniline and azo compounds in soil. *Science*, 156(3782):1617–1618, 1967.
- [6] M. Berg, J. Bolotin, and T. B. Hofstetter. Compound-specific nitrogen and carbon isotope analysis of nitroaromatic compounds in aqueous samples using solid-phase microextraction coupled to GC/IRMS. *Anal. Chem.*, 79(6):2386–2393, 2007.
- [7] A. Bernstein, Z. Ronen, E. Adar, R. Nativ, H. Lowag, W. Stichler, and R. U. Meckenstock. Compound-specific isotope analysis of RDX and stable isotope fractionation during aerobic and anaerobic biodegradation. *Environ. Sci. Technol.*, 42(21):7772–7777, 2008.

- [8] H. M. Bialk and J. A. Pedersen. NMR investigation of enzymatic coupling of sulfonamide antimicrobials with humic substances. *Environ. Sci. Technol.*, 42(1):106–112, 2008.
- [9] M. Blessing, M. A. Jochmann, and T. C. Schmidt. Pitfalls in compound-specific isotope analysis of environmental samples. *Anal. Bioanal. Chem.*, 390(2):591–603, 2008.
- [10] Y. Bloom, R. Aravena, D. Hunkeler, E. Edwards, and S. K. Frape. Carbon isotope fractionation during microbial dechlorination of trichloroethene, cis-1,2-dichloroethene, and vinyl chloride: implications for assessment of natural attenuation. *Environ. Sci. Technol.*, 34(13):2768–2772, 2000.
- [11] D. Bouchard, D. Hunkeler, P. Gaganis, R. Aravena, P. Hohener, M. M. Broholm, and P. Kjeldsen. Carbon isotope fractionation during diffusion and biodegradation of petroleum hydrocarbons in the unsaturated zone: field experiment at Vaerlose airbase, Denmark, and modeling. *Environ. Sci. Technol.*, 42(2):596–601, 2008.
- [12] A. B. A. Boxall, C. J. Sinclair, K. Fenner, D. Kolpin, and S. J. Maud. When synthetic chemicals degrade in the environment. *Environ. Sci. Technol.*, 38(19):368A–375A, 2004.
- [13] W. A. Brand, A. R. Tegtmeier, and A. Hilkert. Compound-specific isotope analysis - extending toward  $^{15}\text{N}/^{14}\text{N}$  and  $^{18}\text{O}/^{16}\text{O}$ . *Org. Geochem.*, 21(6-7):585–594, 1994.
- [14] A. J. Bridgeman, G. Cavigliasso, L. R. Ireland, and J. Rothery. The Mayer bond order as a tool in inorganic chemistry. *J. Chem. Soc.-Dalton Trans.*, (14):2095–2108, 2001.
- [15] S. Brunauer, P. H. Emmett, and E. Teller. Adsorption of gases in multimolecular layers. *J. Am. Chem. Soc.*, 60:309–319, 1938.
- [16] R.G. Burns and V.M. Burns. *Manganese Oxides*. Mineralogical Society of America, 1979.
- [17] S. Canonica, T. Kohn, M. Mac, F. J. Real, J. Wirz, and U. Von Gunten. Photosensitizer method to determine rate constants for the reaction of carbonate radical with organic compounds. *Environ. Sci. Technol.*, 39(23):9182–9188, 2005.

- 
- [18] J. Clark and D. D. Perrin. Prediction of the strengths of organic bases. *Quarterly Reviews*, 18(3):295–320, 1964.
- [19] D. Colon, E. J. Weber, and G. L. Baughman. Sediment-associated reactions of aromatic amines. 2. QSAR development. *Environ. Sci. Technol.*, 36(11):2443–2450, 2002.
- [20] P. F. Cook and W. W. Cleland. *Enzyme Kinetics and Mechanism*. Garland Science, New York, 416 pp 2007.
- [21] C. J. Cramer. *Essentials of Computational Chemistry: Theories and Models*. John Wiley & Sons, Chichester, 2<sup>nd</sup> edition, 2004.
- [22] G. D’Aprano, E. Proynov, M. Leboeuf, M. Leclerc, and D. R. Salahub. Spin densities and polymerizabilities of aniline derivatives deduced from density functional calculations. *J. Am. Chem. Soc.*, 118(40):9736–9742, 1996.
- [23] H. S. Dempster, B. S. Lollar, and S. Feenstra. Tracing organic contaminants in groundwater: A new methodology using compound-specific isotopic analysis. *Environ. Sci. Technol.*, 31(11):3193–3197, 1997.
- [24] J. P. Dinnocenzo, S. B. Karki, and J. P. Jones. On isotope effects for the cytochrome P450 oxidation of substituted *N,N*-dimethylanilines. *J. Am. Chem. Soc.*, 115(16):7111–7116, 1993.
- [25] M. Dodd, M. Buffle, and U. Von Gunten. Oxidation of antibacterial molecules by aqueous ozone: Moiety-specific reaction kinetics and application to ozone-based wastewater treatment. *Environ. Sci. Technol.*, 40(6):1969–1977, 2006.
- [26] A. Dybala-Defratyka, L. Szatkowski, R. Kaminski, M. Wujec, A. Siwek, and P. Paneth. Kinetic isotope effects on dehalogenations at an aromatic carbon. *Environ. Sci. Technol.*, 42(21):7744–7750, 2008.
- [27] M Eigen. Proton transfer, acid-base catalysis, and enzymatic hydrolysis Part I: Elementary processes. *Angew. Chem. Int. Ed.*, 3(1):1–72, 1964.
- [28] M. Elsner. Stable isotope fractionation to investigate natural transformation mechanisms of organic contaminants: Principles, prospects and limitations. *J. Environ. Monit.*, 12(11):2005–2031, 2010.

- [29] M. Elsner, L. Zwank, D. Hunkeler, and R. P. Schwarzenbach. A new concept linking observable stable isotope fractionation to transformation pathways of organic pollutants. *Environ. Sci. Technol.*, 39(18):6896–6916, 2005.
- [30] M. Elsner, J. McKelvie, G. L. Lacrampe-Couloume, and B. Sherwood Lollar. Insight into methyl tert-butyl ether (MTBE) stable isotope fractionation from abiotic reference experiments. *Environ. Sci. Technol.*, 41(16):5693–5700, 2007.
- [31] M. Elsner, M. A. Jochmann, T. B. Hofstetter, D. Hunkeler, A. Bernstein, T. C. Schmidt, and A. Schimmelmann. Current challenges in compound-specific stable isotope analysis of environmental organic contaminants. *Anal. Bioanal. Chem.*, In press, 2011.
- [32] B. I. Escher and K. Fenner. Recent advances in environmental risk assessment of transformation products. *Environ. Sci. Technol.*, 45(9):3835–3847, 2011.
- [33] G. R. Eykholt and D. T. Davenport. Dechlorination of the chloroacetanilide herbicides alachlor and metolachlor by iron metal. *Environ. Sci. Technol.*, 32(10):1482–1487, 1998.
- [34] A. Fischer, I. Herklotz, S. Herrmann, M. Thullner, S. A. B. Weelink, A. J. M. Stams, M. Schlömann, H.-H. Richnow, and C. Vogt. Combined carbon and hydrogen isotope fractionation investigations for elucidating benzene biodegradation pathways. *Environ.*, 42(12):4356–4363, 2008.
- [35] A. Fischer, M. Gehre, J. Breithfeld, H. H. Richnow, and C. Vogt. Carbon and hydrogen isotope fractionation of benzene during biodegradation under sulfate-reducing conditions: A laboratory to field site approach. *Rapid Commun. Mass Spectrom.*, 23(16):2439–2447, 2009.
- [36] L. Fishbein. *The Handbook of Environmental Chemistry - Anthropogenic Compounds*, volume 3, Part C. Springer, Berlin, Germany, 1984.
- [37] P. F. Fitzpatrick. Oxidation of amines by flavoproteins. *Arch. Biochem. Biophys.*, 493(1):13–25, 2010.
- [38] M. J. Frisch, G. W. Trucks, H. B. Schlegel, G. E. Scuseria, M. A. Robb, J. R. Cheeseman, G. Scalmani, V. Barone, B. Mennucci, G. A. Petersson, H. Nakatsuji, M. Caricato, X. Li, H. P. Hratchian, A. F. Izmaylov, J. Bloino, G. Zheng, J. L.

- Sonnenberg, M. Hada, M. Ehara, K. Toyota, R. Fukuda, J. Hasegawa, M. Ishida, T. Nakajima, Y. Honda, O. Kitao, H. Nakai, T. Vreven, J.A. Montgomery, Jr., J. E. Peralta, F. Ogliaro, M. Bearpark, J. J. Heyd, E. Brothers, K. N. Kudin, V. N. Staroverov, R. Kobayashi, J. Normand, K. Raghavachari, A. Rendell, J. C. Burant, S. S. Iyengar, J. Tomasi, M. Cossi, N. Rega, J. M. Millam, M. Klene, J. E. Knox, J. B. Cross, V. Bakken, C. Adamo, J. Jaramillo, R. Gomperts, R. E. Stratmann, O. Yazyev, A. J. Austin, R. Cammi, C. Pomelli, J. W. Ochterski, R. L. Martin, K. Morokuma, V. G. Zakrzewski, G. A. Voth, P. Salvador, J. J. Dannenberg, S. Dapprich, A. D. Daniels, Ö. Farkas, J. B. Foresman, J. V. Ortiz, J. Cioslowski, and D. J. Fox. Gaussian 09 rev. a.01. Technical report, Gaussian, Inc.
- [39] M. J. Frisch, G. W. Trucks, H. B. Schlegel, G. E. Scuseria, M. A. Robb, J. R. Cheeseman, J. A. Montgomery, Jr., T. Vreven, K. N. Kudin, J. C. Burant, J. M. Millam, S. S. Iyengar, J. Tomasi, V. Barone, B. Mennucci, M. Cossi, G. Scalmani, N. Rega, G. A. Petersson, H. Nakatsuji, M. Hada, M. Ehara, K. Toyota, R. Fukuda, J. Hasegawa, M. Ishida, T. Nakajima, Y. Honda, O. Kitao, H. Nakai, M. Klene, X. Li, J. E. Knox, H. P. Hratchian, J. B. Cross, V. Bakken, C. Adamo, J. Jaramillo, R. Gomperts, R. E. Stratmann, O. Yazyev, A. J. Austin, R. Cammi, C. Pomelli, J. W. Ochterski, P. Y. Ayala, K. Morokuma, G. A. Voth, P. Salvador, J. J. Dannenberg, V. G. Zakrzewski, S. Dapprich, A. D. Daniels, M. C. Strain, O. Farkas, D. K. Malick, A. D. Rabuck, K. Raghavachari, J. B. Foresman, J. V. Ortiz, Q. Cui, A. G. Baboul, S. Clifford, J. Cioslowski, B. B. Stefanov, G. Liu, A. Liashenko, P. Piskorz, I. Komaromi, R. L. Martin, D. J. Fox, T. Keith, M. A. Al-Laham, C. Y. Peng, A. Nanayakkara, M. Challacombe, P. M. W. Gill, B. Johnson, W. Chen, M. W. Wong, C. Gonzalez, and J. A. Pople. Gaussian 03, revision c.02. Technical report, Gaussian, Inc., 2004.
- [40] M. J. Frisch, G. W. Trucks, H. B. Schlegel, G. E. Scuseria, M. A. Robb, J. R. Cheeseman, G. Scalmani, V. Barone, B. Mennucci, G. A. Petersson, H. Nakatsuji, M. Caricato, X. Li, H. P. Hratchian, A. F. Izmaylov, J. Bloino, G. Zheng, J. L. Sonnenberg, M. Hada, M. Ehara, K. Toyota, R. Fukuda, J. Hasegawa, T. Ishida, M. and Nakajima, Y. Honda, O. Kitao, H. Nakai, T. Vreven, J. A. Montgomery, J. E. Peralta, F. Ogliaro, M. Bearpark, J. J. Heyd, E. Brothers, K. N. Kudin, V. N. Staroverov, R. Kobayashi, J. Normand, K. Raghavachari, A. Rendell, J. C. Burant, S. S. Iyengar, J. Tomasi, M. Cossi, N. Rega, J. M. Millam, M. Klene,

- J. E. Knox, J. B. Cross, V. Bakken, C. Adamo, J. Jaramillo, R. Gomperts, R. E. Stratmann, O. Yazyev, A. J. Austin, R. Cammi, C. Pomelli, J. W. Ochterski, R. L. Martin, K. Morokuma, V. G. Zakrzewski, G. A. Voth, P. Salvador, J. J. Dannenberg, S. Dapprich, A. D. Daniels, Ö. Farkas, J. B. Foresman, J. V. Ortiz, J. Cioslowski, and D. J. Fox. Gaussian 09, revision a.02. Technical report, Gaussian, Inc., 2010.
- [41] F. Fukumori and C. P. Saint. Nucleotide sequences and regulational analysis of genes involved in conversion of aniline to catechol in *Pseudomonas putida* UCC22(pTDN1). *J. Bacteriol.*, 179(2):399–408, 1997.
- [42] C. A. Gorski, J. T. Nurmi, P. G. Tratnyek, T. B. Hofstetter, and M. M. Scherer. Redox behavior of magnetite: Implications for contaminant reduction. *Environ. Sci. Technol.*, 44(1):55–60, 2010.
- [43] G. Grabner and C. Richard. *Mechanisms of direct photolysis of biocides based on halogenated phenols and anilines*, volume 2 of *Handbook of Environmental Chemistry*. 2005.
- [44] C. Griebl, L. Adrian, R. U. Meckenstock, and H. H. Richnow. Stable carbon isotope fractionation during aerobic and anaerobic transformation of trichlorobenzene. *Fems Microbiol. Ecol.*, 48(3):313–321, 2004.
- [45] F. P. Guengerich, O. Okazaki, Y. Seto, and T. L. Macdonald. Radical-cation intermediates in *N*-dealkylation reactions. *Xenobiotica*, 25(7):689–709, 1995.
- [46] F. P. Guengerich, C. H. Yun, and T. L. Macdonald. Evidence for a 1-electron oxidation mechanism in *N*-dealkylation of *N,N*-dialkylanilines by cytochrome P450 2B1 - Kinetic hydrogen isotope effects, linear free energy relationships, comparisons with horseradish peroxidase, and studies with oxygen surrogates. *J. Biol. Chem.*, 271(44):27321–27329, 1996.
- [47] D.C. Harris. *Quantitative Chemical Analysis*. 3<sup>rd</sup> edition, 1991.
- [48] A. Hartenbach, T. B. Hofstetter, M. Berg, J. Bolotin, and R. P. Schwarzenbach. Using nitrogen isotope fractionation to assess abiotic reduction of nitroaromatic compounds. *Environ. Sci. Technol.*, 40(24):7710–7716, 2006.

- 
- [49] A. E. Hartenbach, T. B. Hofstetter, M. Aeschbacher, M. Sander, D. Kim, T. J. Strathmann, W. A. Arnold, C. J. Cramer, and R. P. Schwarzenbach. Variability of nitrogen isotope fractionation during the reduction of nitroaromatic compounds with dissolved reductants. *Environ. Sci. Technol.*, 42(22):8352–8359, 2008.
- [50] A. E. Hartenbach, T. B. Hofstetter, P. R. Tentscher, S. Canonica, M. Berg, and R. P. Schwarzenbach. Carbon, hydrogen, and nitrogen isotope fractionation during light-induced transformations of atrazine. *Environ. Sci. Technol.*, 42(21):7751–7756, 2008.
- [51] Schleyer P.v.R. Hehre W., Radom L. *Ab Initio Molecular Orbital Theory*. Wiley: New York, 1986.
- [52] D. Hofmann, M. Gehre, and K. Jung. Sample preparation techniques for the determination of natural  $^{15}\text{N}/^{14}\text{N}$  variations in amino acids by gas chromatography-combustion-isotope ratio mass spectrometry (GC-C-IRMS). *Isot. Environ. Health Stud.*, 39(3):233–244, 2003.
- [53] T. B. Hofstetter and M. Berg. Assessing transformation processes of organic contaminants by compound-specific stable isotope analysis. *TrAC-Trends Anal. Chem.*, 30(4):618–627, 2011.
- [54] T. B. Hofstetter, M. Skarpeli-Liati, S. G. Pati, J. Bolotin, J. C. Spain, and K. A. Shin. Distinct nitrogen and carbon isotope fractionation trends of *N*-aryl dioxygenation. *unpublished work*.
- [55] T. B. Hofstetter, A. Neumann, and R. P. Schwarzenbach. Reduction of nitroaromatic compounds by Fe(II) species associated with iron-rich smectites. *Environ. Sci. Technol.*, 40(1):235–242, 2006.
- [56] T. B. Hofstetter, C. M. Reddy, L. J. Heraty, M. Berg, and N. C. Sturchio. Carbon and chlorine isotope effects during abiotic reductive dechlorination of polychlorinated ethanes. *Environ. Sci. Technol.*, 41(13):4662–4668, 2007.
- [57] T. B. Hofstetter, A. Neumann, W. A. Arnold, A. E. Hartenbach, J. Bolotin, C. J. Cramer, and R. P. Schwarzenbach. Substituent effects on nitrogen isotope fractionation during abiotic reduction of nitroaromatic compounds. *Environ. Sci. Technol.*, 42(6):1997–2003, 2008.

- [58] T. B. Hofstetter, R. P. Schwarzenbach, and S. M. Bernasconi. Assessing transformation processes of organic compounds using stable isotope fractionation. *Environ. Sci. Technol.*, 42(21):7737–7743, 2008.
- [59] T. B. Hofstetter, J. C. Spain, S. F. Nishino, J. Bolotin, and R. P. Schwarzenbach. Identifying competing aerobic nitrobenzene biodegradation pathways using compound-specific isotope analysis. *Environ. Sci. Technol.*, 42(13):4764–4770, 2008.
- [60] D. Hunkeler and S. M. Bernasconi. *Environmental isotopes in biodegradation and bioremediation*. CRC Press: Boca Raton, 2010.
- [61] D. Hunkeler, N. Anderson, R. Aravena, S. M. Bernasconi, and B. J. Butler. Hydrogen and carbon isotope fractionation during aerobic biodegradation of benzene. *Environ. Sci. Technol.*, 35(17):3462–3467, 2001.
- [62] D. Hunkeler, B. J. Butler, R. Aravena, and J. F. Barker. Monitoring biodegradation of methyl tert-butyl ether (MTBE) using compound-specific carbon isotope analysis. *Environ. Sci. Technol.*, 35(4):676–681, 2001.
- [63] D. Hunkeler, R. Aravena, K. Berry-Spark, and E. Cox. Assessment of degradation pathways in an aquifer with mixed chlorinated hydrocarbon contamination using stable isotope analysis. *Environ. Sci. Technol.*, 39(16):5975–5981, 2005.
- [64] D. Hunkeler, R. U. Meckenstock, B. Sherwood Lollar, T. C. Schmidt, and J. T. Wilson. *A guide for assessing biodegradation and source identification of organic ground water contaminants using compound specific isotope analysis (CSIA)*. EPA, Office of Research and Development, National Risk Management Research Laboratory, Ada, Oklahoma 74820, 2008.
- [65] D. Job and H. B. Dunford. Substituent effect on oxidation of phenols and aromatic amines by horseradish peroxidase compound-I. *Eur. J. Biochem.*, 66(3):607–614, 1976.
- [66] M. A. Jochmann, M. Blessing, S. B. Haderlein, and T. C. Schmidt. A new approach to determine method detection limits for compound-specific isotope analysis of volatile organic compounds. *Rapid Commun. Mass Spectrom.*, 20(24):3639–3648, 2006.



- [67] S. B. Karki, J. P. Dinnocenzo, J. P. Jones, and K. R. Korzekwa. Mechanism of oxidative amine dealkylation of substituted *N,N*-dimethylanilines by cytochrome P-450 - Application of isotope effect profiles. *J. Am. Chem. Soc.*, 117(13):3657–3657, 1995.
- [68] A. Kavner, F. Bonet, A. Shahar, J. Simon, and E. Young. The isotopic effects of electron transfer: An explanation for Fe isotope fractionation in nature. *Geochim. Cosmochim. Acta*, 69(12):2971–2979, 2005.
- [69] G. L. Kedderis and P. F. Hollenberg. Characterization of the *N*-demethylation reactions catalyzed by horseradish peroxidase. *J. Biol. Chem.*, 258(13):8129–8138, 1983.
- [70] S. Kern, K. Fenner, H. P. Singer, R. P. Schwarzenbach, and J. Hollender. Identification of transformation products of organic contaminants in natural waters by computer-aided prediction and high-resolution mass spectrometry. *Environ. Sci. Technol.*, 43(18):7039–7046, 2009.
- [71] J. Klausen, S. P. Tröber, S. B. Haderlein, and R. P. Schwarzenbach. Reduction of substituted nitrobenzenes by Fe(II) in aqueous mineral suspensions. *Environ. Sci. Technol.*, 29(9):2396–2404, 1995.
- [72] J. Klausen, S. B. Haderlein, and R. P. Schwarzenbach. Oxidation of substituted anilines by aqueous MnO<sub>2</sub>: Effect of co-solutes on initial and quasi steady state kinetics. *Environ. Sci. Technol.*, 31(9):2642–2649, 1997.
- [73] F. D. Kopinke, A. Georgi, M. Voskamp, and H. H. Richnow. Carbon isotope fractionation of organic contaminants due to retardation on humic substances: Implications for natural attenuation studies in aquifers. *Environ. Sci. Technol.*, 39(16):6052–6062, 2005.
- [74] T. Kuder, J. T. Wilson, P. Kaiser, R. Kolhatkar, P. Philp, and J. Allen. Enrichment of stable carbon and hydrogen isotopes during anaerobic biodegradation of MTBE: microcosm and field evidence. *Environ. Sci. Technol.*, 39(1):213–220, 2005.
- [75] R. A. Kwiecien, R. Molinie, P. Paneth, V. Silvestre, J. Lebreton, and R. J. Robins. Elucidation of the mechanism of *N*-demethylation catalyzed by cytochrome P-450 monooxygenase is facilitated by exploiting <sup>15</sup>N-heavy isotope effects. *Arch. Biochem. Biophys.*, 510(1):35–41, 2011.

- [76] Renata A. Kwiecień, Katarzyna Kosieradzka, Jean-Yves Le Questel, Jacques Lebreton, Anaïs Fournial, Emmanuel Gentil, Marcel Delaforge, Piotr Paneth, and Richard J. Robins. Cytochrome P450 monooxygenase-catalyzed ring opening of the bicyclic amine, nortropine: An experimental and DFT computational study. *Chem. Cat. Chem*, 4(4):530–539, 2012.
- [77] E. M. LaBolle, G. E. Fogg, J. B. Eweis, J. Gravner, and D. G. Leaist. Isotopic fractionation by diffusion in groundwater. *Water Resour. Res.*, 44(7), 2008.
- [78] S. Laha and R. G. Luthy. Oxidation of aniline and other primary aromatic amines by manganese-dioxide. *Environ. Sci. Technol.*, 24(3):363–373, 1990.
- [79] M. F. Lehmann, S. M. Bernasconi, A. Barbieri, and J. A. McKenzie. Preservation of organic matter and alteration of its carbon and nitrogen isotope composition during simulated and in situ early sedimentary diagenesis. *Geochim. Cosmochim. Acta*, 66(20):3573–3584, 2002.
- [80] Dongmei Li, Yong Wang, and Keli Han. Recent density functional theory model calculations of drug metabolism by cytochrome P450. *Coord. Chem. Rev.*, 256(11–12):1137 – 1150, 2012.
- [81] S. G. Lias. *Ionization energy evaluation*. National Institute of Standards and Technology. NIST Chemistry WebBook, NIST Standard Reference Database Number 69, Gaithersburg, MD 20899, 2011.
- [82] K Lippa, S Demel, I Lau, and A Roberts. Kinetics and mechanism of the nucleophilic displacement reactions of chloroacetanilide herbicides: Investigation of  $\alpha$ -substituent effects. *J. Agric. Food Chem.*, 52(10):3010–3021, 2004.
- [83] B. S. Lollar, S. K. Hirschorn, M. M. G. Chartrand, and G. Lacrampe-Couloume. An approach for assessing total instrumental uncertainty in compound-specific carbon isotope analysis: Implications for environmental remediation studies. *Anal. Chem.*, 79(9):3469–3475, 2007.
- [84] Haiting Lu, Xi Chen, and Chang-Guo Zhan. First-principles calculation of  $pK_a$  for cocaine, nicotine, neurotransmitters, and anilines in aqueous solution. *J. Phys. Chem. B*, 111(35):10599–10605, 2007.

- 
- [85] S. A. Macko, M. E. Uhle, M. H. Engel, and V. Andrusevich. Stable nitrogen isotope analysis of amino acid enantiomers by gas chromatography combustion/isotope ratio mass spectrometry. *Anal. Chem.*, 69(5):926–929, 1997.
- [86] S. A. Mancini, A. C. Ulrich, G. Lacrampe-Couloume, B. Sleep, E. A. Edwards, and B. S. Lollar. Carbon and hydrogen isotopic fractionation during anaerobic biodegradation of benzene. *Appl. Environ. Microbiol.*, 69(1):191–198, 2003.
- [87] J. March. *Advanced Organic Chemistry*. Wiley Interscience Publication. John Wiley & Sons, New York, 3rd edition, 1985.
- [88] R. A. Marcus. Chemical and electrochemical electron-transfer theory. *Annu. Rev. Phys. Chem.*, 15:155–196, 1964.
- [89] J. F. Marlier. Multiple isotope effects on the acyl group transfer reactions of amides and esters. *Acc. Chem. Res.*, 34(4):283–290, 2001.
- [90] MarvinSketch v 5.2.1. ChemAxon. <http://www.chemaxon.com/marvin/sketch/index.php>, 2009.
- [91] R.M. McKenzie. *Manganese Oxides and Hydroxides*, pages 439–465. SSSA Book Series 1, Madison WI, USA, 1989.
- [92] D. A. Merritt and J. M. Hayes. Factors controlling precision and accuracy in isotope-ratio-monitoring mass-spectrometry. *Anal. Chem.*, 66(14):2336–2347, 1994.
- [93] D. A. Merritt and J. M. Hayes. Nitrogen isotopic analyses by isotope-ratio-monitoring gas-chromatography mass-spectrometry. *J. Am. Soc. Mass Spectrom.*, 5(5):387–397, 1994.
- [94] A. H. Meyer, H. Penning, H. Lowag, and M. Elsner. Precise and accurate compound specific carbon and nitrogen isotope analysis of atrazine: critical role of combustion oven conditions. *Environ. Sci. Technol.*, 42(21):7757–7763, 2008.
- [95] A. H. Meyer, H. Penning, and M. Elsner. C and N isotope fractionation suggests similar mechanisms of microbial atrazine transformation despite involvement of different enzymes (AtzA and TrzN). *Environ. Sci. Technol.*, 43(21):8079–8085, 2009.
- [96] F. J. Millero. The ionization of acids in estuarine waters. *Geochim. Cosmochim. Acta*, 45(11):2085–2089, 1981.

- [97] F. J. Millero and D. R. Schreiber. Use of the ion-pairing model to estimate activity-coefficients of the ionic components of natural waters. *Am. J. Sci.*, 282(9):1508–1540, 1982.
- [98] G. T. Miwa, J. S. Walsh, G. L. Kedderis, and P. F. Hollenberg. The use of intramolecular isotope effects to distinguish between deprotonation and hydrogen-atom abstraction mechanisms in cytochrome P450 catalyzed and peroxidase catalyzed *N*-demethylation reactions. *J. Biol. Chem.*, 258(23):4445–4449, 1983.
- [99] R. Molinié, R. A. Kwiecien, P. Paneth, W. Hatton, J. Lebreton, and R. J. Robins. Investigation of the mechanism of nicotine demethylation in *Nicotiana* through  $^2\text{H}$  and  $^{15}\text{N}$  heavy isotope effects: Implication of cytochrome P450 oxidase and hydroxyl ion transfer. *Arch. Biochem. Biophys.*, 458(2):175–183, 2007.
- [100] J. A. Montgomery, M. J. Frisch, J. W. Ochterski, and G. A. Petersson. A complete basis set model chemistry. VII. Use of the minimum population localization method. *J. Chem. Phys.*, 112(15):6532–6542, 2000.
- [101] J. W. Murray. Surface chemistry of hydrous manganese-dioxide. *J. Colloid Interface Sci.*, 46(3):357–371, 1974.
- [102] H. W. Nesbitt, G. W. Canning, and G. M. Bancroft. XPS study of reductive dissolution of 7 Å-birnessite by  $\text{HAsO}_3$ , with constraints on reaction mechanism. *Geochim. Cosmochim. Acta*, 62(12):2097–2110, 1998.
- [103] J. Neuwoehner, T. Zilberman, K. Fenner, and B. I. Escher. QSAR-analysis and mixture toxicity as diagnostic tools: Influence of degradation on the toxicity and mode of action of diuron in algae and daphnids. *Aquat. Toxicol.*, 97(1):58–67, 2010.
- [104] A. Nitzan. *Chemical Dynamics in Condensed Phases*. Oxford University Press, New York, 2006.
- [105] F. E. Norrington, R. M. Hyde, S. G. Williams, and R. Wootton. Physicochemical-activity relations in practice 1. Rational and self-consistent data bank. *J. Med. Chem.*, 18(6):604–607, 1975.
- [106] J. W. Ochterski, G. A. Petersson, and J. A. Montgomery. A complete basis set model chemistry. V. Extensions to six or more heavy atoms. *J. Chem. Phys.*, 104(7):2598–2619, 1996.

- 
- [107] O. Okazaki and F. P. Guengerich. Evidence for specific base catalysis in *N*-dealkylation reactions catalyzed by cytochrome P450 and chloroperoxidase - differences in rates of deprotonation of aminium radicals as an explanation for high kinetic hydrogen isotope effects observed with peroxidases. *J. Biol. Chem.*, 268(3):1546–1552, 1993.
- [108] G. E. Parris. Covalent binding of aromatic-amines to humates 1. Reactions with carbonyls and quinones. *Environ. Sci. Technol.*, 14(9):1099–1106, 1980.
- [109] T. Paul, P. L. Miller, and T. J. Strathmann. Visible-light-mediated TiO<sub>2</sub> photocatalysis of fluoroquinolone antibacterial agents. *Environ. Sci. Technol.*, 41(13):4720–4727, 2007.
- [110] T. Paul, M. C. Dodd, and T. J. Strathmann. Photolytic and photocatalytic decomposition of aqueous ciprofloxacin: Transformation products and residual antibacterial activity. *Water Res.*, 44(10):3121–3132, 2010.
- [111] H. Penning and M. Elsner. Intramolecular carbon and nitrogen isotope analysis by quantitative dry fragmentation of the phenylurea herbicide isoproturon in a combined injector/capillary reactor prior to GC separation. *Anal. Chem.*, 79:8399–8405, 2007.
- [112] H. Penning, C. J. Cramer, and M. Elsner. Rate-dependent carbon and nitrogen kinetic isotope fractionation in hydrolysis of isoproturon. *Environ. Sci. Technol.*, 42(21):7764–7771, 2008.
- [113] H. Penning, S. R. Sorensen, A. H. Meyer, J. Aamand, and M. Elsner. C, N, and H isotope fractionation of the herbicide isoproturon reflects different microbial transformation pathways. *Environ. Sci. Technol.*, 44(7):2372–2378, 2010.
- [114] J. Perdew and Y. Wang. Accurate and simple density functional for the electronic exchange energy: Generalized gradient approximation. *Phys. Rev. B*, 33(12):8800–8802, 1986.
- [115] J. P. Perdew. *Unified Theory of Exchange and Correlation Beyond the Local Density Approximation*. Electronic Structure of Solids. Akademie Verlag, Berlin, p. 11-20, 1991.
- [116] G. A. Petersson. Complete basis-set thermochemistry and kinetics. *ACS Symposium series*, Vol. 667, 1998.

- [117] K. S. Pitzer. Thermodynamics of electrolytes. 1. Theoretical basis and general conclusions. *J. Phys. Chem.*, 77(2):268–277, 1973.
- [118] K. S. Pitzer. *Activity coefficients in electrolyte solutions*, volume 2. CRC; Press: Boca Raton, 1991.
- [119] M. D. R. Pizzigallo, P. Ruggiero, C. Crecchio, and G. Mascolo. Oxidation of chloroanilines at metal oxide surfaces. *J. Agric. Food Chem.*, 46(5):2049–2054, 1998.
- [120] Affolter C. Pretsch E., Bühlmann P. and Badertscher M. *Spektroskopische Daten zur Strukturaufklärung organischer Verbindungen*. Springer Verlag, 4th edition, 2001.
- [121] E. C. Ralph, J. S. Hirschi, M. A. Anderson, W. W. Cleland, D. A. Singleton, and P. F. Fitzpatrick. Insights into the mechanism of flavoprotein-catalyzed amine oxidation from nitrogen isotope effects on the reaction of *N*-methyltryptophan oxidase. *Biochemistry*, 46(25):7655–7664, 2007.
- [122] Z. Rappoport. *The Chemistry of Anilines*, volume 1139 of *Wiley Interscience Publication*. John Wiley & Sons Ltd, Chichester, 2007.
- [123] S. D. Richardson and T. A. Ternes. Water analysis: emerging contaminants and current issues. *Anal. Chem.*, 83(12):4614–4648, 2011.
- [124] K. Schirmer and M. Schirmer. Who is chasing whom? A call for a more integrated approach to reduce the load of micro-pollutants in the environment. *Water Sci. Technol.*, 57(1):145–150, 2008.
- [125] T. C. Schmidt, L. Zwank, M. Elsner, M. Berg, R. U. Meckenstock, and S. B. Haderlein. Compound-specific stable isotope analysis of organic contaminants in natural environments: a critical review of the state of the art, prospects, and future challenges. *Anal. Bioanal. Chem.*, 378(2):283–300, 2004.
- [126] R. P. Schwarzenbach, P. M. Gschwend, and D. M. Imboden. *Environmental Organic Chemistry*. Wiley Interscience Publication. John Wiley & Sons, New York, 2nd edition, 2003.

- 
- [127] R. P. Schwarzenbach, B. I. Escher, K. Fenner, T. B. Hofstetter, C. A. Johnson, U. von Gunten, and B. Wehrli. The challenge of micropollutants in aquatic systems. *Science*, 313(5790):1072–1077, 2006.
- [128] R. P. Schwarzenbach, T. Egli, T. B. Hofstetter, U. von Gunten, and B. Wehrli. Global water pollution and human health. *Annu. Rev. Environ. Resour.*, 35:109–36, 2010.
- [129] K. M. Scott, X. Lu, C. M. Cavanaugh, and J. S. Liu. Optimal methods for estimating kinetic isotope effects from different forms of the Rayleigh distillation equation. *Geochim. Cosmochim. Acta*, 68(3):433–442, 2004.
- [130] A. L. Sessions. Isotope-ratio detection for gas chromatography. *J. Sep. Sci.*, 29(12):1946–1961, 2006.
- [131] J. Y. Shin and M. A. Cheney. Abiotic dealkylation and hydrolysis of atrazine by birnessite. *Environ. Sci. Technol.*, 24(6):1353–1360, 2005.
- [132] K. A. Shin and J. C. Spain. Pathway and evolutionary implications of diphenylamine biodegradation by *Burkholderia* sp Strain JS667. *Appl. Environ. Microbiol.*, 75(9):2694–2704, 2009.
- [133] K. E. Simmons, R. D. Minard, and J. M. Bollag. Oligomerization of 4-chloroaniline by oxidoreductases. *Environ. Sci. Technol.*, 21(10):999–1003, 1987.
- [134] M. Skarpeli-Liati, W. A. Arnold, A. Turgeon, C. J. Cramer, and T. B. Hofstetter. pH-Dependent equilibrium isotope fractionation associated with compound-specific nitrogen and carbon isotope analysis by SPME-GC/IRMS. *Anal. Chem.*, 83(5):1641–1648, 2011.
- [135] M. Skarpeli-Liati, M. Jiskra, A. Turgeon, A. N. Garr, W. A. Arnold, C. J. Cramer, R. P. Schwarzenbach, and T. B. Hofstetter. Using nitrogen isotope fractionation to assess the oxidation of substituted anilines by manganese oxide. *Environ. Sci. Technol.*, 45(13):5596–5604, 2011.
- [136] A. T. Stone. Reductive dissolution of manganese(III/IV) oxides by substituted phenols. *Environ. Sci. Technol.*, 21(10):979–988, 1987.
- [137] W. Stumm and J. J. Morgan. *Aquatic Chemistry*. John Wiley & Sons, New York, 3rd edition, 1996.

- [138] A. K. Styring, J. C. Sealy, and R. P. Evershed. Resolving the bulk  $\delta^{15}\text{N}$  values of ancient human and animal bone collagen via compound-specific nitrogen isotope analysis of constituent amino acids. *Geochim. Cosmochim. Acta*, 74(1):241–251, 2010.
- [139] J. C. Suatoni, R. E. Snyder, and R. O. Clark. Voltammetric studies of phenol and aniline ring substitution. *Anal. Chem.*, 33(13):1894–1897, 1961.
- [140] N. Tanaka, A. Yamaguchi, M. Araki, and K. Kimata. Separation of nitrogen isotopic compounds by reversed-phase liquid-chromatography on the basis of nitrogen isotope effects on the dissociation of amines. *J. Am. Chem. Soc.*, 107(25):7781–7782, 1985.
- [141] K. A. Thorn, P. J. Pettigrew, W. S. Goldenberg, and E. J. Weber. Covalent binding of aniline to humic substances. 2.  $^{15}\text{N}$ -NMR studies of nucleophilic addition reactions. *Environ. Sci. Technol.*, 30(9):2764–2775, 1996.
- [142] N. B. Tobler, T. B. Hofstetter, and R. P. Schwarzenbach. Assessing iron-mediated oxidation of toluene and reduction of nitroaromatic contaminants in anoxic environments using compound-specific isotope analysis. *Environ. Sci. Technol.*, 41(22):7773–7780, 2007.
- [143] N. B. Tobler, T. B. Hofstetter, and R. P. Schwarzenbach. Carbon and hydrogen isotope fractionation during anaerobic toluene oxidation by *Geobacter metallireducens* with different Fe(III) phases as terminal electron acceptors. *Environ. Sci. Technol.*, 42(21):7786–7792, 2008.
- [144] J. Tomasi, B. Mennucci, and E. Cancès. The IEF version of the PCM solvation method: an overview of a new method addressed to study molecular solutes at the QM ab initio level. *Theochem - J. Mol. Struct.*, 464(1-3):211–226, 1999.
- [145] J. Tomasi, B. Mennucci, and R. Cammi. Quantum mechanical continuum solvation models. *Chem. Rev.*, 105(8):2999–3093, 2005.
- [146] D. G. Truhlar, B. C. Garrett, and S. J. Klippenstein. Current status of transition-state theory. *J. Phys. Chem.*, 100(31):12771–12800, 1996.
- [147] J. Van Der Zee, D. R. Duling, R. P. Mason, and T. E. Eling. The oxidation of *N*-substituted aromatic amines by horseradish peroxidase. *J. Biol. Chem.*, 264(33):19828–19836, 1989.



- 
- [148] M. J. H. Van Haandel, M. M. J. Claassens, N. Van der Hout, M. G. Boersma, J. Vervoort, and I.M.C.M. Rietjens. Differential substrate behaviour of phenol and aniline derivatives during conversion by horseradish peroxidase. *Biochim. Biophys. Acta-Protein Struct. Molec. Enzym.*, 1435(1-2):22–29, 1999.
- [149] A. Vieth, J. Muller, G. Strauch, M. Kastner, M. Gehre, R. U. Meckenstock, and H. H. Richnow. In-situ biodegradation of tetrachloroethene and trichloroethene in contaminated aquifers monitored by stable isotope fractionation. *Isot. Environ. Health Stud.*, 39(2):113–124, 2003.
- [150] C. Vogt, E. Cyrus, I. Herklotz, D. Schlosser, A. Bahr, S. Herrmann, H.-H. Richnow, and A. Fischer. Evaluation of toluene degradation pathways by two-dimensional stable isotope fractionation. *Environ. Sci. Technol.*, 42(21):7793–7800, 2008.
- [151] D. J. Wang, J. Y. Shin, M. A. Cheney, G. Sposito, and T. G. Spiro. Manganese dioxide as a catalyst for oxygen-independent atrazine dealkylation. *Environ. Sci. Technol.*, 33(18):3160–3165, 1999.
- [152] Y. Wang, D. Kumar, C. Yang, K. Han, and S. Shaik. Theoretical study of *N*-demethylation of substituted *N,N*-dimethylanilines by cytochrome P450: The mechanistic significance of kinetic isotope effect profiles. *J. Phys. Chem. B*, 111(26):7700–7710, 2007.
- [153] Y. Wang, D. M. Li, K. L. Han, and S. Shaik. An acyl group makes a difference in the reactivity patterns of cytochrome P450 catalyzed *N*-demethylation of substituted *N,N*-dimethylbenzamides - High spin selective reactions. *J. Phys. Chem. B*, 114(8):2964–2970, 2010.
- [154] E. J. Weber and R. L. Adams. Chemical-mediated and sediment-mediated reduction of the azo-dye disperse-blue-79. *Environ. Sci. Technol.*, 29(5):1163–1170, 1995.
- [155] E. J. Weber, D. L. Spidle, and K. A. Thorn. Covalent binding of aniline to humic substances. 1. Kinetic studies. *Environ. Sci. Technol.*, 30(9):2755–2763, 1996.
- [156] E. J. Weber, D. Colon, and G. L. Baughman. Sediment-associated reactions of aromatic amines. 1. Elucidation of sorption mechanisms. *Environ. Sci. Technol.*, 35(12):2470–2475, 2001.
- [157] M. Wolfsberg, Alexander van Hook, P. Paneth, and L. P. N. Rebelo. *Isotope Effects in Chemical, Geological, and Bio Sciences*. Springer, Heidelberg, 2010.

- [158] J. Zeyer, A. Wasserfallen, and K. N. Timmis. Microbial mineralization of ring-substituted anilines through an ortho-cleavage pathway. *Appl. Environ. Microbiol.*, 50(2):447–453, 1985.
- [159] H. C. Zhang and C. H. Huang. Oxidative transformation of fluoroquinolone antibacterial agents and structurally related amines by manganese oxide. *Environ. Sci. Technol.*, 39(12):4474–4483, 2005.
- [160] H. C. Zhang, W. R. Chen, and C. H. Huang. Kinetic modeling of oxidation of antibacterial agents by manganese oxide. *Environ. Sci. Technol.*, 42(15):5548–5554, 2008.
- [161] J. Zhang, J.-W. Zheng, B. Liang, C.-H. Wang, S. Cai, Y.-Y. Ni, J. He, and S.-P. Li. Biodegradation of chloroacetamide herbicides by *Paracoccus* sp. FLY-8 in vitro. *J. of Agric. Food Chem.*, 59(9):4614–4621, 2011.
- [162] T. Zhang, H.-F. Ren, Y. Liu, B.-L. Zhu, and Z.-P. Liu. A novel degradation pathway of chloroaniline in *Diaphorobacter* sp. PCA039 entails initial hydroxylation. *World J. Microbiol. Biotechnol.*, 26(4):665–673, 2010.
- [163] M. Q. Zhu, K. W. Paul, J. D. Kubicki, and D. L. Sparks. Quantum chemical study of arsenic (III/V) adsorption on Mn-oxides: Implications for arsenic(III) oxidation. *Environ. Sci. Technol.*, 43(17):6655–6661, 2009.
- [164] L. Zwank, M. Berg, T. C. Schmidt, and S. B. Haderlein. Compound-specific carbon isotope analysis of volatile organic compounds in the low-microgram per liter range. *Anal. Chem.*, 75(20):5575–5583, 2003.
- [165] L. Zwank, M. Berg, M. Elsner, T. C. Schmidt, R. P. Schwarzenbach, and S. B. Haderlein. New evaluation scheme for two-dimensional isotope analysis to decipher biodegradation processes: Application to groundwater contamination by MTBE. *Environ. Sci. Technol.*, 39(4):1018–1029, 2005.

# Curriculum Vitae

Marita Skarpeli-Liati

Born July 30<sup>th</sup>, 1983 in Athens, Greece

Citizen of Greece and Zürich, Switzerland

- 1989 – 1997     Primary and High school in Athens, Greece
- 1997 – 2002     High school, "Matura Type C" (Mathematics and Natural Sciences),  
MNG Rämibühl, Zürich
- 2002 – 2007     B.Sc. and M.Sc. Degree in Chemistry, Department of Chemistry  
and Applied Biosciences, ETH Zurich
- 2007             Master Thesis "*Reductive Transformation of Chlorinated Ethanes  
by Fe(II)-Species in Clay Minerals*", Group of Prof. R. P. Schwarzenbach,  
Department of Environmental Sciences, ETH Zurich
- 2008 – 2012     Doctoral Student and Teaching Assistant  
in the Institute of Biogeochemistry and Pollutant Dynamics (IBP)  
of the Department of Environmental Sciences, ETH Zurich  
and Department of Environmental Chemistry  
of the Swiss Federal Institute of Aquatic Science and Technology (EAWAG)  
"*Oxidative Transformation of Aromatic Amines: Mechanistic Insights  
from Multielement Stable Isotope Analyses*", Prof. R. P. Schwarzenbach.